People assume that time is a strict progression of cause to effect,
but, actually, from a non-linear, non-subjective point of view,
it's more like a big ball of... wibbily-wobbly... timey-wimey... stuff.
— Doctor Who (David Tennant)

5 Estimation of rare allele age

Contents

5.1 Introduction

The inference of the genealogical history of a sample is of interest to a myriad of applications in genetic research, both in population and medical genetics. The "age" of an allele, which simply refers to the time since the allele was created by a mutation event, is of particular interest; for example, to observe demographic processes and events, or to better understand the effects of disease-related variants by their time of emergence in the population.

In this chapter, I propose a novel method to estimate the age of an allele, which is based on a collection of statistical models that derive from coalescent theory. The method is inspired by *composite likelihood* approaches, which recently have gained in popularity for various applications in genetic research. The coalescent-based approach was pioneered by Hudson (2001) and has been used successfully, for example, for the fine-scale estimation of recombination rates (McVean *et al.*, 2004; Myers *et al.*, 2005).

In contrast to existing methods for allele age estimation (*e.g.*, see review by Slatkin and Rannala, 2000), the method I present in this chapter does not require prior knowledge about past demographic processes or events. Although an assumption of certain population parameters is required, such as effective population size (N_e) or mutation rate (μ), these are expected to *mostly* affect the scaling of time, such that differences between age estimates for different alleles are proportionally constant.

The age estimation framework presented in this chapter is based on allele sharing at a particular variant site observed in the sample, where the underlying IBD structure is inferred locally around the chromosomal position of the variant under consideration. The methodology for targeted IBD detection presented in Chapters 3 and 4 is therefore essential for this approach; *i.e.* the `tidy` algorithm which includes the four-gamete test (FGT), discordant genotype test (DGT), and the probabilistic IBD model for inference using a Hidden Markov Model (HMM). I implemented the age estimation method as a computational tool written in `C++`, referred to as the **`rvage`** algorithm (for rare variant age estimation) which incorporates the full functionality of the previously presented `tidy` algorithm for IBD detection.*

I begin this chapter by introducing the concept of the method, which is followed by a detailed description of the statistical framework. The method is evaluated in extensive simulation studies, which also consider data error as a source of estimation bias. Although the method can be applied to single-nucleotide polymorphisms (SNP) occurring at any frequency, here, I focus on rare alleles in particular. Finally, I apply this method to data from the 1000 Genomes Project (1000G) Phase III.

5.2 Approach

Consider a set of haplotypes which share a given allele by descent from a common ancestor who lived at some point in the past. Suppose that the genealogical history of the sample is known such that the ancestral origin of the allele can be found by tracing back to

* Rare variant age estimation (`rvage`): https://github.com/pkalbers/rvage

the most recent common ancestor (MRCA) of the haplotypes that share the allele. In a finite population, however, the MRCA is unlikely to indicate the individual in which the allele arose through mutation; therefore the actual age of the allele is expected to be older than the time to the most recent common ancestor (T_{MRCA}) of the set of haplotypes which share the focal allele. The mutation from which the allele derived can be seen as a distinguishing event in the history of the population, immediately after which only one individual in the population carried the mutant allele. It follows that the allele is expected to be younger than the MRCA of that one individual and any of the non-carrier individuals in the contemporary population. This insight is of particular interest as it suggests that the actual time of the mutation event lies somewhere in between those two points in time.

There are two main sources of information available from the data which relate to the T_{MRCA}. First, mutation events occur independently in each lineage and mutations accumulate along the sequence as the chromosome is passed on over generations. Second, recombination events break down the length of the shared haplotype in each generation independently in each lineage. The number of mutations which segregate in the two haplotypes as well as the genetic length of the pairwise shared haplotype segment can be used to infer the T_{MRCA} of two chromosomes; *i.e.* the time of the coalescent event at which the two lineages join.

In the following section, I derive the formulations for three estimators of the T_{MRCA} of a pair of chromosomes, two of which are the *mutation clock* and the *recombination clock* model and are denoted by $\mathcal{T}_{\mathcal{M}}$ and $\mathcal{T}_{\mathcal{R}}$, respectively. The third estimator combines both the number of mutations and the genetic length of the segment; referred to as the *combined clock* model, denoted by $\mathcal{T}_{\mathcal{MR}}$.

5.2.1 Coalescent time estimators

The presented age estimation method is based on the computation of the posterior probability of the T_{MRCA} of a pair of haplotypes. It is assumed that no recombination has occurred along the sequence in the haplotype segment considered, such that the genealogical relationship between the two haplotypes does not change along the region. This facilitates the analysis under a coalescent process, where the posterior probability is proportional to the prior probability of the time to coalescence multiplied by the likelihood of the time given the estimator. The derivation of the coalescent prior follows from the results given in Section 1.3.2 (page 16), but is briefly reiterated below.

Let t be the number of discrete generations that separate two haplotypes in relation to the MRCA. As shown by Tajima (1983), the probability that two haplotypes are derived from one common ancestral haplotype t generations in the past is

$$f(t) \approx \frac{1}{2N_e} \mathrm{e}^{-\frac{t}{2N_e}} \quad \text{CORRECTED}$$

where N_e is the effective population size. The expression above relates to the probability distribution of the branch length in the underlying genealogical tree. Further, the probability that the two haplotypes do not share an ancestral haplotype more recently than t generations in the past is given by

$$P(T_c > t \mid N_e) \approx \mathrm{e}^{-\frac{t}{2N_e}} \quad \text{CORRECTED}$$

where T_c is the time of the coalescent event between two lineages. It is convenient to use a continuous time approximation and measure time in units of $2N_e$ generations, in the context of the coalescent, such that $\tau = t/2N_e$ Thus, the coalescent prior can be expressed as

$$\pi(\tau) \propto \mathrm{e}^{-\tau} \quad \text{CORRECTED}$$

which was already given in Equation (1.11) (page 19).

The sections below describe each clock model in detail. Recall that the *breakpoints* of past recombination events are inferred for a pair of individuals, independently on the left and right-hand side of a target variant. Under this *variant-centric* approach, a given IBD segment is composed of two intervals, each delimited by the focal site and one distal breakpoint, where at least one recombination event was inferred to have occurred within each interval. If no evidence of recombination was found on either the left or the right-hand side, a *boundary case* is recorded where the chromosomal end position is taken as a breakpoint to delimit the length of the interval.

5.2.1.1 Mutation clock model ($\mathcal{I}_{\mathcal{M}}$)

Let the physical length of a given haplotype region be denoted by D, measured in basepairs. The number of mutational differences observed along the sequence in the pair of haplotypes is denoted by S. The value of S refers to the number of segregating sites in a sample of $N = 2$ haplotypes, for which the infinite sites model is assumed without recombination; *e.g.* see Watterson (1975) and Tavaré *et al.* (1997). Mutations

are assumed to occur only once at each site in the history of the sample (Kimura, 1969), such that S reflects the total number of mutation events that have occurred along both lineages since the split from the MRCA.

Given the time of the MRCA, mutation events are Poisson distributed, as each mutation represents an independent Bernoulli trial over a large number of sites, where each site has a small probability of mutation. The mutation rate per site per generation is given by μ. In the coalescent, the mutation rate is scaled by population size, which is expressed by the composite mutation parameter $\theta = 4N_e\mu$. It follows that $\theta \times D$ is equal to the expected number of pairwise differences per coalescent time unit over the length of the segment. Thus, the probability of observing a discrete number S over distance D and time τ is modelled as a Poisson process, such that $S \sim \text{Pois}(\theta D\tau)$, for which the probability mass function (PMF) is defined as

$$P(S \mid \theta, D, \tau) = \frac{(\theta D\tau)^S}{S!} \mathrm{e}^{-\theta D\tau} \tag{5.1}$$

for $S = 0, 1, 2, \ldots$ and $\theta, D, \tau > 0$. Note that the equation above is the *joint* probability of observing mutational differences at each site along the sequence. The likelihood function for the time parameter τ is proportional to the joint PMF, but requires only those terms that involve τ and where constant terms can be dropped, such that

$$\mathcal{L}(\tau \mid \theta, D, S) \propto \tau^S \mathrm{e}^{-\theta D\tau} . \tag{5.2}$$

The posterior probability of the time to coalescence can now be written as

$$\begin{aligned} p(\tau \mid \theta, D, S) &\propto \pi(\tau) \times \mathcal{L}(\tau \mid \theta, D, S) \\ &\propto \tau^S \mathrm{e}^{-\tau(\theta D+1)} \end{aligned} \tag{5.3}$$

where $\pi(\tau)$ is the coalescent prior, reflecting the assumption that the expected time to a coalescent event grows exponentially back in time.

5.2.1.2 Recombination clock model ($\mathcal{T}_\mathcal{R}$)

In reference to the position of a focal allele that is shared by descent in two chromosomes, the length of the shared haplotype is delimited by two recombination events between the two lineages that occurred on either side of the focal position. The recombination rate per site per generation is given by ρ;* again, the rate is rescaled by population size and

* Note that the literature often specifies ρ as the population-scaled recombination rate and r as the rate per site per generation.

the composite recombination parameter $\psi = 4N_e\rho$ is used. The interval on the left and right-hand side of the focal position is distinguished by defining the distance variable D_X, where $X \in \{L, R\}$. The genetic distance to the first recombination event is geometrically distributed along the sequence, but can be approximated by the exponential distribution if time is continuously measured and provided that N_e is large; *e.g.* see Hein *et al.* (2004). The probability of observing a recombination breakpoint can therefore be modelled such that $D_X \sim \text{Exp}(\psi\tau)$, for which the probability density function (PDF) is defined as

$$P(D_X \mid \psi, \tau) \;=\; 2\psi\tau \; \mathrm{e}^{-2\psi D_X \tau} \tag{5.4}$$

which is equal to the joint probability of recombination between consecutive sites along the sequence. The factor of 2 is included to consider that recombination events occur independently in the two lineages. Note that D_X may refer to the entire length of interval if recombination rate is uniform, but it is straightforward to compute a variable recombination rate over the interval (*e.g.* by using a genetic map) to derive the genetic length expressed in ψD_X.

Considering Equation (5.4), the likelihood function for τ can be written as

$$\mathcal{L}(\tau \mid \psi, D_X) \;\propto\; \tau^{\mathrm{I}_X} \; \mathrm{e}^{-2\psi D_X \tau} \tag{5.5}$$

where I_X is an indicator function of the detected breakpoint. Recall that an IBD segment may extend to the end of a chromosome if no recombination occurred on one or both sides of the focal position; *i.e.* a boundary case. The indicator function is therefore defined as

$$\mathrm{I}_X \;=\; \begin{cases} 0 & \text{if boundary case on side } X \\ 1 & \text{otherwise .} \end{cases}$$

Thus, to consider the intervals on both sides simultaneously by the length of the whole IBD segment, D, the following likelihood function is defined.

$$\mathcal{L}(\tau \mid \psi, D) \;\propto\; \tau^{\mathrm{I}_L + \mathrm{I}_R} \; \mathrm{e}^{-2\psi D \tau} \,. \tag{5.6}$$

As a result, the posterior probability of the time to coalescence under the recombination clock can be written as

$$\begin{aligned} p(\tau \mid \psi, D) \;&\propto\; \pi(\tau) \;\times\; \mathcal{L}(\tau \mid \psi, D) \\ &\propto\; \tau^{\mathrm{I}_L + \mathrm{I}_R} \, \mathrm{e}^{-\tau(2\psi D + 1)} \,. \end{aligned} \tag{5.7}$$

Note that the inference of recombination breakpoints does not require haplotype data; thus, the recombination clock model may provide a convenient solution if only genotype data is available.

5.2.1.3 Combined clock model ($\mathcal{T}_{\mathcal{MR}}$)

Given the information available for both the mutation and the recombination clocks, the posterior probability of τ is readily calculated; see below.

$$\begin{aligned} p(\tau \mid \theta, \psi, D, S) &\propto \pi(\tau) \times \mathcal{L}(\tau \mid \theta, D, S) \times \mathcal{L}(\tau \mid \psi, D) \\ &\propto \mathrm{e}^{-\tau} \times \tau^{S} \mathrm{e}^{-\theta D \tau} \times \tau^{\mathrm{I}_L + \mathrm{I}_R} \mathrm{e}^{-2\psi D \tau} \\ &\propto \tau^{S + \mathrm{I}_L + \mathrm{I}_R} \mathrm{e}^{-\tau(D(\theta + 2\psi) + 1)} \end{aligned} \tag{5.8}$$

However, it is worth to consider the following. Both clocks, $\mathcal{T}_{\mathcal{M}}$ and $\mathcal{T}_{\mathcal{R}}$, can be consolidated by their conjugate prior distributions which, for both, is the Gamma distribution. The PDF of the Gamma distribution in support of τ is

$$\frac{\beta^{\alpha}}{\Gamma(\alpha)} \tau^{\alpha - 1} \mathrm{e}^{-\beta \tau}$$

where α is the shape and β the rate parameter of the distribution. Given the variables at hand for the combined clock, and under consideration of the coalescent prior, the parameters can be defined as $\alpha = 1 + S + \mathrm{I}_L + \mathrm{I}_R$ and $\beta = D(\theta + 2\psi) + 1$. Note that because α is an integer, the Erlang distribution can be used instead of the Gamma distribution, *e.g.* to facilitate faster computation;

$$\begin{aligned} P(S, L \mid \theta, \psi, \tau) &= P(S \mid \theta, D, \tau) \times P(D \mid \psi, \tau) \\ &= \frac{(D(\theta + 2\psi) + 1)^{1 + S + \mathrm{I}_L + \mathrm{I}_R}}{(S + \mathrm{I}_L + \mathrm{I}_R)!} \tau^{S + \mathrm{I}_L + \mathrm{I}_R} \mathrm{e}^{-\tau(D(\theta + 2\psi) + 1)} \end{aligned} \tag{5.9}$$

for which the likelihood function for τ is identical to Equation (5.8). Note that a similar derivation has been used by Schroff (2016).

5.2.2 Cumulative coalescent function

Each clock model described above computes the posterior probability for two lineages to have coalesced at a particular point in time. This is extended such that the posterior distribution of coalescent times is calculated over a continuous time prior such that the $\mathrm{T}_{\mathrm{MRCA}}$ can be derived from the cumulative distribution function (CDF). Here, this approach is referred to as the cumulative coalescent function (CCF) which is defined as

$$\Lambda_{ij}(t \mid \cdot) = \int_0^t p(\tau \mid \cdot)\, d\tau \tag{5.10}$$

where t denotes the coalescent time prior and i, j denote the two haplotypes under consideration. The parameterisation of the clock model used is indicated by "$\cdot$". In practise, the posterior probability $p(\tau \mid \cdot)$ is calculated from the Gamma (Erlang) distribution in each clock model, due to the conjugate relation described in the previous section.

5.2.3 Composite likelihood estimation of mutation time

Consider a sample of haplotypes and an allele shared by some of the haplotypes. The time at which this allele was created by a mutation event is bound by the times of the two coalescent events that delimit the length of the branch on which the mutation occurred in the underlying coalescent tree; see the example provided in Figure 5.1. The haplotypes which co-inherited the allele (*sharers*) are distinguished from the other haplotypes which do not carry the allele (*non-sharers*). Thus, the sample is divided into two disjoint subsamples; let X_c denote the set of chromosomes which share a given allele and X_d the set of chromosomes which do not share that allele. Importantly, all lineages in the X_c subsample coalesce before any of them can coalesce with a lineage in the X_d subsample.

It follows that any coalescent event between two lineages in X_c must have occurred *earlier* that the focal mutation event (back in time). On the other hand, any coalescent event between one lineage in X_c and one lineage in X_d must have occurred *later* than the focal mutation event. In the following, pairs of haplotypes in X_c are referred to as *concordant* pairs and pairs from X_c and X_d as *discordant* pairs. The sets Ω_c and Ω_d are defined to contain all concordant and discordant pairs, respectively.

The time of a focal mutation event is found at the "sweet spot" in between the earlier coalescent event at time t_c and the later coalescent event at time t_d. The CCF is computed for concordant pairs in Ω_c to infer the $\mathrm{T_{MRCA}}$ of the X_c subsample, such that the oldest MRCA indicates the lower bound in the estimation of the focal allele age. The upper bound is found by computing the CCF for discordant pairs in Ω_d, where the youngest MRCA is closest in time to the focal mutation event. The information provided from these pairwise CCF analyses are used in the calculation of the composite likelihood, which is defined below.

$$\Phi(\tau) \;\propto\; \prod_{i,j \in \Omega_c} \Lambda_{ij}(\tau \mid \cdot) \times \prod_{i,j \in \Omega_d} \Big(1 - \Lambda_{ij}(\tau \mid \cdot)\Big) \tag{5.11}$$

The lower and upper bounds on the estimated age are provided by the incomplete gamma functions

$$P_{i,j}(\tau > t) \;=\; \int_0^{\tau} \Phi(t \mid i, j)\, dt \tag{5.12}$$

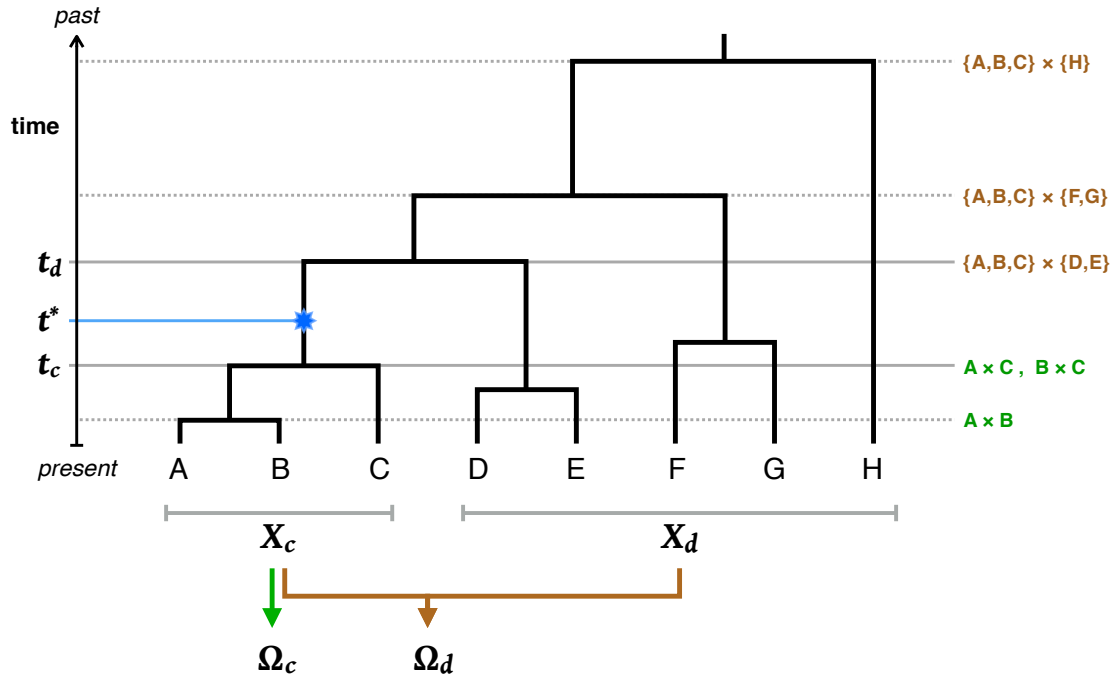

Figure 5.1: Allele age in relation to concordant and discordant pairs. The genealogy of a sample of eight haplotypes is shown of which A, B, and C share a focal allele that derived from a mutation event as indicated in the tree (*star*). These chromosomes constitute the set of *sharers*, denoted by X_c, which are differentiated from the set of *non-sharers*, denoted by X_d. Horizontal lines indicate the time of each coalescent event in the history of the sample within the local genealogy. The time of the focal mutation event is denoted by t^*; the two coalescent events at time t_c and t_d define the length of the branch on which the focal mutation event occurred. In particular, t_c and t_d correspond to the time until all haplotypes in X_c have coalesced and the time at which the derived lineage joins the ancestral lineage of the most closely related haplotype in X_d, respectively.

and

$$P_{i,j}(\tau < t) \;=\; \int_{\tau}^{\infty} \Phi(t \mid i, j)\, dt\,. \tag{5.13}$$

The composite likelihood estimate of the time is scaled in units of $2N_e$. The mean, median, and mode of the posterior distribution were taken as age estimates. In the following, the estimated age is reported using the median, which is denoted by $\hat{t}$ and expressed in units of generations. The example shown in Figure 5.2 (next page) illustrates the output produced for a single focal variant.

5.2.3.1 Reduction of the computational burden

A major caveat to the estimation of allele age is the computationally demanding analysis of each haplotype pair in Ω_c and Ω_d per target site. The numbers of concordant and discordant pairs are denoted by n_c and n_d, respectively, and the overall number of pairwise

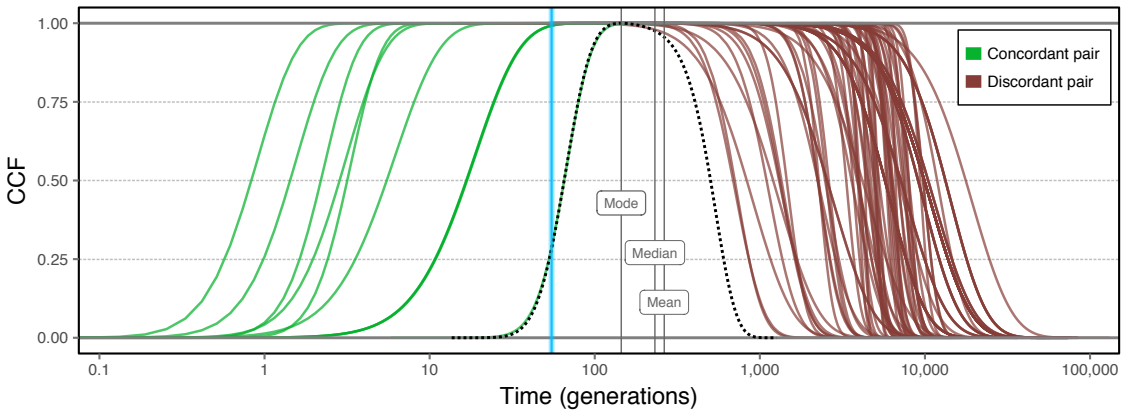

Figure 5.2: Example of the age estimation result for a focal variant. A target variant was randomly selected from simulated data. Each of the possible concordant pairs was formed and analysed using the CCF. A subset of $n_d = 100$ discordant pairs was randomly selected and analysed using the CCF. Vertical lines indicate the mode, median, and mean of the composite likelihood distribution. The *blue* line marks the true age of the mutation, as determined from simulation records.

analyses varies dependent on the observed frequency of the focal allele and the sample size. For a given f_k variant, the number of possible concordant pairs is

$$\max[n_c] = \binom{k}{2} = \frac{k(k-1)}{2} \tag{5.14}$$

where k is the number of allele copies observed in the sample; *i.e.* the size of X_c. The number of possible discordant pairs is given by

$$\max[n_d] = k(2N-k) \tag{5.15}$$

where N refers to the diploid sample size. The total number of pairwise analyses conducted per target site is the sum of n_c and n_d. However, the estimation process for a single focal allele quickly becomes intractable if the allele is observed at higher frequencies or if sample size is large, which is particularly problematic if many target sites are considered. For example, if $N = 1{,}000$, each f_2 variant has $n_c = 2$ and $n_d = 3{,}996$, whereas each f_{20} variant already has $n_c = 190$ and $n_d = 19{,}600$.

To make the age estimation analysis computationally tractable, a sampling regime was employed which randomly pairs individual chromosomes drawn from X_c and X_d until a nominal threshold of unique pairs in Ω_c and Ω_d is reached. Note that the `rvage` algorithm in its current implementation includes all possible concordant pairs in Ω_c, because $\max[n_c]$ is assumed to be reasonably small if the focal allele frequency is low, even in larger samples of thousands of individuals. Hence, the method specifies a sampling threshold as the upper limit of n_d.

5.2.4 Inference of IBD around shared and unshared alleles

The age estimation method relies on the inference of the underlying IBD structure of the sample. In particular, IBD around a given target position is detected in each pair in Ω_c and Ω_d in order to obtain the parameter values required by the clock model used. This is accomplished through the targeted IBD detection methodology incorporated from the `tidy` algorithm; namely the FGT, DGT, and the HMM, which detect IBD in pairs of diploid individuals. However, these methods were originally designed to detect IBD segments in individuals sharing a focal allele. While this condition is fulfilled when considering concordant pairs, the IBD detection in discordant pairs is problematic as these are defined by not sharing the focal allele.

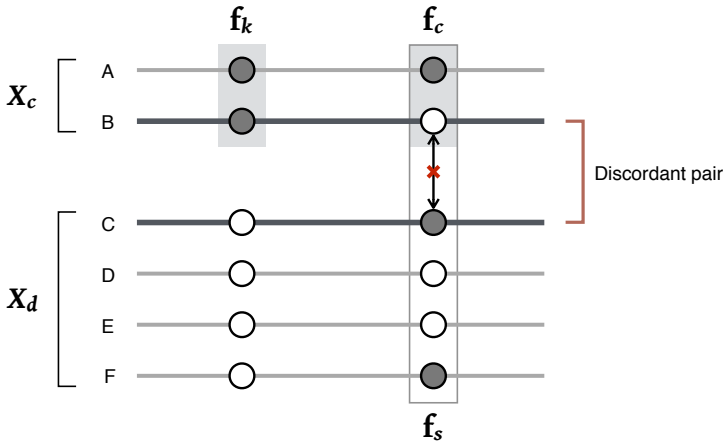

Figure 5.3: Breakpoint detection in discordant pairs. A discordant pair is formed by one haplotype from X_c (which share the focal allele) and one haplotype from X_d (which do not share the focal allele). The lines indicate the chromosomal sequence where the alleles at two sites are indicated; allelic states are distinguished as the ancestral (*hollow* circle) and derived state (*solid*). The conditions that lead to the detection of a recombination breakpoint is indicated between the focal site (*left*) and another, distal site (*right*), where f_k denotes the number of allele copies at the focal site within the subsample X_c, f_c denotes the number of allele copies observed at the distal site within the subsample X_c, and f_s denotes the number of allele copies at the distal site within the whole sample. The FGT is passed if all four allelic configurations are observed at four haplotypes in the sample.

Recall that the FGT is applied to the four haplotypes observed in two diploid individuals. A recombination event is inferred to have occurred between two variant sites if all four possible allelic configurations are observed. Let the focal site be denoted by b_i and another, distal site by b_j. In the four haplotypes, the alleles observed at (b_i, b_j) confirm a breakpoint if, for example, $(0, 0)$, $(1, 0)$, $(0, 1)$, and $(1, 1)$ are observed, where 0 denotes the ancestral allelic state and 1 the derived state. Since breakpoints are inferred

on both sides of a given focal variant, the genotypes at the focal site are both heterozygous in concordant pairs. But because the two individuals considered in a discordant pair do not share the focal allele, the required configuration cannot be observed.

To maintain the variant-centric concept, breakpoints are detected in discordant pairs as follows. Let f_k denote the number of allele copies at the focal site b_i. At a distal site, b_j, let f_c denote the number of allele copies observed only within the subsample X_c, and f_s the number of allele copies in the whole sample. A recombination breakpoint is indicated at b_j if the two haplotypes carry different alleles and if $f_c < f_k$ and $f_c < f_s$; additionally $f_s > 1$ to exclude singletons and $(f_s - f_c) > (2N - f_k)$ to exclude sites that are monomorphic within X_d, where $2N$ refers to the number of haplotypes in the sample. The condition implies the existence of the four allelic configurations at any of the haplotypes in the sample but is not bound by haplotype occurrence in two diploid individuals. The FGT thereby still holds but is practically inverted. An example is illustrated in Figure 5.3 (page 185).

Note that both the DGT and the HMM-based approach may operate on genotype data alone. Importantly, if haplotype information is not available, the sets X_c and X_d are formed by assigning all individuals that are heterozygous to X_c while all others are assigned to X_d, but excluding individuals that are homozygous for the focal allele. This may reduce the information available from the sample, but the effect is expected to be negligible, in particular if the focal allele is rare. Since haplotype data are required to determine pairwise differences, S, along haplotype sequences, $\mathcal{T}_{\mathcal{M}}$ and $\mathcal{T}_{\mathcal{MR}}$ cannot be used with genotype data.

Recall that the DGT is a special case of the FGT which detects breakpoints at genotypic configurations that would also pass the FGT if haplotypes were available. Given the two heterozygous genotypes at the focal variant, a breakpoint is found at a distal site if opposite homozygous genotypes are observed; for example, $(1, 0)$ and $(1, 2)$, where 0 denotes a genotype homozygous for the ancestral allele, 1 a heterozygous genotype, and 2 a genotype homozygous for the derived allele. Again, in discordant pairs, such a configuration cannot be observed. The observation of opposite homozygous genotypes nonetheless implies that the two individuals do not share a haplotype at this site and is therefore also applied for breakpoint detection in discordant pairs.

The HMM-based approach includes a probabilistic model for observing each possible genotype pair in pairs of diploid individuals in *ibd* and *non*, which are the hidden states defined in the underlying IBD model; see Chapter 4. Both the emission and initial probabilities were determined empirically, from data before and after the inclusion of realistic genotype error rates. The initial state probability corresponds to the probability

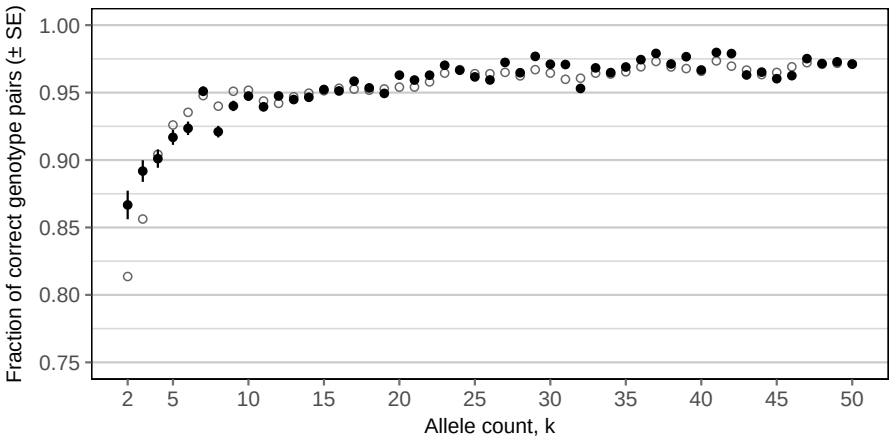

Figure 5.4: Initial state probability of discordant pairs in the Hidden Markov Model (HMM). The proportion of discordant pairs that were correctly identified by their genotypes was empirically determined from data before and after the inclusion of realistic genotype error rates. The mean per f_k was used as the initial state probability of the HMM-based approach for IBD detection around target sites. For comparison, the initial state probability of concordant pairs is shown (*hollow* circles).

of correctly observing a concordant pair by allele sharing, *i.e.* the true positive rate of observing heterozygous genotypes at a given target site where both individuals share the focal allele, which was determined per focal allele frequency (f_k). To extend the model to consider discordant pairs, here, initial state probabilities were estimated as the true positive rate of observing the focal allele as a heterozygous genotype in the X_c individual and not observing the focal allele in a homozygous genotype, g_0, in the X_d individual; again, based on the comparison between genotype data before and after error (using the same dataset as available in Chapter 4). For each f_k category, I randomly selected 1,000 target sites in the dataset before error and randomly selected 1,000 discordant pairs per target site, which I then compared to the genotypes observed in the dataset after error to determine the true positive rate. The mean per f_k was taken as the empirical initial state probability. The resulting probability distribution is shown in Figure 5.4 (this page); the initial state probabilities used for discordant pairs are indicated for comparison. Notably, the discordant probability of initialisation is similar to the concordant one. A possible explanation is that this is particularly driven by the heterozygous status being false.

5.2.4.1 Anticipated limitations

Since the estimation of allele age is dependent on parameters inferred from the underlying IBD structure of the sample, the accuracy of IBD detection is expected to affect the accuracy of the estimated age.

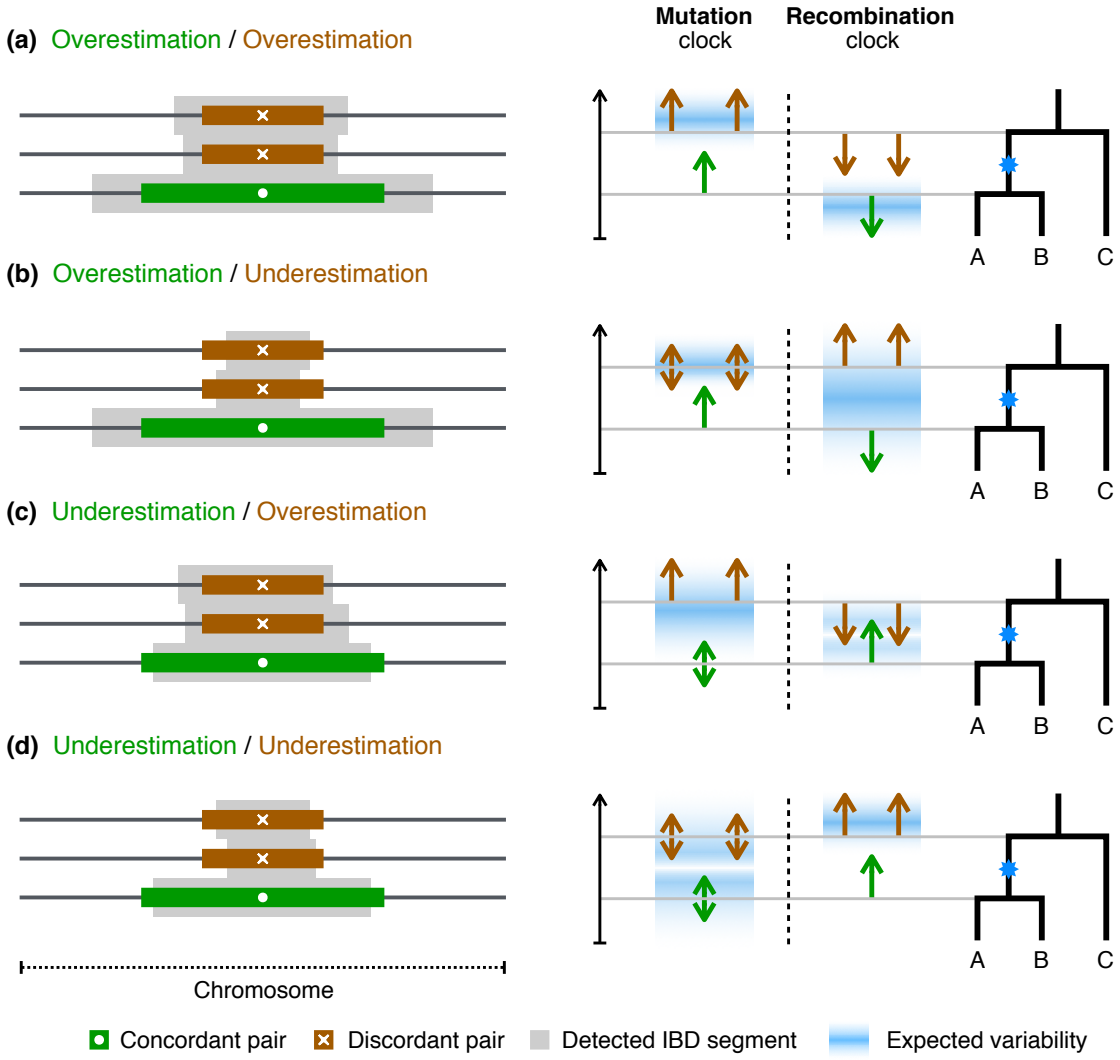

Figure 5.5: Expected estimation bias due to deficient IBD inference. A minimal example is illustrated for a sample of three chromosomes where $A, B \in X_c$ and $C \in X_d$. The focal mutation event is indicated in the genealogy of the sample (*star*). Each pair shares some haplotype region identical by decent, where the actual extent of the underlying IBD segment is shown for the concordant pair $\{A, B\}$ and the discordant pairs $\{A, C\}$ and $\{B, C\}$; indicated by *green* and *brown* bars, respectively. The allele shared in concordant pairs is indicated (*circle*), as well as the absence of allele sharing in discordant pairs (*cross*). Inferred IBD segments are shown as *grey* bars at each true IBD segment, which may overestimate or underestimate the actual shared haplotype length. Panels **(a)** to **(d)** illustrate the possible cases of over and underestimation when observed in concordant and discordant pairs. The arrows shown in relation to the times of coalescent events in the genealogy indicate the direction to which the estimation under a given clock model is expected to tend, given the respective pattern of over and underestimation in concordant and discordant pairs. The expected variability of the estimated age posterior distribution is indicated (*blue*). Note that only the mutation clock, $\mathcal{T}_{\mathcal{M}}$, and the recombination clock, $\mathcal{T}_{\mathcal{R}}$, are shown because $\mathcal{T}_{\mathcal{MR}}$ is a combination of both models.

Possible consequences of inaccurately inferred lengths of IBD segments are summarised in Figure 5.5 (page 188), which illustrates a minimal example for the different cases possible when concordant or discordant IBD length is over or underestimated. For instance, in cases where IBD is overestimated in both concordant and discordant pairs (Figure 5.5a), both the the genetic length and the number of pairwise differences, S, may be inflated, which affects the computation of the CCF under the mutation and recombination clock differently. Notably, because the pairwise probability distributions computed by the CCF in the set of pairs are multiplied to calculate the composite likelihood in Equation (5.11), it is possible that some analyses my return invalid results, as probabilities may cancel out or become too small to be distinguishable from zero given machine limits. In the following, the term *conflict* is used to refer to sites at which the analysis returned an invalid age estimate.

5.3 Evaluation

The method was assessed using data generated in coalescent simulations. First, the validity of the method under each clock model was demonstrated based on the true IBD structure of the sample as known from simulation records. Second, the analysis was repeated for each IBD detection method. Third, each approach was then assessed with regard to genotype error, which also considered the effects of phasing error.

5.3.1 Data generation

The performance of the age estimation method was evaluated using several simulated datasets. First, sample data were simulated under a simple demographic model of constant population size (N_e = 10,000) with mutation rate $\mu = 1 \times 10^{-8}$ per site per generation and constant recombination rate $\rho = 1 \times 10^{-8}$ per site per generation, using `msprime` (Kelleher *et al.*, 2016). Note that by setting the mutation and recombination rates to constant and equal values, the physical and genetic lengths are identical when measured in Megabase (Mb) and centiMorgan (cM), respectively. The size of the simulated dataset was 2,000 haplotypes, which were randomly paired to form a sample of N = 1,000 diploid individuals. The length of the simulated region was 100 Mb (100 cM), resulting in 326,335 variant sites. This dataset is denoted by $\mathcal{D}_A$.

Second, the dataset simulated in Chapter 3 was included here to evaluate the age estimation method in presence of genotype error. Briefly, the simulation was performed under a demographic model that recapitulates the human expansion out of Africa;

following Gutenkunst *et al.* (2009). A sample of 5,000 haplotypes was simulated with N_e = 7,300, a mutation rate of $\mu = 2.35 \times 10^{-8}$ per site per generation, and variable recombination rates taken from human chromosome 20; Build 37 of the International HapMap Project (HapMap) Phase II (International HapMap Consortium *et al.*, 2007; International HapMap 3 Consortium *et al.*, 2010), yielding 0.673 million segregating sites over a chromosomal length of 62.949 Mb (108.267 cM). The simulated haplotypes were randomly paired to form a sample of N = 2,500 diploid individuals. Haplotype data were converted into genotypes and subsequently phased using `SHAPEIT2` (Delaneau *et al.*, 2008, 2013). Here, this permitted the assessment of the impact of phasing error on the age estimation process.

Third, the dataset described above was retrofitted in Chapter 4 to include realistic proportions of empirically estimated error, which was equally distributed in the derived genotype and haplotype datasets. Here, data *before* and *after* the inclusion of error are distinguished by referring to dataset $\mathcal{D}_B$ and dataset $\mathcal{D}_B^*$, respectively. Note that in the following the term *genotype error* is used, even in analyses that operate on haplotype data, as error proportions were estimated from misclassified genotypes (see Chapter 4).

In each dataset, simulation records were queried to determine the underlying IBD structure of each pair of individuals analysed in this work. Note that the simulated genealogy underlying $\mathcal{D}_B$ was identical to $\mathcal{D}_B^*$, such that direct comparisons were possible between results obtained before and after error. True IBD intervals were found in simulated genealogies by scanning the sequence until the MRCA of a given pair of haplotypes changed, on both sides of a given target position. Interval breakpoints were identified on basis of the observed variant sites in the sample, such that the resulting true IBD segment defined the smallest interval detectable from available data. Note that this allowed overestimation of the actual genetic length of the IBD segment, but thereby provided a realistic benchmark for comparisons with IBD detection methods; namely the FGT, DGT, and the HMM-based approach as implemented in the `rvage` algorithm.

5.3.2 Accuracy analysis

Coalescent simulators may not define the exact time point at which a mutation event occurred, because mutations are independent of the genealogical process (if simulated under neutrality) and can therefore be placed randomly along the branches of the simulated tree; *i.e.* mutation times are not specified in `msprime`, but the times of coalescent events are recorded. In simulations, the probability of placing a mutation on a particular

branch is directly proportional to its length, which itself is delimited by the time of the coalescent event below (joining the lineages that derive from that branch) and the time of the coalescent event above (joining that branch with the tree back in time). Here, the times of coalescence below and above a particular mutation event are denoted by t_c and t_d, respectively, against which the accuracy of the estimated allele age is measured.

Although the true time of a mutation event was not known from the simulations performed, an indicative value for the age of an allele was derived from the logarithmic "midpoint" (or *log-average*) between coalescent events, which is denoted by t_m and calculated as the geometric mean of t_c and t_d; see below.

$$t_m = \exp\left[\log\left[t_c\right] + \frac{1}{2}\left(\log\left[t_d\right] - \log\left[t_c\right]\right)\right] = \sqrt{t_c\, t_d} \tag{5.16}$$

Accuracy was measured using Spearman's rank correlation coefficient, r_S, which is a robust measure for the strength of the monotonic relationship between two variables; *i.e.* the inferred allele age ($\hat{t}$) and true time proxies (t_c, t_m, or t_d). Note that the squared Pearson correlation coefficient, r^2, was used in previous chapters but is less suitable here, as both the inferred and true age are expected to vary on log-scale, and the Pearson coefficient measures the linear relationship between variables.. In addition, the root mean squared logarithmic error (RMSLE) was calculated as a descriptive score for the magnitude of error (here defined on $\log_{10}$).

To better illustrate the distribution of age estimates obtained in an analysis, the *relative age* was computed, $\hat{t}_{rel}$, for each allele by normalising the time scale conditional on the time interval between the coalescent events at t_c and t_d, such that age estimates were "mapped" on the same scale relative to the branch length spanned between t_c and t_d; this was calculated as below.

$$\hat{t}_{rel} = \frac{\log\left[\frac{\hat{t}}{t_c}\right]}{\log\left[\frac{t_d}{t_c}\right]} \tag{5.17}$$

As a result, the times of coalescent events at t_c and t_d are mapped to 0 and 1, respectively. An age estimate is defined as being "correct" if $t_c \leq \hat{t} \leq t_d$, which is equal to the condition $0 \leq \hat{t}_{rel} \leq 1$, such that $\hat{t}_{rel} < 0$ indicates underestimation and $\hat{t}_{rel} > 1$ overestimation in relation to the true interval in which the mutation event could have occurred.

5.4 Results

In each dataset, 10,000 rare variants were randomly selected as target sites for estimation of allele age. These were selected at shared allele frequency $\leq 1\,\%$, *i.e.* $f_{[2,20]}$ variants, in $\mathcal{D}_A$. Identical sets of target sites were randomly selected in $\mathcal{D}_B$ and $\mathcal{D}_B^*$, at shared allele frequency $\leq 0.5\%$ ($f_{[2,25]}$ variants). Note that these were sampled from the subset of variants unaffected by genotype error, to ensure that alleles correctly identified haplotype sharing.

5.4.1 Validation of the method under different thresholds

Because an exhaustive analysis of all possible discordant pairs becomes computationally intractable, it is convenient to reduce the number of pairwise analyses that are conducted per target allele. For example, although the sample size of dataset $\mathcal{D}_A$ was modest ($N = 1{,}000$), the total number of possible pairwise analyses for the set of 10,000 selected rare variants would have been 145.725 million. For realistic applications of the method, it is therefore essential to limit the number of discordant pairs, n_d, such that Ω_d consists of a substantially smaller set of randomly formed pairs. In this section, I analyse the impact on the accuracy of estimated allele age under different nominal thresholds of n_d (listed below). Importantly, to focus on the impact resulting from different n_d thresholds, the analysis was conducted using true IBD segments as determined from simulation records. Thus, this section provides a general validation analysis of the age estimation method.

n_d	Pairwise analyses
10	0.462 million
50	0.862 million
100	1.362 million
500	5.362 million
1,000	10.366 million

Each clock model was considered separately and the same set of 10,000 target sites was analysed under each threshold. This resulted in a total of 276.133 million pairwise analyses in this section alone. None of the analyses returned conflicting results; recall that *conflicts* were defined as invalid estimates resulting from erroneous patterns of coalescent times as computed through the CCF for the set of pairs considered. Note that discordant pairs were formed randomly and therefore differed in each analysis. The results are illustrated in Figure 5.6 (next page), which shows the density of true and

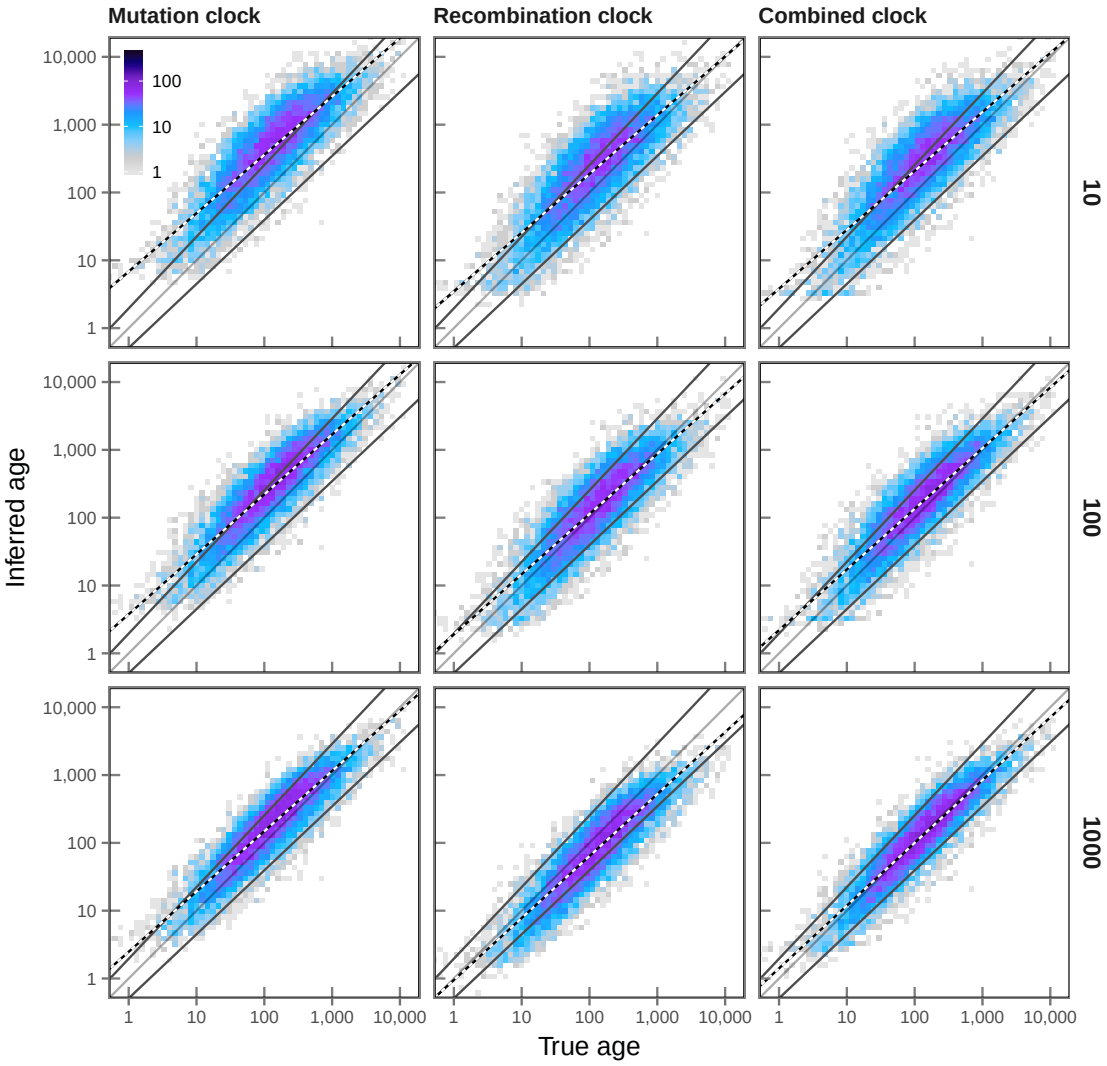

Figure 5.6: True and inferred age under varying numbers of discordant pairs. A set of 10,000 target sites was randomly drawn in $f_{[2,20]}$ (shared allele frequency ≤ 1%) in a simulated sample of 2,000 haplotypes. Different numbers of sampled discordant pairs were analysed on the same set of target variants, which is shown for $n_d = 10$, $n_d = 100$, and $n_d = 1{,}000$ (indicated at the *right* of each row). True IBD was used to estimate allele age. IBD breakpoints were determined from simulation records and defined as the first variant sites observed in the data following the two recombination events on each side of a given focal position. Age was estimated under each of the three clock models; *i.e.* mutation clock, $\mathcal{T}_{\mathcal{M}}$, recombination clock, $\mathcal{T}_{\mathcal{R}}$, and combined clock, $\mathcal{T}_{\mathcal{MR}}$ (indicated at the *top* of each column). Each panel shows the density distribution of true and inferred age (numbers indicated by the colour-gradient). The true age of a focal allele was set at t_m, which is the geometric mean of t_c and t_d, *i.e.* the true time of the coalescent event from which the focal allele derived (t_c) and the true time of the coalescent event immediately preceding that event (t_d) in the history of the sample; these are indicated by their linear regression trend lines *below* and *above* the dividing line at t_m, respectively. The *black-white* line indicates the line of best fit resulting from linear regression of age estimates, using the posterior mode of the composite likelihood distribution as the inferred age value. Note that both true and inferred age are compared on log-scale, as the time to a coalescent event is expected to increase exponentially back in time.

estimated age under each clock model; results are shown for $n_d = 10$, $n_d = 100$, and $n_d = 1{,}000$, to better distinguish differences visually. Note that true age is set at t_m, but t_c and t_d are indicated in Figure 5.6.

Despite the substantial difference in the number of pairwise analyses, overall accuracy was high for each threshold and under each clock model. A higher n_d threshold was generally found to improve overall accuracy. At lower thresholds, each model showed a tendency to overestimate allele age, which most likely resulted from the smaller set of discordant pairs, as the individuals that are more closely related to the focal haplotypes may or may not be captured.

Interestingly, the recombination clock, $\mathcal{T}_{\mathcal{R}}$, showed a tendency to underestimate allele age at higher thresholds, despite using true IBD segments. This observation may be the result of an overestimation of true IBD lengths, since IBD breakpoints were determined from the set of variant sites observed in the data, to provide a realistic benchmark for comparisons with IBD detection methods (see next section). Note that allele age is generally expected to be underestimated if genetic lengths in concordant or discordant pairs are overestimated, as a longer IBD segment is indicative for more recent haplotype sharing (*i.e.* recombination had less time the break down the length of a shared haplotype). The average distance between consecutive variant sites in $\mathcal{D}_A$ was 3.064×10^{-4} cM (306.431 basepairs), showing that even small inaccuracies in IBD can affect the estimation of allele age (under the recombination clock).

The proportion of target alleles for which age was correctly estimated increased with higher n_d thresholds under each clock model. This was lowest in $\mathcal{T}_{\mathcal{M}}$, where 36.610 %, 51.110 %, and 66.280 % were correctly inferred for n_d at 10, 100, and 1,000, respectively, and relatively high in $\mathcal{T}_{\mathcal{R}}$, where 55.790 %, 70.600 %, and 70.510 % were correct, respectively. The highest proportion of correct alleles was 79.930 % in $\mathcal{T}_{\mathcal{MR}}$ and $n_d = 1{,}000$. The proportion of overestimated alleles ($\hat{t} > t_d$) decreased in all clock models at higher n_d thresholds, showing a modest decrease in $\mathcal{T}_{\mathcal{M}}$ (63.380 % to 32.660 % for n_d at 10 and 1,000, respectively), a substantial decrease in $\mathcal{T}_{\mathcal{R}}$ (43.450 % to 6.450 %, respectively), and a notable decrease in $\mathcal{T}_{\mathcal{MR}}$ (46.780 % to 15.640 %, respectively). Since $\mathcal{T}_{\mathcal{M}}$ showed a tendency to overestimate allele age, the proportion of underestimated alleles was low (1.060 % for $n_d = 1{,}000$), which was similarly low in $\mathcal{T}_{\mathcal{MR}}$ (4.430 %), and highest in $\mathcal{T}_{\mathcal{R}}$ (23.040 %).

A complete summary of results is given in Table 5.1 (next page). Throughout, rank correlation (r_S) was highest for $n_d = 1{,}000$; see Table 5.1. However, for all thresholds, correlations with t_c were higher than correlations with t_m, which in turn were higher than

Table 5.1: Estimation accuracy under varying numbers of discordant pairs. Different thresholds for the number of randomly formed discordant pairs, n_d, were analysed to evaluate the impact on the accuracy of allele age estimation. Note that all possible concordant pairs were included in each analysis; *i.e.* n_c was not reduced. True IBD segments were used to focus on the differences induced by varying n_d thresholds. Each analysis was conducted on the same set of 10,000 randomly selected rare variants at allele frequency ≤ 1%. Accuracy was measured using the rank correlation coefficient, r_S, and the magnitude of error, RMSLE, between the estimated age, $\hat{t}$ and the the times of coalescent events; *i.e.* the time until all haplotypes in X_c have coalesced, t_c, and the time of the immediately preceding coalescent event, t_d, which joined the lineages in X_c and X_d back in time, as well as the geometric mean of both, t_m.

Clock	n_d	Rank correlation (r_S)			RMSLE		
		t_c	t_m	t_d	t_c	t_m	t_d
$\mathcal{T}_\mathcal{M}$	10	**0.907**	0.842	0.632	0.963	0.624	**0.574**
	50	**0.918**	0.872	0.674	0.823	**0.487**	0.528
	100	**0.920**	0.884	0.692	0.763	**0.431**	0.521
	500	**0.920**	0.907	0.731	0.626	**0.308**	0.533
	1,000	**0.923**	0.904	0.723	0.606	**0.299**	0.547
$\mathcal{T}_\mathcal{R}$	10	**0.881**	0.816	0.612	0.714	**0.443**	0.609
	50	**0.889**	0.844	0.651	0.578	**0.349**	0.633
	100	**0.892**	0.857	0.671	0.519	**0.319**	0.653
	500	**0.892**	0.886	0.720	0.390	**0.304**	0.728
	1,000	0.889	**0.895**	0.739	0.345	**0.329**	0.772
$\mathcal{T}_{\mathcal{MR}}$	10	**0.891**	0.829	0.624	0.745	**0.455**	0.589
	50	**0.901**	0.865	0.675	0.624	**0.348**	0.586
	100	**0.905**	0.881	0.699	0.574	**0.309**	0.593
	500	0.909	**0.914**	0.753	0.469	**0.243**	0.626
	1,000	0.911	**0.914**	0.751	0.464	**0.243**	0.629

correlations with t_d. Such a pattern may be expected as the number of concordant pairs, n_c, was not reduced, such that the t_c was inferred with higher accuracy. Highest accuracy was seen for the mutation clock model, $\mathcal{T}_\mathcal{M}$, where r_S for n_d = 1,000 was 0.923, 0.904, and 0.723 for t_c, t_m, and t_d, respectively. By comparison, the recombination clock, $\mathcal{T}_\mathcal{R}$, yielded the lowest levels of overall accuracy at each threshold, but did not differ markedly from $\mathcal{T}_\mathcal{M}$; *e.g.* r_S for n_d = 1,000 was 0.889, 0.895, and 0.739 for t_c, t_m, and t_d, respectively. The combined clock, $\mathcal{T}_{\mathcal{MR}}$, was found to be more accurate for t_m and t_d at higher thresholds. The magnitude of error, measured by RMSLE scores, was lowest for t_m, indicating that the majority of alleles were correctly dated between t_c and t_d; except in $\mathcal{T}_\mathcal{M}$ for n_d = 10, in which allele age was overestimated and therefore closer to t_d.

The difference between n_d = 500 and n_d = 1,000 was small overall (see Table 5.1), suggesting that further improvements in accuracy may not be attained by increasing the threshold.

A comparison of the inferred age distributions at distinct f_k ranges is presented in Figure 5.7 (next page), again shown for n_d = 10, n_d = 100, and n_d = 1,000. Notably, the accuracy of target alleles at lower frequencies was overall higher compared to alleles

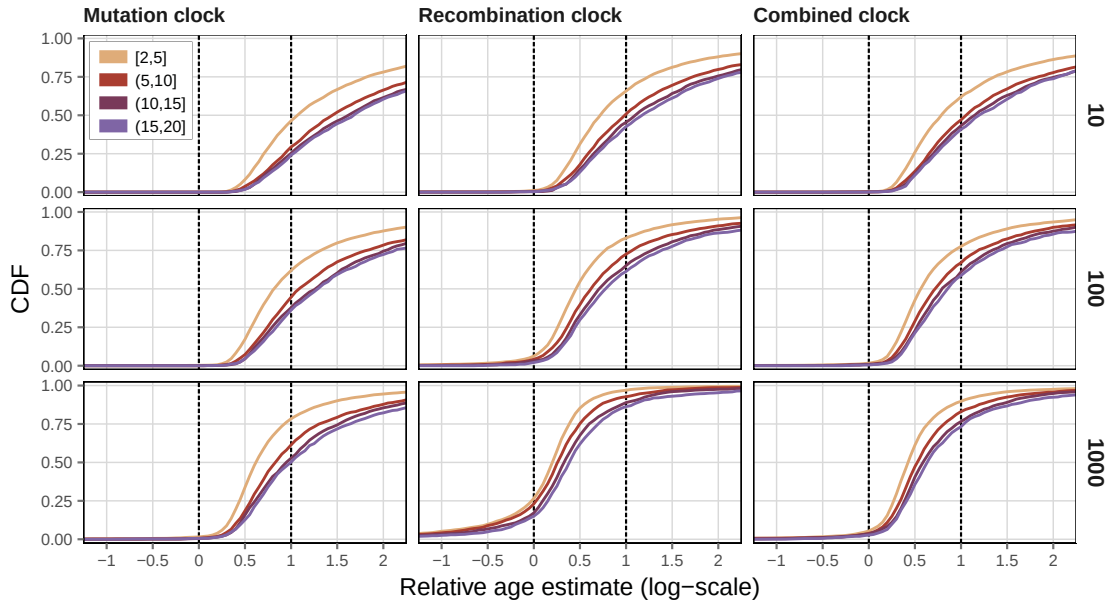

Figure 5.7: Relative age under varying numbers of discordant pairs. A randomly drawn set of 10,000 target sites at allele frequency ≤ 1%, *i.e.* $f_{[2,20]}$, was analysed under each of the three clock models (indicated at the *top* of each column) and with different numbers of sampled discordant pairs; $n_d = 10$, $n_d = 100$, and $n_d = 1{,}000$ (indicated at the *right* of each row). The analysis was conducted using the true IBD breakpoints as derived from simulation records, defined as the first variant sites observed in the data that immediately follow the two recombination events on each side distal to a given focal site. The relative age, $\hat{t}_{rel}$, was calculated as given in Equation (5.17), such that the true times of concordant and discordant coalescent events, t_c and t_d, sit at 0 and 1, respectively (*dashed* lines). Note that $\hat{t}_{rel}$ is defined on log-scale. The CDF of relative age estimates is shown per f_k group, where target variants were pooled by their allele count in the data, in ranges of $f_{[2,5]}$, $f_{(5,10]}$, $f_{(10,15]}$, and $f_{(15,20]}$.

observed at higher frequencies. This difference was consistent across n_d thresholds under the mutation clock model, $\mathcal{T}_{\mathcal{M}}$. For example, at $n_d = 10$, the proportion of correctly dated alleles was higher in the $f_{[2,5]}$ range (48.356 %) compared to alleles at $f_{(5,10]}$ (29.445 %). At $n_d = 1{,}000$, overall accuracy was increased but the difference for alleles at lower and higher frequencies remained; *i.e.* 77.819 % and 60.834 % at $f_{[2,5]}$ and $f_{(5,10]}$, respectively. Under the recombination clock model, $\mathcal{T}_{\mathcal{R}}$, these differences were reduced at higher n_d thresholds. At $n_d = 10$, 66.608 % and 50.344 % of alleles were correctly dated at $f_{[2,5]}$ and $f_{(5,10]}$, respectively, whereas at $n_d = 1{,}000$ these proportions were 72.258 % and 69.826 % at the same frequency ranges, respectively.

In summary, these results demonstrate that the method as well as the clock models proposed are able to estimate allele age from IBD information alone, without prior knowledge of the demographic history of the sample. However, because data were simulated under a simple demographic model (dataset $\mathcal{D}_A$), further evaluation is appropriate (*e.g.* using datasets $\mathcal{D}_B$ and $\mathcal{D}_B^*$; see further below). The analysis considered

true IBD segments and therefore evaded the effects that would result from inexact IBD detection. Since true IBD was determined conditional on the observed variation in the data, the analysis reflected the practical feasibility of age estimation given available data.

The implemented sampling process seeks to find a compromise between computational tractability and the chance of randomly selecting haplotypes that are informative for the estimation. However, ideally, to minimise the computational burden while simultaneously improving estimation accuracy, it would be desirable to consider the nearest neighbours to the focal shared haplotypes in the local genealogy. If the nearest neighbours are found among the haplotypes in X_d and paired with the focal haplotypes in X_c they are likely to coalesce at t_d and are therefore most informative for the estimation of focal allele age. For instance, a simple approach would be to compute the Hamming distance between haplotypes in X_c and X_d within a short region around the position of a given target site, such that a subset of presumed nearest neighbours can be selected based on a distance ranking. In practice, however, there are three caveats to such an approach.

First, it would be computationally expensive to conduct an additional pairwise analysis for the (whole) sample at each target site, which may not outweigh the improvement gained through the reduction of n_d. Second, the identification of nearest neighbours may be less accurate if only genotype data are available. Both the DGT and the HMM-based approach implemented in `rvage` are able to infer IBD in absence of haplotype information; thus, a method to identify nearest neighbours in genotype data would be required to achieve full compatibility with the algorithm. Regardless, third, a dilemma arises in presence of genotype error, as the identification of nearest neighbours is likely to give preference to haplotypes in which the focal allele has been missed. Such *false negatives* distort the estimation of allele age as the CCF computed for false discordant pairs would bias (or cancel out) the resulting composite likelihood distribution. In such cases, the estimated age is expected to be approximately equal to or smaller than t_c, such that $\hat{t}$ is likely to be underestimated.

It is important to note that the problem of finding false negatives in the data (if genotype error is present) cannot be avoided if discordant pairs are formed by a random sampling process, but the chance of including false negatives is reduced if n_d is small in comparison to the (haploid) sample size. Hence, the n_d threshold defines a balance between accuracy and expected bias. Subsequent analyses were conducted using a threshold equal to the diploid sample size, N; that is $n_d = 1{,}000$ in analyses using $\mathcal{D}_A$, and $n_d = 2{,}500$ using $\mathcal{D}_B$ or $\mathcal{D}_B^*$. Since the results presented in this section were obtained on true IBD information, they serve as a benchmark against which different IBD detection methods are compared in the section below.

5.4.2 Comparison of IBD detection methods

The `tidy` algorithm for targeted IBD detection (see Chapters 3 and 4) was fully integrated in `rvage`, such that the FGT, DGT, and the HMM-based approach were available for the inference of IBD segments around focal variants. Note that genotype data are sufficient for IBD detection using the DGT and HMM, but haplotypes are required for estimation under the mutation clock model; *i.e.* to count pairwise differences, S, along haplotype sequences. Thus, analyses were conducted on the simulated haplotype dataset ($\mathcal{D}_A$), but haplotype phase was ignored during IBD detection in the DGT and HMM. The parameters required by the `rvage` algorithm were specified accordingly with simulation parameters ($N_e = 10{,}000$; $\mu = 1 \times 10^{-8}$ per site per generation; $\rho = 1 \times 10^{-8}$ per site per generation). Here, because simulated data did not include genotype error, theoretical emission model was used in the HMM.

The results presented in this section were obtained on the previously selected 10,000 rare allele target sites, which were analysed using each of the three IBD detection methods and under each clock model, resulting in a total of 93.295 million pairwise analyses. The fraction of conflicting age estimates differed by clock model as well as IBD detection method; no conflicting estimates were returned when true IBD was used. Under the mutation clock, $\mathcal{T}_{\mathcal{M}}$, analyses using the FGT returned 1.809 % conflicts. This fraction was higher using the DGT and HMM, with 2.601 % and 2.327 %, respectively. Conflicts were seen less under the recombination clock, $\mathcal{T}_{\mathcal{R}}$, where none were returned using the FGT, but 0.010 % and 0.030 % using the DGT and HMM. The fraction under the combined clock, $\mathcal{T}_{\mathcal{MR}}$, was smaller compared to $\mathcal{T}_{\mathcal{M}}$, with 1.097 %, 2.266 %, and 1.819 % of conflicted sites using the FGT, DGT, and HMM, respectively. The remaining sites were intersected to compare clock models and IBD methods on the same set of target sites, retaining 9,434 variants.

The density distribution of true and inferred allele age is given in Figure 5.8 (next page). In all three methods, a tendency to overestimate allele age was seen, in particular under the mutation clock, $\mathcal{T}_{\mathcal{M}}$. This overestimation was elevated when the DGT was used, and less prominent for the FGT or HMM. The latter methods showed similar age distributions in $\mathcal{T}_{\mathcal{M}}$ and under the combined clock model, $\mathcal{T}_{\mathcal{MR}}$, in which alleles appeared to be less overestimated. Under the recombination clock, $\mathcal{T}_{\mathcal{R}}$, alleles were underestimated in each method, but more severely in both the DGT and HMM.

Specifically, the method with the highest proportion of correctly estimated alleles was the FGT in all three clock models, where accuracy was highest under the recombination clock, $\mathcal{T}_{\mathcal{R}}$, at 72.610 %, and lowest under the mutation clock, $\mathcal{T}_{\mathcal{M}}$, with 34.460 %; under

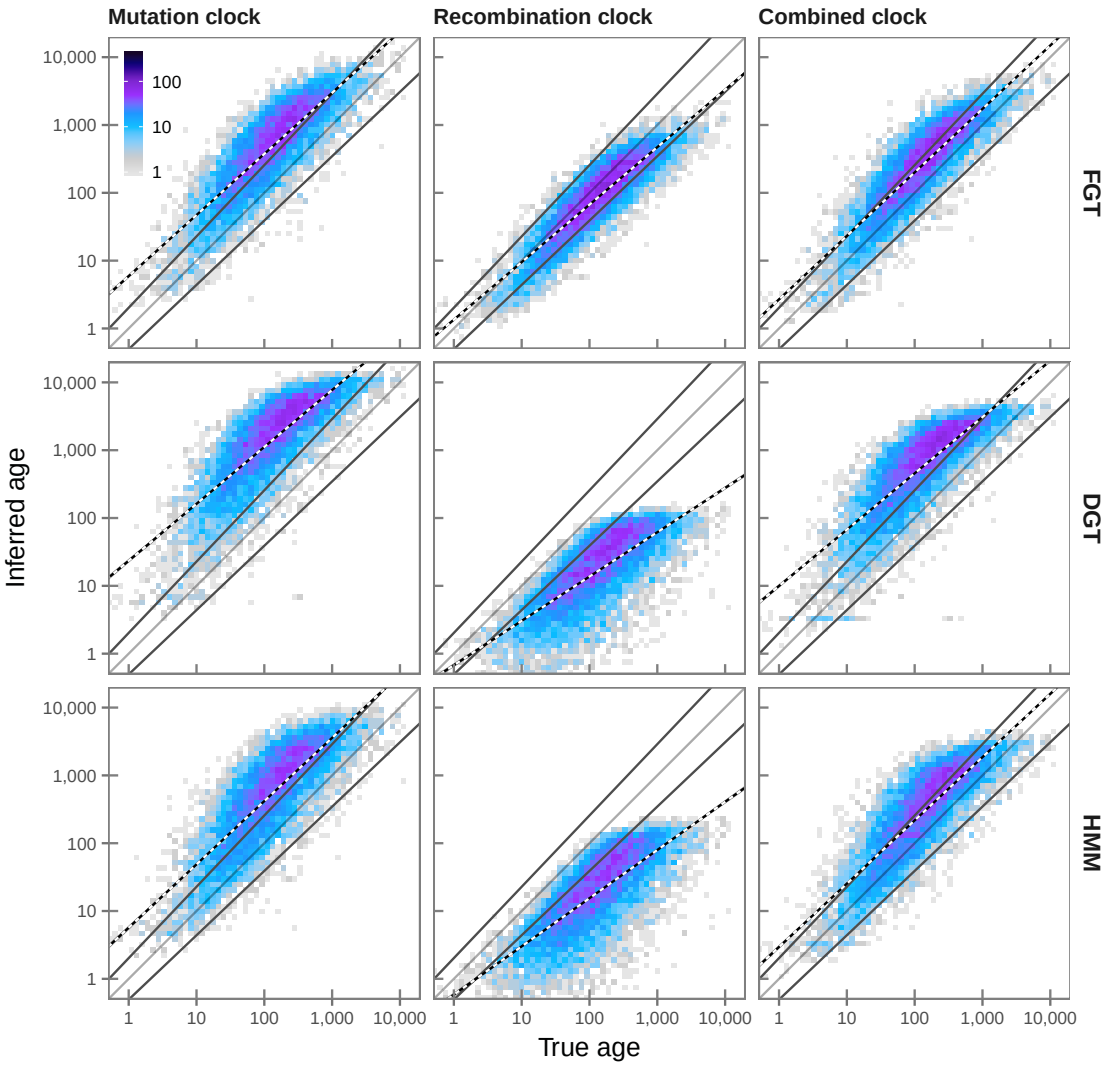

Figure 5.8: Distribution of true and inferred age using different IBD detection methods. The three IBD detection methods implemented in `rvage` were compared, *i.e.* FGT, DGT, and HMM (indicated at the *right* of each row), under each clock model (indicated at the *top* of each column). Analyses were compared on the same set of 9,434 target sites that were drawn from available $f_{[2,20]}$ variants in the simulated dataset of 2,000 haplotypes (allele frequency $\leq 1\%$). Each panel shows the density of true age (t_m) and inferred age (numbers indicated by the colour-gradient). Lines *below* and *above* the dividing line are regression trend lines of the corresponding true coalescent times around each mutation event, t_c and t_d, respectively. The regression trend line of inferred age ($\hat{t}$) is indicated by the *black-white* line, using the posterior mode of the composite likelihood estimation as the inferred age value.

the combined clock, $\mathcal{T}_{\mathcal{MR}}$, 55.395 % of alleles were correctly estimated when the FGT was used. The HMM achieved similar levels of accuracy, but the accuracy in $\mathcal{T}_{\mathcal{R}}$ was noticeably reduced (10.950 %) compared to $\mathcal{T}_{\mathcal{MR}}$ (51.876 %) and $\mathcal{T}_{\mathcal{M}}$ 32.415 %. Throughout, the lowest proportions of correctly inferred alleles were found for the DGT, which also showed the lowest accuracy in $\mathcal{T}_{\mathcal{R}}$ (8.226 %) and comparatively low levels of accuracy in $\mathcal{T}_{\mathcal{M}}$ and $\mathcal{T}_{\mathcal{MR}}$ (14.554 % and 29.659 %, respectively). Overestimation of allele age was highest in $\mathcal{T}_{\mathcal{M}}$, where 65.084 %, 85.277 %, and 66.960 % of alleles were underestimated by the FGT, DGT, and HMM, respectively. Conversely, the proportion of underestimated alleles was lowest in $\mathcal{T}_{\mathcal{M}}$, at $\leq 1\%$ in each method, and similarly low in $\mathcal{T}_{\mathcal{MR}}$ with $\leq 2\%$ in each method. In contrast, alleles were markedly underestimated in $\mathcal{T}_{\mathcal{R}}$; the FGT resulted in 20.140 % of underestimated alleles, whereas 91.753 % and 88.934 % of alleles were underestimated when the DGT and the HMM were used for IBD inference, respectively.

Table 5.2: Estimation accuracy per IBD detection method. The accuracy was measured in analyses based on IBD detected by different methods; namely the FGT, DGT, and the HMM-based approach. See Table 5.1 (page 195) for comparison to results obtained using true IBD segments (for n_d = 1,000).

Clock	Method	Rank correlation (r_S)			RMSLE		
		t_c	t_m	t_d	t_c	t_m	t_d
$\mathcal{T}_{\mathcal{M}}$	FGT	**0.841**	**0.839**	**0.686**	**1.011**	**0.653**	**0.554**
	DGT	0.830	0.813	0.650	1.460	1.086	0.832
	HMM	0.806	0.806	0.662	1.078	0.725	0.607
$\mathcal{T}_{\mathcal{R}}$	FGT	**0.899**	**0.887**	**0.718**	**0.339**	**0.330**	**0.775**
	DGT	0.820	0.749	0.554	0.577	0.941	1.396
	HMM	0.821	0.751	0.556	0.533	0.892	1.348
$\mathcal{T}_{\mathcal{MR}}$	FGT	**0.863**	**0.873**	**0.723**	**0.755**	**0.422**	**0.524**
	DGT	0.840	0.829	0.669	1.083	0.727	0.600
	HMM	0.826	0.834	0.692	0.806	0.485	0.554

The accuracy measured for each analysis is summarised in Table 5.2 (this page). The FGT under the recombination clock model, $\mathcal{T}_{\mathcal{R}}$, showed a higher correlation and slightly reduced error with regard to t_d. There, rank correlation was $r_S = 0.899$ for the FGT and $r_S = 0.889$ for true IBD; likewise the magnitude of error (RMSLE) was 0.339 and 0.345 for FGT and true IBD, respectively. However, note that a higher accuracy at t_c does not necessarily reflect an improvement in the estimation of actual allele age. For example, the accuracy with regard to t_m or t_d was lower for the FGT compared to true IBD. In comparison to the other detection methods, the FGT outperformed both the DGT and HMM with regard to each time measure. The HMM showed slightly higher levels of

accuracy than the DGT in $\mathcal{T}_{\mathcal{R}}$, where r_S was higher and RMSLE lower in terms of each time measure for the HMM. Similarly, in both $\mathcal{T}_{\mathcal{M}}$ and $\mathcal{T}_{\mathcal{MR}}$, RMSLE scores were lower for the HMM compared to the DGT, whereas r_S measures were similar.

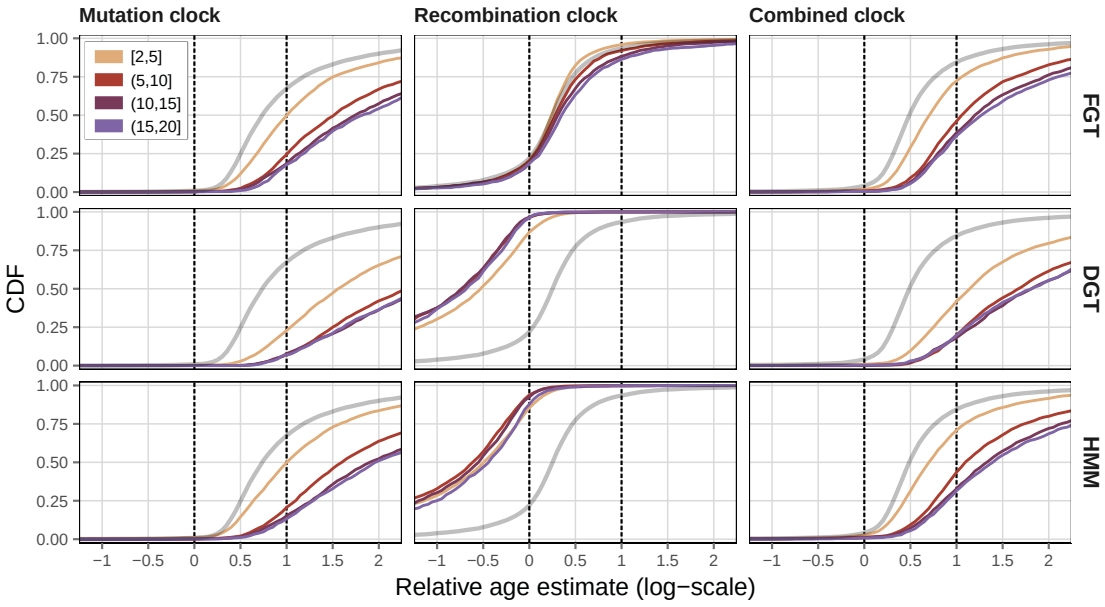

Figure 5.9: Relative age using different IBD detection methods. The three IBD detection methods implemented in `rvage` were compared, *i.e.* FGT, DGT, and HMM (indicated at the *right* of each row), under each clock model (indicated at the *top* of each column). The relative age, $\hat{t}_{rel}$, was calculated as given in Equation (5.17), such that t_c and t_d sit at 0 and 1, respectively (*dashed* lines). The CDF of relative age estimates is shown for different frequency ranges; namely $f_{[2,5]}$, $f_{(5,10]}$, $f_{(10,15]}$, and $f_{(15,20]}$.

Relative age estimates are shown for distinct f_k ranges in Figure 5.9 (this page), where the relative age of true IBD is indicated for comparison per clock model (calculated on the full f_k range). Analyses under the mutation clock and the combined clock models, $\mathcal{T}_{\mathcal{M}}$ and $\mathcal{T}_{\mathcal{MR}}$, showed a substantial difference between alleles at lower and higher frequencies; *e.g.* overall accuracy of $f_{[2,5]}$ variants was increased compared to f_k variants at higher frequencies in each method. This difference was reduced under the recombination clock model, $\mathcal{T}_{\mathcal{R}}$, but the DGT showed an accuracy decrease for $f_{[2,5]}$ variants.

The distribution of IBD lengths inferred using the FGT, DGT, and the HMM-based approach are shown in Figure 5.10 (next page). Segments inferred using the HMM were close to those detected using the FGT in concordant pairs. However, for discordant pairs, only the FGT produced IBD segments that were close to the length distribution of true IBD segments. The DGT showed the highest degree of overestimation for both concordant and discordant pairs.

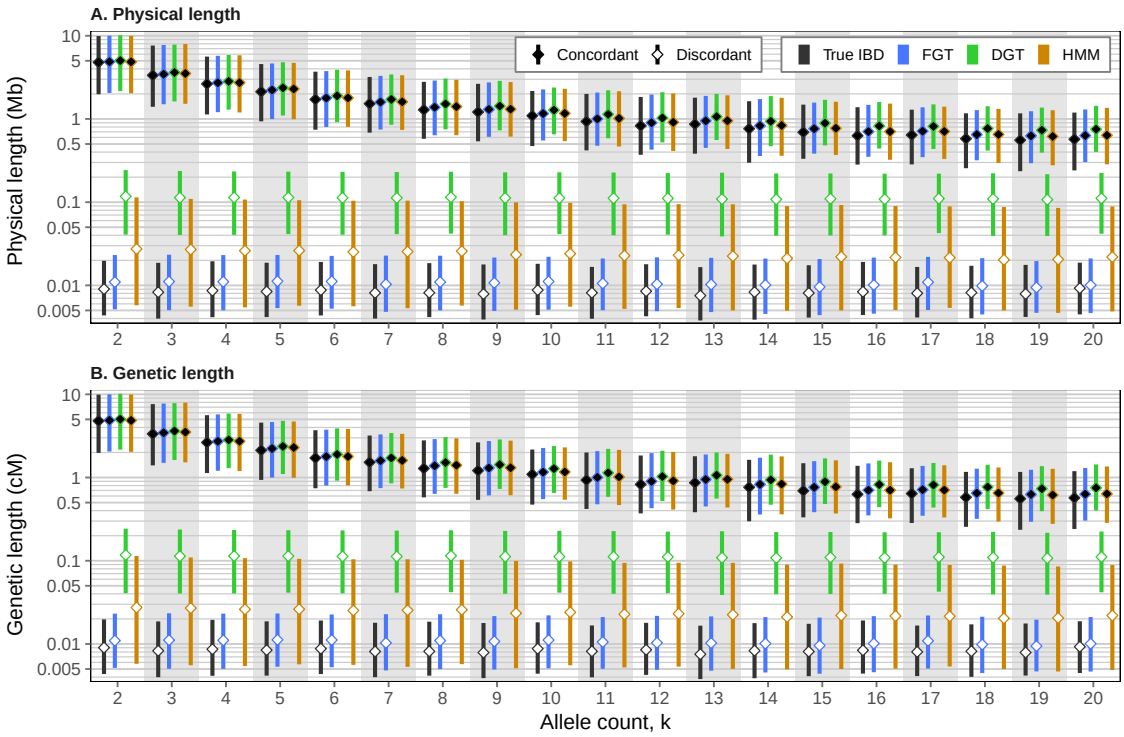

Figure 5.10: Length distribution of inferred IBD segments. Bottom and top of each bar indicate 1st and 3rd quartiles, respectively, between which the median (2nd quartile) is marked (*diamonds*). IBD detected for concordant and discordant pairs is distinguished; *solid* and *hollow* diamonds, respectively.

In summary, these results suggest that the accuracy of estimated allele age is crucially dependent on correct inference of the underlying IBD structure. The overestimation of IBD lengths, which is generally expected for each method, affected each clock model differently. While $\mathcal{T}_{\mathcal{M}}$ overall resulted in an overestimation of allele age when IBD is overestimated, this pattern was reversed in $\mathcal{T}_{\mathcal{R}}$. Although both models are combined in $\mathcal{T}_{\mathcal{MR}}$, the impact of mutational differences, seen at the overestimated regions of detected IBD segments, was substantial and could not be mitigated by considering recombinational length. Further, I confirmed that the FGT was the best performing method for the targeted detection of IBD segments, in that the estimation of allele age was similar to the expectations defined by true IBD information. However, the estimation was more accurate for target sites at lower allele frequencies. The DGT was least accurate in terms of estimated allele age in this comparison.

Recall that the probabilistic model of the HMM was developed to overcome the effects of genotype error encountered in real data (see Chapter 4). Thus, the results in this section reflect theoretical limitations of age estimation given IBD detected in flawless data, but may change drastically in presence of genotype error. This was explored in the section below.

5.4.3 Impact of genotype error on allele age estimation

The allele age estimation method was evaluated under each clock model and each method for IBD detection, on data before and after the inclusion of genotype error; *i.e.* using datasets $\mathcal{D}_B$ and $\mathcal{D}_B^*$, respectively. Each analysis was performed on the same set of 10,000 target sites selected at $f_{[2,25]}$ in a sample of $N = 2{,}500$ diploid individuals, using a threshold of $n_d = 2{,}500$, which amounted to 25.281 million pairwise analyses per comparison. The FGT was applied to both the simulated (*true*) haplotypes as well as phased haplotype data. The HMM used theoretical emission model in analyses on $\mathcal{D}_B$ and the empirical error model in analyses on $\mathcal{D}_B^*$. To enable direct comparisons, true IBD segments were determined from simulation records and separately analysed on the same number of concordant and discordant pairs in data before and after error. In total, for the results presented in this section, 758.437 million pairwise analyses were conducted.

Table 5.3: Conflicted estimates in analyses before and after error.

Method	Conflicts before error (%)			Conflicts after error (%)		
	$\mathcal{T}_{\mathcal{M}}$	$\mathcal{T}_{\mathcal{R}}$	$\mathcal{T}_{\mathcal{MR}}$	$\mathcal{T}_{\mathcal{M}}$	$\mathcal{T}_{\mathcal{R}}$	$\mathcal{T}_{\mathcal{MR}}$
FGT*	6.396	0.000	3.695	5.131	0.141	2.189
FGT**	6.587	0.422	4.388	4.940	0.341	3.123
DGT	10.945	0.161	8.384	5.211	1.767	3.956
HMM	5.884	0.392	4.418	13.335	0.823	9.268
True IBD	0.000	0.000	0.000	9.583	0.000	1.030

* FGT applied to true haplotypes
** FGT applied to phased haplotypes

As in the previous section, some of the analyses returned conflicting estimates; see Table 5.3. Again, no conflicts were seen when true IBD information was used. However, this changed after the inclusion of genotype error; the fraction of conflicting estimates was high in $\mathcal{T}_{\mathcal{M}}$, zero in $\mathcal{T}_{\mathcal{R}}$, and small in $\mathcal{T}_{\mathcal{MR}}$. Before error, the largest fraction of conflicts was seen for the DGT in $\mathcal{T}_{\mathcal{M}}$. Data from analyses before and after error were intersected across results obtained under each clock model and for each IBD method, which retained a set of 5,015 identical target sites. A complete summary of the accuracy per analysis is given below in Table 5.4 (page 213).

Estimation based on the true IBD structure of the sample is compared before and after error in Figure 5.11a (next page). The most striking discovery is the extent of overestimation after error under the mutation clock model, $\mathcal{T}_{\mathcal{M}}$, which was similarly high in the combined clock, $\mathcal{T}_{\mathcal{MR}}$. Alleles were overestimated because the presence of misclassified

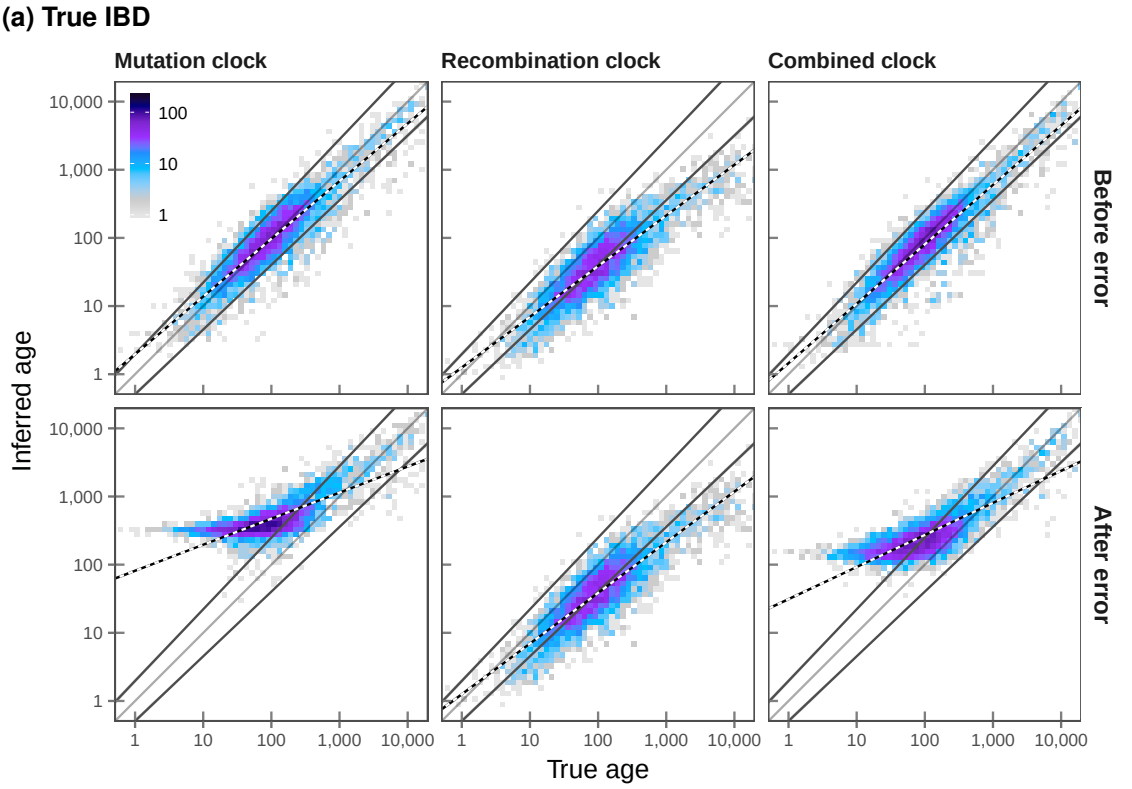

Figure 5.11: Density distribution of allele age before and after the inclusion of genotype error in simulated data. Allele age estimation was conducted on data in which empirical distributions of genotype error were simulated. The effects on the estimation process *before* and *after* error are compared (*top* and *bottom*, respectively). The dividing line is fixed at the true age (t_m), around which the lines *below* and *above* correspond to the regression trend lines of the times of coalescent events delimiting the branch on which focal mutations sit; *i.e.* t_c and t_d, respectively. The *black-white* line indicates the regression trend of the inferred age ($\hat{t}$). This panel (**a**) compares the distributions of true and inferred ages, which were estimated on basis of the true IBD structure of the sample as determined from simulation records. The other panels show estimation results based on the different IBD detection methods; FGT on both true and phased haplotypes (**b**, **c**; page 206), DGT (**d**; page 207), and the HMM-based approach (**e**; page 208). Each analysis was conducted on the same set of retained 5,015 target variants at allele frequency ≤ 0.5% in simulated data of N = 2,500 diploid individuals.

alleles substantially increased the number of observed mutational differences, S, along the sequence. For example, accuracy decreased in $\mathcal{T}_{\mathcal{M}}$ from $r_S = 0.870$ to $r_S = 0.518$ with regard to t_c, before and after error respectively, similarly in $\mathcal{T}_{\mathcal{MR}}$, where r_S at t_c decreased from 0.884 to 0.593, respectively. The proportion of correctly estimated alleles ($t_c < \hat{t} < t_d$) in $\mathcal{T}_{\mathcal{M}}$ was 75.394 % before and 24.068 % after error, which was similar in $\mathcal{T}_{\mathcal{MR}}$, where 80.518 % of alleles were correct before but only 39.402 % after error. The proportion of overestimated alleles was 18.046 % in $\mathcal{T}_{\mathcal{M}}$ and 9.212 % in $\mathcal{T}_{\mathcal{MR}}$ before error, but 74.397 % and 57.926 %, respectively, after error. Note that this did not vary noticeably by focal allele frequency; for example, the proportion of overestimated alleles in $\mathcal{T}_{\mathcal{M}}$ was

75.659 % at lower frequencies ($f_{[2,5]}$) and 79.375 % at higher frequencies ($f_{[20,25]}$), which was also the case in $\mathcal{T}_{\mathcal{MR}}$, where 61.831 % and 1.250 % of alleles were overestimated at $f_{[2,5]}$ and $f_{[20,25]}$, respectively.

In contrast, the estimation under the recombination clock model, $\mathcal{T}_{\mathcal{R}}$, was not affected by genotype error, due to using true IBD information to derive recombinational segment lengths. Note that analyses were performed on the same sets of concordant and discordant pairs, which is why the results in $\mathcal{T}_{\mathcal{R}}$ are identical before and after error. As in the previous analysis, alleles showed a tendency to be underestimated in $\mathcal{T}_{\mathcal{R}}$. The average distance between consecutive SNPs was 1.609×10^{-4} cM (93.557 basepairs) in $\mathcal{D}_B$ and $\mathcal{D}_B^*$; *i.e.* the density of variant sites is higher compared to $\mathcal{D}_A$, such that a potential bias resulting from overestimation of true IBD lengths is expected to be reduced. Overall, 42.891 % of alleles were correctly inferred, but this was higher for at $f_{[2,5]}$ and lower at $f_{[20,25]}$; 48.681 % and 39.375 %, respectively. The proportion of underestimated alleles was 55.553 %, where 50.528 % and 52.500 % were underestimated at $f_{[2,5]}$ and $f_{[20,25]}$, respectively. The correlation between inferred and true age was generally high (r_S: 0.818, 0.843, and 0.666 at t_c, t_m, and t_d, respectively) but nonetheless slightly lower compared to corresponding results from dataset $\mathcal{D}_A$ (0.889, 0.895, and 0.739, respectively); although, note that these results are not directly comparable as the underlying demographies were different and only half the number of target sites was analysed here.

When IBD was inferred, the accuracy of the estimation analysis was differently affected dependent on the IBD detection method used. Results based on the FGT are shown in Figure 5.11b and 5.11c (next page), which compare age estimates obtained on the same set of target sites based on IBD detected in true and phased haplotypes, respectively, both before and after error. Without genotype error, 53.021 %, 50.847 %, and 60.040 % of alleles were correctly inferred from true haplotype data in $\mathcal{T}_{\mathcal{M}}$, $\mathcal{T}_{\mathcal{R}}$, and $\mathcal{T}_{\mathcal{MR}}$, respectively. When phased data were used, this changed only slightly; 50.828 %, 51.366 %, and 59.182 % of correct alleles in $\mathcal{T}_{\mathcal{M}}$, $\mathcal{T}_{\mathcal{R}}$, and $\mathcal{T}_{\mathcal{MR}}$, respectively. Note that the proportion of correctly inferred alleles increased in $\mathcal{T}_{\mathcal{R}}$ due to phasing error. This is because the underestimation that was generally seen under the recombination clock model may have been mitigated by further reduction of IBD segment lengths resulting from flip or switch errors in phased data. The small difference between true and phased data was further reflected in the accuracy of each analysis, where r_S changed from 0.680 to 0.660 in $\mathcal{T}_{\mathcal{M}}$, 0.780 to 0.764 in $\mathcal{T}_{\mathcal{R}}$, and 0.742 to 0.731 in $\mathcal{T}_{\mathcal{MR}}$, with regards to t_d.

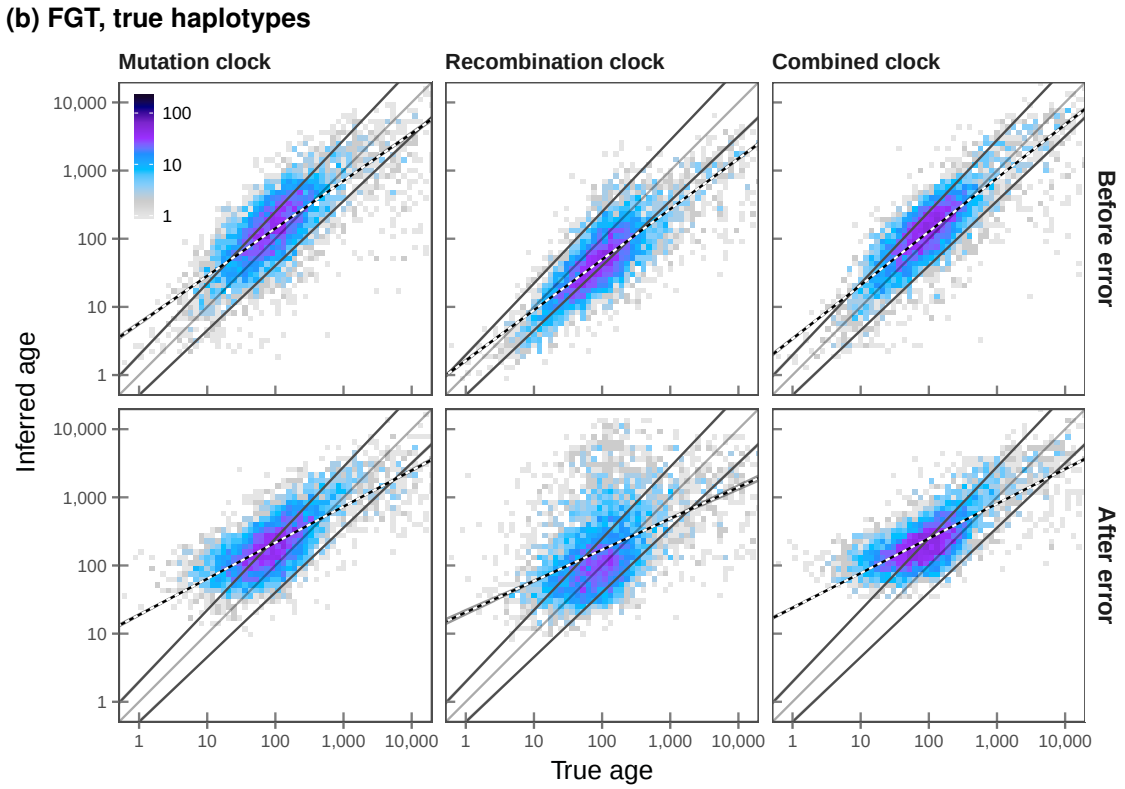

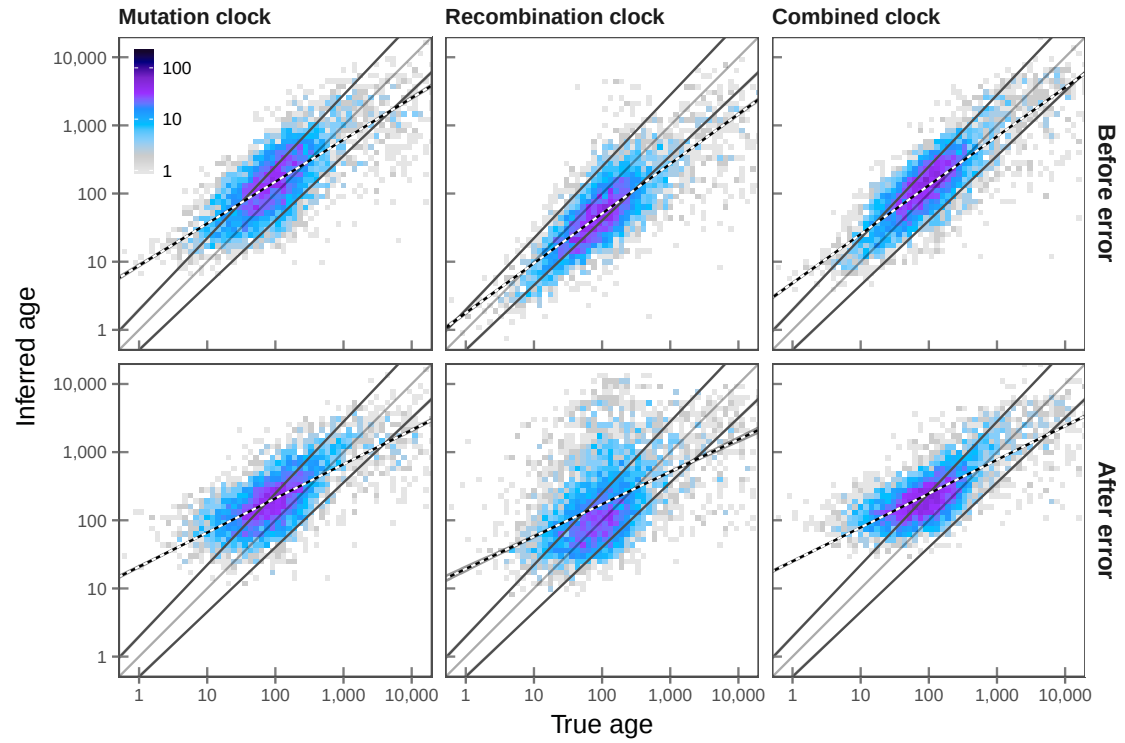

Figure 5.11: Continued.

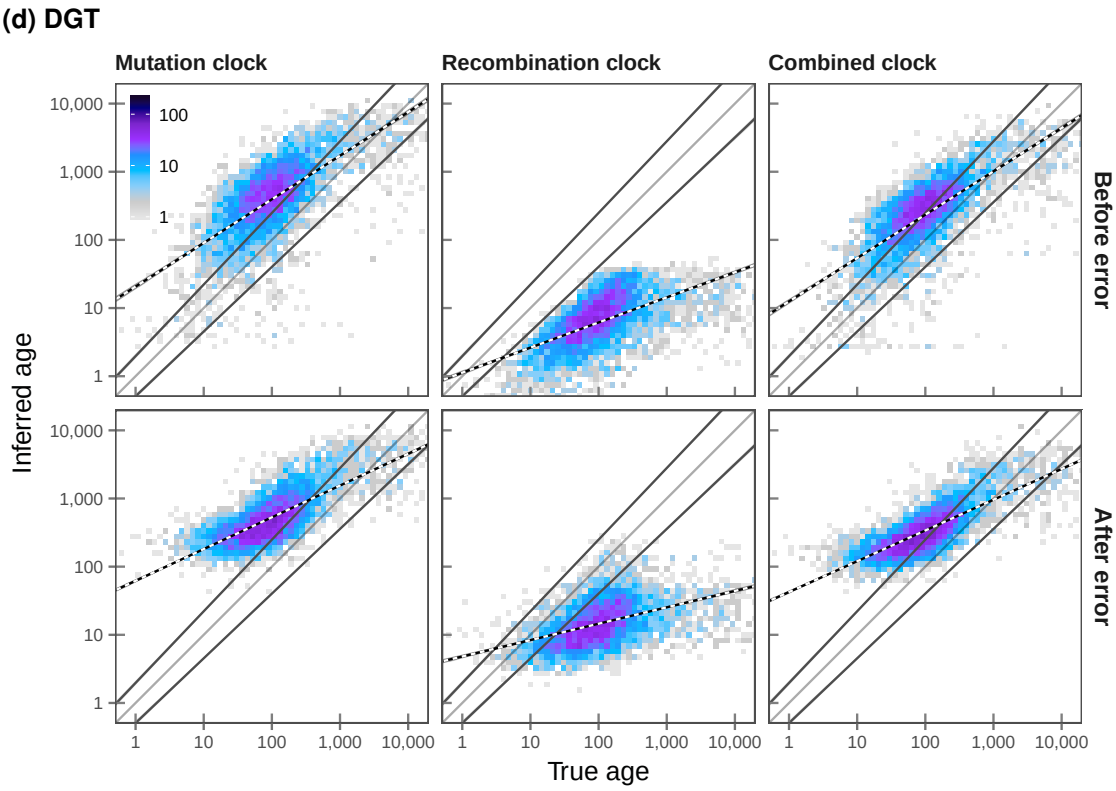

Figure 5.11: Continued.

When analyses were performed on data with genotype error, the overall proportion of correct alleles was reduced, but again the differences seen from true and phased data were small. On true haplotypes, the proportion of correct alleles was 44.267 %, 45.025 %, and 42.034 % in $\mathcal{T}_{\mathcal{M}}$, $\mathcal{T}_{\mathcal{R}}$, and $\mathcal{T}_{\mathcal{MR}}$, respectively, whereas 43.549 %, 46.002 %, and 41.635 % of alleles were correct using phased haplotypes in $\mathcal{T}_{\mathcal{M}}$, $\mathcal{T}_{\mathcal{R}}$, and $\mathcal{T}_{\mathcal{MR}}$, respectively. Likewise, accuracy was overall reduced but r_S and RMSLE scores did not suggest notable differences between estimation results from true and phased haplotypes; see Table 5.4 (page 213). Notably, the analysis on true IBD suggested that genotype error induces an overall overestimation of allele age in $\mathcal{T}_{\mathcal{M}}$ and $\mathcal{T}_{\mathcal{MR}}$. However, this effect was mitigated by underestimating IBD lengths in the FGT, such that the number of pairwise differences, S, may not be elevated as genotype errors that would increase the value of S may also lead to the premature detection of interval breakpoints.

Estimation results based on the DGT for IBD detection are shown in Figure 5.11d (this page). Before error, the proportions of correctly inferred allele age were the lowest in the present comparison in each clock model. Under both the mutation and combined clocks, $\mathcal{T}_{\mathcal{M}}$ and $\mathcal{T}_{\mathcal{MR}}$, DGT-based age estimation resulted in 26.341 % and 36.949 % of correct alleles, respectively, whereas only 2.413 % were correct in $\mathcal{T}_{\mathcal{R}}$. While the majority

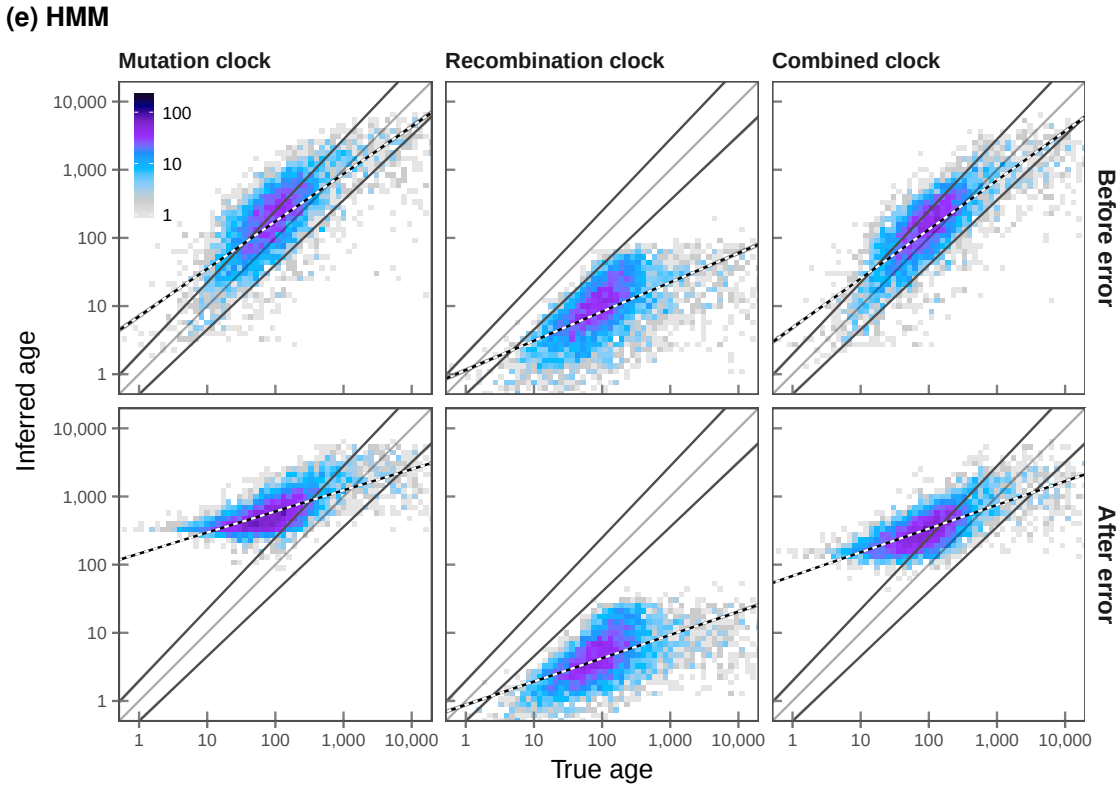

Figure 5.11: Continued.

of alleles in $\mathcal{T}_{\mathcal{M}}$ and $\mathcal{T}_{\mathcal{MR}}$ were overestimated, 70.050 % and 57.846 % respectively, 97.587 % were underestimated in $\mathcal{T}_{\mathcal{R}}$ (none were overestimated). The tendency to overestimate allele age was increased after error; the proportions of alleles overestimated were 77.308 % and 67.856 % in $\mathcal{T}_{\mathcal{M}}$ and $\mathcal{T}_{\mathcal{MR}}$, respectively. As this was also the case in $\mathcal{T}_{\mathcal{R}}$, the proportion of correctly inferred alleles increased to 15.693 %, but this was an artefact resulting from an overall underestimation of IBD lengths. However, the loss in accuracy was reflected in the correlation between true and inferred allele age; r_S at t_c, t_m, and t_d was 0.746, 0.628, and 0.406 before error, and 0.588, 0.504, and 0.328 after error. Note that rank correlations at t_m and t_d were higher in $\mathcal{T}_{\mathcal{M}}$ and $\mathcal{T}_{\mathcal{MR}}$, both before and after error. However, the same measures taken after error actually suggested that the accuracy increased in $\mathcal{T}_{\mathcal{M}}$ and $\mathcal{T}_{\mathcal{MR}}$; see Table 5.4 (page 213). Regardless, rank correlation measured at t_c was decreased after error under each clock model.

The accuracy of age estimation based on IBD inference using the HMM-based approach was overall highly accurate before error; more accurate in comparison to the FGT in $\mathcal{T}_{\mathcal{M}}$, similar in accuracy to the DGT in $\mathcal{T}_{\mathcal{R}}$, and similar to the FGT in $\mathcal{T}_{\mathcal{MR}}$. The density distribution for results obtained using the HMM is given in Figure 5.11e (this page). Before error, the proportion of correct alleles was 47.537 % in $\mathcal{T}_{\mathcal{M}}$, 3.629 % in $\mathcal{T}_{\mathcal{R}}$, and

57.827 % in $\mathcal{T}_{\mathcal{MR}}$. The majority of alleles was underestimated in $\mathcal{T}_{\mathcal{R}}$ (96.351 %). This was increased after error, *i.e.* 98.305 % in $\mathcal{T}_{\mathcal{R}}$, as the proportion of correct alleles was overall reduced; 16.650 % and 27.657 % in $\mathcal{T}_{\mathcal{M}}$ and $\mathcal{T}_{\mathcal{MR}}$, respectively. For example, RMSLE scores were lowest for the HMM under each clock model after error; see Table 5.4 (page 213). The accuracy before and after error, measured as r_S at t_c, decreased from 0.702 to 0.535 in $\mathcal{T}_{\mathcal{M}}$, and from 0.733 to 0.569 in $\mathcal{T}_{\mathcal{MR}}$. However, importantly, the HMM-based estimation showed the highest levels of accuracy in $\mathcal{T}_{\mathcal{R}}$ compared to the other methods, *i.e.* r_S at t_c was 0.751 before and 0.737 after error. Although allele age was vastly underestimated, deviations appeared to be consistent.

The distribution of inferred IBD segment lengths for each approach are given in Figure 5.12 (next page). Notably, IBD segments detected using the FGT and DGT were overall underestimated after error; only the HMM maintained similarly accurate lengths before and after error, for both concordant and discordant pairs.

5.4.3.1 Generation of error correction models

Although the estimation showed strong tendencies to either over- or underestimate allele age, dependent on the clock model and IBD method used, some settings maintained relatively high levels of accuracy after error; in particular the HMM-based inference in $\mathcal{T}_{\mathcal{R}}$. This suggested that deviations from the true age may follow a consistent pattern. As it is hoped that the age estimation method presented in this chapter is able to produce credible results when used on real data, I evaluated the reliability of each estimation approach by constructing error correction models specific to each setting.

The deviation of the estimated age, $\hat{t}$, from the actual true age of an allele, denoted by t^*, is simply the absolute value of their difference; calculated as $\delta = |\hat{t} - t^*|$. Given the expectation that the time to coalescence is exponentially distributed, the logarithmic difference is calculated as

$$\xi = \frac{t^* \, \mathrm{e}^{-\delta}}{\hat{t}} \tag{5.18}$$

where $\xi = 0$ if true and estimated age are equal, $0 < \xi < 1$ if the age is overestimated, and $\xi > 1$ if age is underestimated. As the actual age of an allele was not known from coalescent simulations, here, the midpoint of the branch on which the mutation event occurred, t_m, was defined as the reference point against which the estimated age was compared. In reverse, a constant ξ value was used as a correction factor applied to a given set of analysed alleles, considering the results obtained per clock model and IBD method,

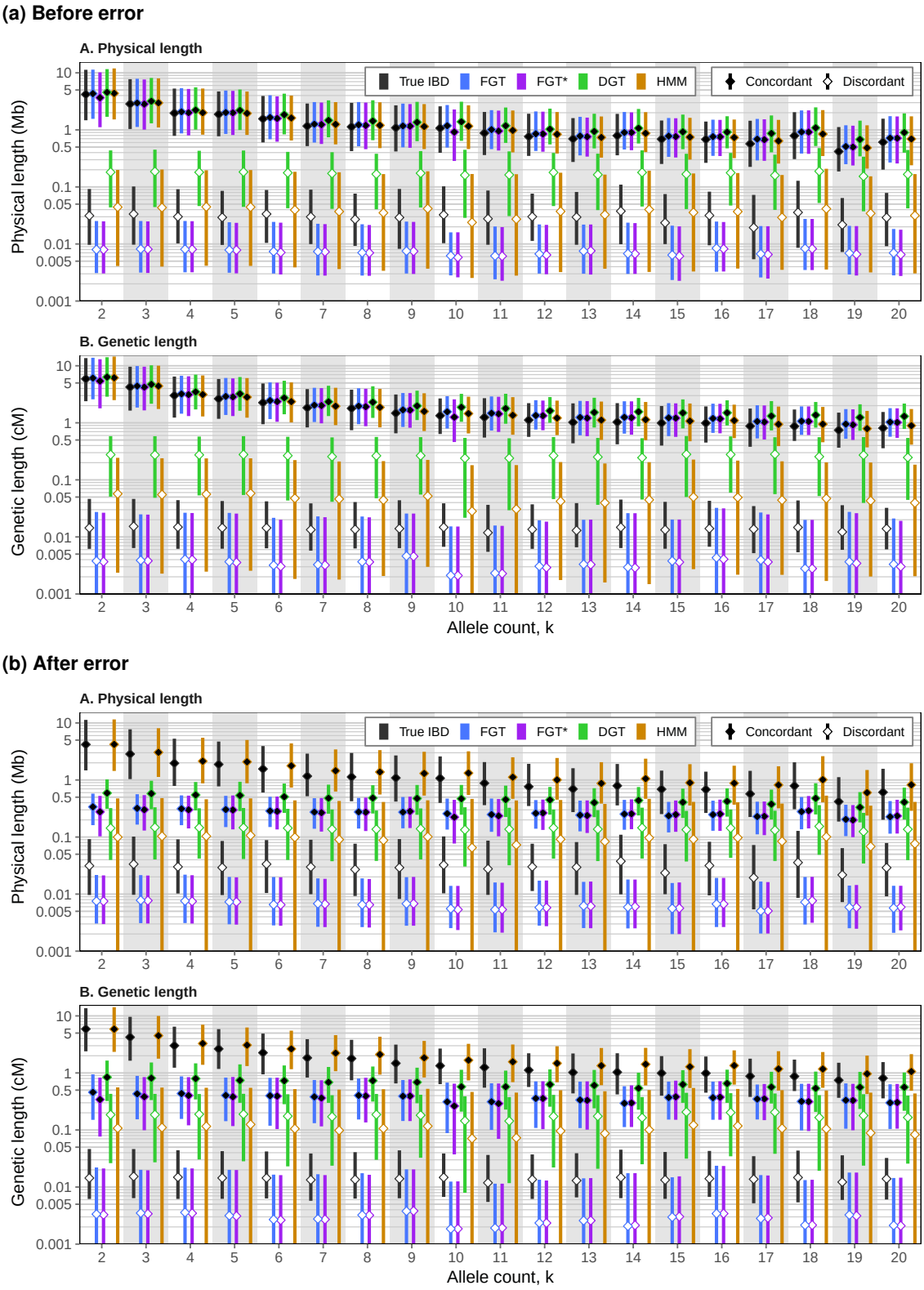

Figure 5.12: Length distribution of inferred IBD segments before and after error. Bottom and top of each bar indicate 1st and 3rd quartiles, respectively, between which the median (2nd quartile) is marked (*diamonds*). IBD detected for concordant and discordant pairs is distinguished; *solid* and *hollow* diamonds, respectively.

in order to minimise the mean of the difference distribution. The value of this correction factor was estimated by iteration through an array, denoted by Ξ, which is defined as a series of l factor values, denoted by $\xi_i \in \Xi$, where $i \in [1, 2, \ldots l]$. The minimum factor value was found through the following operation;

$$i = \underset{\xi_i \in \Xi}{\arg\min} \left(\left| \frac{1}{n} \sum_{j=1}^{n} \log\left[t_{mj}\right] - \log\left[\hat{t}_j \; \xi_i\right] \right| \right) \tag{5.19}$$

which is applied to a given set of n true and corresponding estimated times, t_{mj} and $\hat{t}_j$, respectively, where $j \in 1, 2, \ldots, n$. I applied Equation (5.19) in a recursive algorithm in which I selected ξ_{i-1} and ξ_{i+1} after each step to redefine the limits of Ξ and to recalculate l new factor values for the next step. This greatly improved the speed and resolution of the computation.

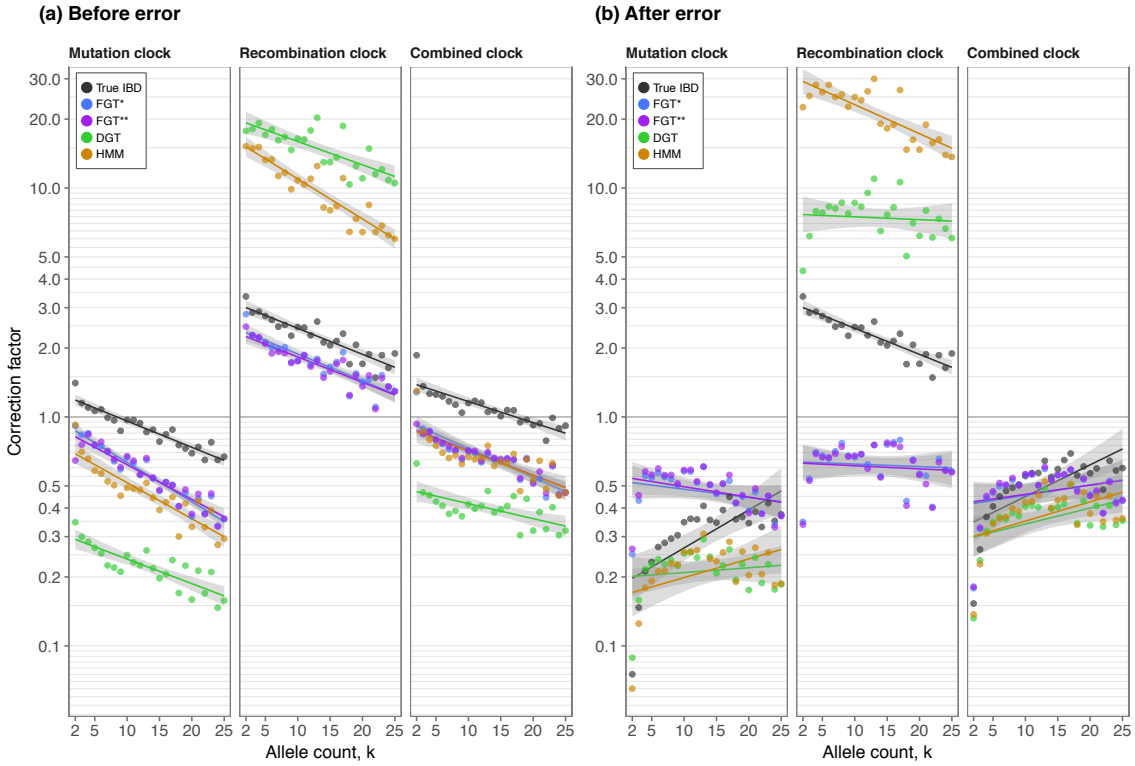

Figure 5.13: Estimated correction factors before and after error. Correction factors were estimated per set of f_k variants for which allele age was estimated in each analysis under a given clock model and IBD detection method. Values below and above 1 indicate that true age was overestimated and underestimated on average, respectively. The line shown per analysis indicates the trend of the corrected deviation (± SE), which was calculated through simple nonlinear regression by allele frequency. Note that IBD detection using the FGT was performed on true haplotype data (*) as well as phased haplotypes (**).

The algorithm outlined above was applied on the results obtained per set of f_k variants estimated in each clock model and IBD method, as well as true IBD, before and after error. Computed correction factors are shown in Figure 5.13, which highlights that deviations followed a general trend in each analysis. For example, before error, allele age estimated using true IBD showed the lowest amount of deviation in $\mathcal{T}_{\mathcal{M}}$ and $\mathcal{T}_{\mathcal{MR}}$, but where alleles at lower frequencies showed a tendency to be overestimated on average and underestimated at higher frequencies. However, in $\mathcal{T}_{\mathcal{R}}$, true IBD showed larger deviations compared to the FGT (on both true and phased haplotype data), but this may result from the assumption that t_m approximates the actual age of an allele. After error, notably, factor deviations showed spurious patterns for most approaches, except for the HMM-based estimation of allele age, which indicated a consistent trend. Note that the factor distributions of true IBD in $\mathcal{T}_{\mathcal{R}}$ were identical before and after error, as genotype error did not affect the estimation under the recombination clock when IBD is known.

Generated error correction factors were applied to the estimated age results, after error, at corresponding f_k variants under each clock model and in each IBD method, which minimised deviations in relation to t_m. As a consequence, accuracy was overall improved in each approach; see Table 5.4 (next page). Notably, however, the rank correlation measured for the HMM in $\mathcal{T}_{\mathcal{R}}$ was least affected; before applying correction factors, r_S was 0.737, 0.621, and 0.398 at t_c, t_m, and t_d, respectively, which was marginally improved after correction, yielding 0.738, 0.624, and 0.402, respectively. Nonetheless, the HMM indicated the highest levels of accuracy at these measures in comparison to the other IBD methods. Hence, this result corroborates the reliability of the HMM in $\mathcal{T}_{\mathcal{R}}$.

The HMM was developed to account for genotype error in the inference of IBD segments. It may therefore be expected that the HMM outperformed the FGT and DGT in this comparison. However, this had little influence on the estimation in $\mathcal{T}_{\mathcal{M}}$ and $\mathcal{T}_{\mathcal{MR}}$. This is because the HMM was implemented such that the interval of the IBD segment is reported, but without further guiding the estimation process. For example, but it would be possible to calculate the posterior probabilities of the hidden states (defined as *ibd* and *non*; see Chapter 4) to weight observed mutational differences at each site along the sequence to determine the value of S. This was not considered in the current implementation of the `rvage` algorithm, but could be extended in future versions.

Table 5.4: Effect of genotype error on age estimation accuracy. Allele age was estimated based on IBD inferred using the FGT, DGT, and HMM on the same set rare allele target sites at shared allele frequency ≤ 0.5% in simulated data of 5,000 haplotypes. The number of discordant pairs was limited to n_d = 2,500 in each analysis. Note that the HMM used the theoretical emission model in the analysis before error (dataset $\mathcal{D}_B$), and the empirical emission model after error ($\mathcal{D}^*_B$). True IBD refers to the first breakpoints that are detectable in the data to both sides of a given target position, which were determined from simulation records. The estimates obtained on data with genotype error were additionally corrected using the correction factors calculated per set of f_k variants estimated under each clock model and in each IBD method (including true IBD).

Clock	Method	Before error			After error			After error, corrected		
		t_c	t_m	t_d	t_c	t_m	t_d	t_c	t_m	t_d
Rank correlation coefficient (r_S)										
$\mathcal{T}_{\mathcal{M}}$	FGT*	0.680	0.736	0.597	0.556	0.696	0.615	0.613	0.721	0.607
	FGT**	0.660	0.711	0.576	0.543	0.673	0.591	0.597	0.696	0.582
	DGT	0.618	0.685	0.563	**0.577**	**0.724**	**0.649**	0.669	**0.753**	**0.620**
	HMM	**0.702**	**0.738**	**0.599**	0.535	0.686	0.621	**0.676**	0.715	0.563
	True IBD	0.870	0.871	0.673	0.518	0.694	0.646	0.712	0.752	0.590
$\mathcal{T}_{\mathcal{R}}$	FGT*	**0.780**	**0.782**	0.601	0.405	0.481	0.407	0.462	0.515	0.414
	FGT**	0.764	0.780	**0.603**	0.406	0.485	**0.414**	0.461	0.519	**0.420**
	DGT	0.746	0.628	0.406	0.588	0.504	0.328	0.630	0.530	0.336
	HMM	0.751	0.632	0.411	**0.737**	**0.621**	0.398	**0.738**	**0.624**	0.402
	True IBD	0.818	0.843	0.666	0.818	0.843	0.666	0.801	0.849	0.684
$\mathcal{T}_{\mathcal{MR}}$	FGT*	**0.742**	**0.792**	**0.644**	0.528	0.689	0.629	0.640	0.741	0.617
	FGT**	0.731	0.787	0.643	0.520	0.679	0.619	0.631	0.732	0.609
	DGT	0.666	0.727	0.597	**0.596**	**0.757**	**0.689**	**0.694**	**0.781**	**0.645**
	HMM	0.733	0.781	0.641	0.569	0.693	0.606	0.679	0.718	0.568
	True IBD	0.884	0.885	0.696	0.593	0.735	0.655	0.740	0.778	0.613
Root mean squared logarithmic error (RMSLE)										
$\mathcal{T}_{\mathcal{M}}$	FGT*	**0.696**	**0.436**	0.639	0.864	**0.516**	**0.524**	0.615	0.394	**0.662**
	FGT**	0.715	0.444	**0.623**	**0.859**	0.524	0.547	0.625	0.416	0.678
	DGT	1.083	0.743	0.657	1.190	0.809	0.606	**0.593**	**0.382**	0.668
	HMM	0.754	0.478	0.633	1.250	0.882	0.681	0.598	0.425	0.713
	True IBD	0.454	0.255	0.666	1.146	0.770	0.587	0.562	0.362	0.671
$\mathcal{T}_{\mathcal{R}}$	FGT*	**0.380**	**0.471**	0.909	0.881	**0.638**	0.728	0.738	0.594	0.815
	FGT**	0.413	0.480	**0.903**	0.890	0.641	**0.722**	0.742	0.594	0.811
	DGT	0.905	1.252	1.690	**0.703**	0.991	1.413	0.631	0.533	0.822
	HMM	0.796	1.141	1.585	1.031	1.380	1.814	**0.590**	**0.488**	**0.798**
	True IBD	0.337	0.504	0.960	0.337	0.504	0.960	0.508	0.284	0.645
$\mathcal{T}_{\mathcal{MR}}$	FGT*	**0.624**	**0.364**	0.626	**0.915**	**0.548**	**0.496**	0.601	0.373	**0.649**
	FGT**	0.641	0.367	**0.608**	0.916	0.551	0.503	0.609	0.384	0.654
	DGT	0.869	0.557	0.611	1.019	0.645	0.523	**0.587**	**0.372**	0.661
	HMM	0.644	0.398	0.647	1.021	0.672	0.585	0.595	0.421	0.712
	True IBD	0.381	0.260	0.716	0.919	0.555	0.506	0.542	0.330	0.656

* FGT applied to true haplotypes

** FGT applied to phased haplotypes

5.5 Age of alleles with predicted effects in 1000 Genomes data

The method presented in this chapter was applied the final release dataset of the 1000 Genomes Project (1000G) Phase III (1000 Genomes Project Consortium *et al.*, 2012, 2015), where I estimated allele age on a selected set of target sites using the HMM-based approach under the recombination clock model, $\mathcal{T}_{\mathcal{R}}$. To regard inferred allele age in relation to the functional consequences of specific variants, I prioritised SNPs that have been annotated by the Ensembl Variant Effect Predictor (VEP) (McLaren *et al.*, 2016).* In particular, VEP classifies variants into four *impact* categories which broadly distinguishes the severity of the consequences predicted; namely *high*, *moderate*, and *low* impact, as well as *modifiers*.

5.5.1 Quality control

Because genotype error was expected to be present in the data, alleles observed at selected target sites may not correctly identify haplotype sharing by descent in all individuals. Alleles can either be missed (*false negatives*) or incorrectly observed (*false positives*), such that allocation into the set of sharers, X_c, and the set of non-sharers, X_d, is biased. This is likely to disrupt the estimation of the composite likelihood, *i.e.* by including CCFs at wrong ends of Equation (5.11), to the extent that the resulting posterior probabilities may become spurious or cancel out (referred to as *disconformity*). In general, the identification of missed or falsely observed alleles is not straightforward, in particular towards lower allele frequencies. While it would be possible to reduce the risk of including false negatives in Ω_d by lowering the n_d threshold, the inclusion of false positives would not be affected, but could be reduced by applying a threshold to n_c. However, this would not be possible for f_2 variants, unless they are categorically excluded.

As an alternate solution, here, I attempted to exclude target sites in a *post hoc* analysis using the following quality control measure. The median of the posterior probability of the CCF in each pair was taken to calculate the geometric mean (or *log-average*) across pairs contained in Ω_c and Ω_d, respectively, computed as

$$\tilde{y}_x = \left(\prod_{i,j \in \Omega_x} [\Lambda_{ij}]_2 \right)^{-n_x} \tag{5.20}$$

* Ensemble Variant Effect Predictor (VEP): http://www.ensembl.org/info/docs/tools/vep/index.html [Date accessed: 2017-02-15]

where $x \in \{c, d\}$, referring to either set Ω_c or Ω_d, and $[\Lambda_{ij}]_2$ is the median (2nd quartile) of the CCF computed for individuals i and j taken from that set. The intuition is that $\tilde{y}_c$ and $\tilde{y}_d$ are indicators of the central tendency of the time of coalescent events found through concordant and discordant pairs, such that $\tilde{y}_c < \tilde{y}_d$ is expected if the estimation was not or less affected by false negatives or positives. By also considering $\tilde{y}_m = \sqrt{\tilde{y}_c \tilde{y}_d}$ as a robust measure of allele age, here, target sites were removed if the condition $\tilde{y}_c < \tilde{y}_m < \tilde{y}_d$ was violated.

5.5.2 Error correction based on allele frequency

The error correction model constructed in Section 5.4.3.1 (page 209) was used to correct estimated age values dependent on the allele frequency observed at a given target site. In particular, a simple nonlinear regression model was used to fit empirically computed factor values, such that correction factors could be predicted by the allele frequency observed in 1000G data. The following exponential model was used.

$$\hat{\xi}_k = b\, \mathrm{e}^{ka} \tag{5.21}$$

The fitted model parameters were $a = -0.029$ and $b = 30.975$ for the the HMM in $\mathcal{T}_{\mathcal{R}}$.

5.5.3 Results

Target sites were randomly selected from the set of SNPs in available VEP results, across chromosomes 1–22, at shared allele frequencies below 1 % observed across the whole sample of $N = 2504$ diploid individuals; *i.e.* f_k variants with $k \in [2, 50]$. In total, approximately 150,000 target sites were analysed, using the following model parameters; $N_e = 10{,}000$, constant mutation rate of $\mu = 1.200 \times 10^{-8}$ per site per generation (following Scally and Durbin, 2012), recombination rates according to genetic maps per chromosome provided by HapMap Phase II, Build 37 (International HapMap Consortium *et al.*, 2007), and $n_d = 2{,}504$. The HMM used the empirical emission model that was generated from genotype error identified in 1000G data (chromosome 20); see Chapter 4.

The total number of pairwise analyses conducted was 460.051 million. A fraction of 2.613 % was conflicting and 2.899 % were indicated in quality control; together, 3.497 % of target sites were removed. Notably, the proportion of variants removed in both filtering steps was highest at lower allele frequencies; for example, 10.761 % of f_2 variants and only 0.852 % of f_5 variants were removed.

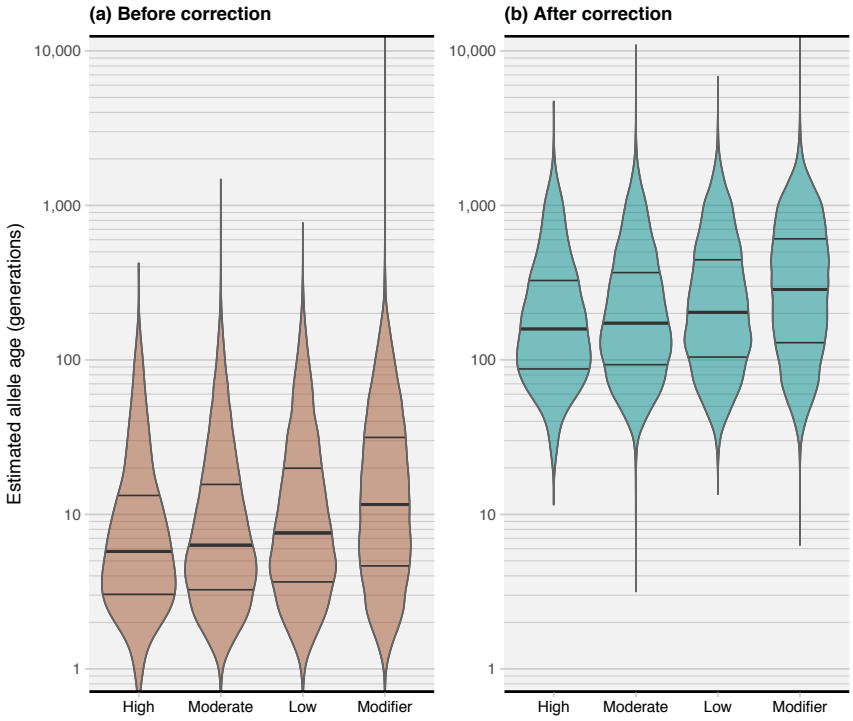

Figure 5.14: Allele age estimated on functionally annotated data in 1000 Genomes. The distribution of inferred allele age is shown in Violin plots by predicted impact category for the whole sample of the 1000G dataset, before and after correction; 1st, 2nd, and 3rd quartiles are indicated.

The number of retained estimates was 141,069, which included 1,255 variants of *high* impact (splice acceptor and splice donor variants, and stop gained and stop lost variants), 44,131 variants with *moderate* impact (missense variants only), 9,990 variants with *low* impact (synonymous variants only), and 85,694 *modifier* variants (non-coding variants, *e.g.* intron and intergenic variants, and regulatory region variants).

The distribution of allele age before and after correction is shown in Figure 5.14 (this page). Before correction, median ages per category were inferred at 5.661, 6.329, 7.567, and 11.828 generations in *high*, *moderate*, *low*, and *modifier*, respectively, which were corrected to 158.163, 174.435, 203.952, and 289.557 generations, respectively. The correlation between estimated age and allele frequency was measured using r_S, which was 0.829, 0.834, 0.851, and 0.867 in *high*, *moderate*, *low*, and *modifier*, respectively. Although differences were small, this suggested that the estimated allele age was less correlated with allele frequency if the severity of the presumed consequences was high.

The 1000G dataset is composed of several continental population samples (or *super-populations*) in which allele frequencies may differ. I applied the correction as per frequency observed in each population; variants were excluded if monomorphic per

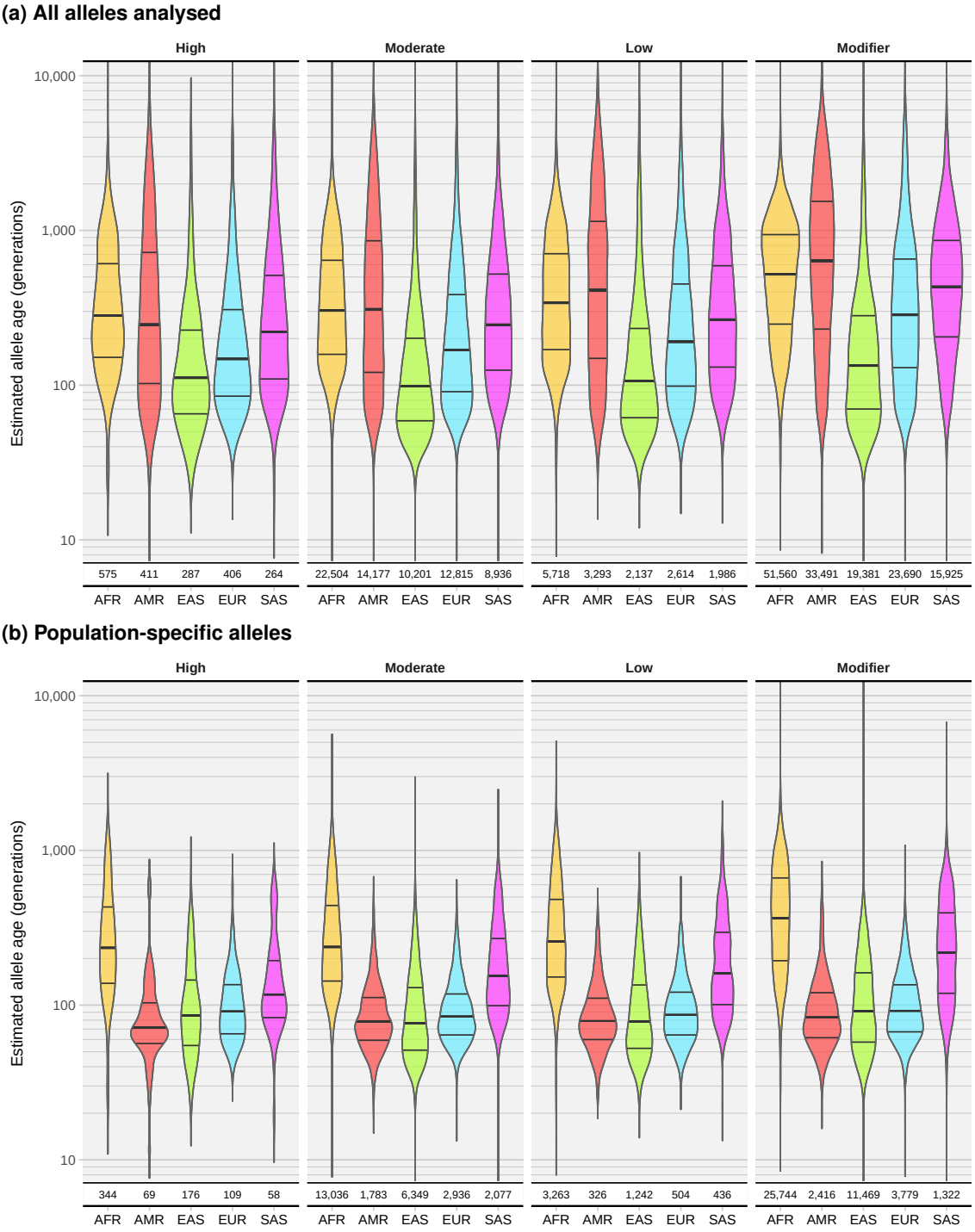

Figure 5.15: Allele age after correction on population-specific frequency in 1000 Genomes. The distribution of inferred allele age is shown in Violin plots by predicted impact category for each population in the 1000G dataset; 1st, 2nd, and 3rd quartiles are indicated. In Panel **(a)**, all variants retained after quality control were included in the comparison, which included n = 141,069 target sites. Note that this also included alleles shared among populations. In Panel **(b)**, only the subset of population-specific variants was included (n = 77,438). The number of alleles retained in each impact category and population are shown below each graph. The colours used follow the 1000G colour-scheme.

population. Although target sites were selected at ≤ 1% allele frequency in the whole sample, some alleles were found at relatively high frequencies in certain populations, but which did not exceed 5% allele frequency. The distribution of allele age per population is shown in Figure 5.15a. Variants of *high* impact were overall estimated to be younger, *e.g.* median age was 276.716 generations in AFR and 113.895 generations in EAS. Non-coding variants, *modifiers*, were older throughout, *e.g.* 528.812 generations in AFR, but were not notably older in EAS, where median age was 135.348 generations. Alleles in the AMR sample were overall more widely distributed and indicated an older median age per impact category. Rank correlation with allele frequency, r_S, was high in AFR (0.731), but not substantial in EAS (0.439), EUR (0.409), and SAS (0.347). In AMR, age and frequency appeared to be weakly related (0.092), which may be the result of population admixture, which characterises this population sample.

Table 5.5: Allele age per population in the 1000 Genomes sample. Inferred allele age was corrected in reference to population allele frequencies in the five population groups in 1000G data, shown per VEP impact category. In total, 141,070 variants were analysed **(a)**, of which 77,439 were population-specific **(b)**.

Impact	Median estimated age (generations)					Correlation with frequency (r_S)				
	AFR	AMR	EAS	EUR	SAS	AFR	AMR	EAS	EUR	SAS
(a) All alleles analysed										
High	276.7	238.3	113.9	145.8	219.0	0.697	0.164	0.445	0.581	0.441
Moderate	305.2	311.5	99.0	169.1	247.7	0.707	0.143	0.432	0.469	0.386
Low	341.4	414.0	105.0	191.9	266.3	0.738	0.116	0.388	0.445	0.410
Modifier	528.8	645.6	135.3	287.3	435.3	0.729	0.058	0.435	0.349	0.340
(b) Population-specific alleles										
High	227.2	67.7	86.9	87.8	116.7	0.886	0.673	0.861	0.738	0.865
Moderate	239.8	77.4	76.8	84.6	154.9	0.892	0.647	0.878	0.746	0.907
Low	256.4	78.0	78.0	87.2	154.9	0.905	0.616	0.881	0.751	0.907
Modifier	369.7	82.7	91.8	91.9	221.6	0.920	0.707	0.897	0.808	0.935

Variants that appeared in more than one population were removed to focus on population-specific, presumably more recent alleles; see Figure 5.15b. This reduced the number of alleles to 77,438. Notably, alleles retained in AMR were youngest in all impact categories, whereas the alleles specific to the AFR sample were seen to be the oldest; *e.g.* median age was 227.240 generations in *high* and 369.733 generations in the *modifier* category. Rank correlation between between allele frequency and inferred age showed a more consistent relationship in each population; AFR (0.917), EAS (0.890), EUR (0.780), SAS (0.921). Notably, the variants specific to AMR now showed a moderately high correlation between age and frequency (0.677). These results are summariesed in Table 5.5 (this page).

5.6 Discussion

I demonstrated the validity of the age estimation framework using simulated data where I showed that age can be estimated with very high accuracy. However, certain problems may arise when working with real data. The impact of phasing error is small in comparison to genotypic (or allelic) misclassification, which is likely to bias the estimation process.

Generally, imperfect data may affect the estimation of allele age in two ways. First, the method was shown to be highly susceptible to inaccurate IBD inference, where each clock model behaves differently to the over or underestimation of IBD length. In this regard, the HMM-based approach for IBD inference was shown to maintain consistency even if genotype error is present. However, second, even if IBD is detected with high accuracy, the alleles observed at a focal variant in the sample may wrongly identify haplotype sharing by descent. To account for the possibility that some concordant pairs may actually be discordant pairs, for example, a separate filtering method would be needed to exclude pairs before or after the computation of the CCF, to reduce the chance that the calculation of the composite likelihood is biased. However, because such a method would effectively predict missed alleles in the data, a solution to this problem may not be straightforward. Yet it would be possible, for example, to exclude pairs on basis of patterns of allele sharing or consistency of the inferred IBD structure. Alternatively, instead of excluding pairs, the target site itself would need to be excluded from the analysis if bias is likely. A simple solution was presented in the previous section, where sites are excluded if the lower and upper bounds indicate a reverse order, but further evaluation is required to determine the effectiveness of this filtering criterion.

Lastly, note that both the DGT and the HMM-based approach operate on genotype data to detect IBD, but because the mutation clock model, $\mathcal{T}_M$, requires haplotypes, it would be desirable to estimate pairwise differences, S, in genotype data, so as to make these methods fully compatible with $\mathcal{T}_M$ and $\mathcal{T}_{MR}$. A possible solution is presented in Chapter 3, where haplotype phase was determined from genotype pairs in detected IBD segments, based on the genealogical constrains that arise under haplotype sharing by descent. Yet, further work is needed to determine the feasibility of such an approach.

The key test for an acronym is to ask whether it helps or hurts communication.

— Elon Musk

Abbreviations

1000G	1000 Genomes Project
CCF	Cumulative coalescent function
CDF	Cumulative distribution function
cM	CentiMorgan
DGT	Discordant genotype test
FGT	Four-gamete test
HapMap	International HapMap Project
HMM	Hidden Markov Model
Mb	Megabase
MRCA	Most recent common ancestor
PDF	Probability density function
PMF	Probability mass function
RMSLE	Root mean squared logarithmic error
SNP	Single-nucleotide polymorphism
$\mathbf{T_{MRCA}}$	Time to the most recent common ancestor
VEP	Variant Effect Predictor

My definition of a scientist is that you can complete the following sentence: 'he or she has shown that . . . '

— E. O. Wilson

Bibliography

1000 Genomes Project Consortium, Abecasis, G. R., Auton, A., Brooks, L. D., DePristo, M. A., Durbin, R. M., Handsaker, R. E., Kang, H. M., Marth, G. T., and McVean, G. A. (2012). An integrated map of genetic variation from 1,092 human genomes. *Nature*, **491**(7422), 56–65.

1000 Genomes Project Consortium, Auton, A., Brooks, L. D., Durbin, R. M., Garrison, E. P., Kang, H. M., Korbel, J. O., Marchini, J. L., McCarthy, S., McVean, G. A., and Abecasis, G. R. (2015). A global reference for human genetic variation. *Nature*, **526**(7571), 68–74.

Abecasis, G. R., Cherny, S. S., and Cardon, L. R. (2001). The impact of genotyping error on family-based analysis of quantitative traits. *European Journal of Human Genetics*, **9**(2), 130–134.

Albrechtsen, A., Korneliussen, T. S., Moltke, I., Hansen, T. v. O., Nielsen, F. C., and Nielsen, R. (2009). Relatedness Mapping and Tracts of Relatedness for Genome-Wide Data in the Presence of Linkage Disequilibrium. *Genetic Epidemiology*, **33**(3), 266–274.

Altshuler, D., Daly, M. J., and Lander, E. S. (2008). Genetic Mapping in Human Disease. *Science*, **322**(5903), 881–888.

Altshuler, D. L., Bentley, D. R., Chakravarti, A., Collins, F. S., Donnelly, P., Gabriel, S. B., Knoppers, B. M., Lander, E. S., Lehrach, H., Mardis, E. R., Nickerson, D. A., Peltonen, L., Wang, J., Wilson, R. K., Gibbs, R. A., Deiros, D., Metzker, M., Wheeler, D., Li, J., Jian, M., Li, G., Li, R., Liang, H., Tian, G., Wang, B., Wang, W., Yang, H., Zhang, X., Zheng, H., Ambrogio, L., Bloom, T., Sougnez, C. L., Gormley, N., Humphray, S., Kingsbury, Z., Koko-Gonzales, P., Stone, J., McKernan, K. J., Costa, G. L., Ichikawa, J. K., Lee, C. C., Borodina, T. A., Dahl, A., Davydov, A. N., Marquardt, P., Mertes, F., Nietfeld, W., ROSENSTIEL, P., Schreiber, S., Soldatov, A. V., Timmermann, B., Tolzmann, M., Egholm, M., Affourtit, J., Ashworth, D., Attiya, S., Bachorski, M., Buglione, E., Burke, A., Caprio, A., Celone, C., Clark, S., Conners, D., Gu, L., Guccione, L., Kao, K., Kebbel, A., Knowlton, J., Labrecque, M., McDade, L., Mealmaker, C., Minderman, M., Nawrocki, A., Niazi, F., Pareja, K., Ramenani, R., Riches, D., Song, W., Turcotte, C., Wang, S., Fulton, L., Weinstock, G., Burton, J., Carter, D. M., Churcher, C., Coffey, A., Cox, A., Quail, M., Skelly, T., Stalker, J., Swerdlow, H. P., Turner, D., De Witte, A., Giles, S., Sabo, A., Yu, J., Fang, X., Guo, X., Li, Y., Luo, R., Tai, S., Wu, H., Zheng, H., Zheng, X., Zhou, Y., Wang, J., Huang, W., Indap, A., Kural, D., Lee, W.-P., Stromberg, M. P., Ward, A. N., Lee, C., Mills, R. E., Shi, X., Daly, M. J., DePristo, M. A., Ball, A. D., Browning, B. L., Cibulskis, K., Garimella, K. V., Grossman, S. R., Hanna, M., Jaffe, D. B., Kernytsky, A. M., Li, H., Maguire, J. R., McCarroll, S. A., McKenna, A., Nemesh, J. C., Philippakis, A. A., Poplin, R. E., Price, A., Rivas, M. A., Sabeti, P. C., Schaffner, S. F., Shefler, E., Shlyakhter, I. A., Cooper, D. N., Ball, E. V., Mort, M., Phillips, A. D., Stenson, P. D., Sebat, J., Makarov, V., Ye, K., Yoon, S. C., Clark, A. G., Boyko, A., Degenhardt, J., Gutenkunst, R. N., Kaganovich, M., Keinan, A., Lacroute, P., Ma, X., Reynolds, A., Clarke, L., Cunningham, F., Herrero, J., Keenen, S., Kulesha, E., Leinonen, R., McLaren, W. M., Radhakrishnan, R., Smith, R. E., Zalunin, V., Zheng-Bradley, X., Korbel, J. O., Stütz, A. M., Bauer, M., Keira Cheetham, R., Cox, T., Eberle, M., James, T., Kahn, S., Murray, L., Ye, K., De La Vega, F. M., Fu, Y., Hyland, F. C. L., Manning, J. M., McLaughlin, S. F., Peckham, H. E., Sakarya, O., Sun, Y. A., Tsung, E. F., Batzer, M. A., Konkel, M. K., Walker, J. A., Sudbrak, R., Albrecht, M. W., Amstislavskiy, V. S., Herwig, R., Parkhomchuk, D. V., Agarwala, R., Khouri, H. M., Morgulis, A. O., Paschall, J. E., Phan, L. D., Rotmistrovsky, K. E., Sanders, R. D., Shumway, M. F., Xiao, C., Lunter, G., Marchini, J. L., Moutsianas, L., Myers, S., Tumian, A., Desany, B., Knight, J., Winer, R., Craig, D. W., Beckstrom-Sternberg, S. M., Christoforides, A., Kurdoglu, A. A., Pearson, J. V., Sinari, S. A., Tembe, W. D., Haussler, D., Hinrichs, A. S., Katzman, S. J., Kern, A., Kuhn, R. M., Przeworski, M., Hernandez, R. D., Howie, B., Kelley, J. L., Cord Melton, S., Abecasis, G. R., Li, Y., Anderson, P., Blackwell, T., Chen, W., Cookson, W. O., Ding, J., Min Kang, H., Lathrop, M., Liang, L., and Moffatt, M. F. a. (2010). A map of human genome variation from population-scale sequencing. *Nature*, **467**(7319), 1061–1073.

Bodmer, W. and Bonilla, C. (2008). Common and rare variants in multifactorial susceptibility to common diseases. *Nature Genetics*, **40**(6), 695–701.

Boehnke, M. and Cox, N. J. (1997). Accurate Inference of Relationships in Sib-Pair Linkage Studies. *The American Journal of Human Genetics*, **61**(2), 423–429.

Boomsma, D. I., Wijmenga, C., Slagboom, E. P., Swertz, M. A., Karssen, L. C., Abdellaoui, A., Ye, K., Guryev, V., Vermaat, M., van Dijk, F., Francioli, L. C., Hottenga, J. J., Laros, J. F. J., Li, Q., Li, Y., Cao, H., Chen, R., Du, Y., Li, N., Cao, S., van Setten, J., Menelaou, A., Pulit, S. L., Hehir-Kwa, J. Y., Beekman, M., Elbers, C. C., Byelas, H., de Craen, A. J. M., Deelen, P., Dijkstra, M., den Dunnen, J. T., de Knijff, P., Houwing-Duistermaat, J., Koval, V., Estrada, K., Hofman, A., Kanterakis, A., van Enckevort, D., Mai, H., Kattenberg, M., van Leeuwen, E. M., Neerincx, P. B. T., Oostra, B., Rivadeneira, F., Suchiman, E. H. D., Uitterlinden, A. G., Willemsen, G., Wolffenbuttel, B. H., Wang, J., de Bakker, P. I. W., van Ommen, G.-J., and van Duijn, C. M. (2013). The Genome of the Netherlands: design, and project goals. *European Journal of Human Genetics*, **22**(2), 221–227.

Borodulin, K., Vartiainen, E., Peltonen, M., Jousilahti, P., Juolevi, A., Laatikainen, T., Mannisto, S., Salomaa, V., Sundvall, J., and Puska, P. (2015). Forty-year trends in cardiovascular risk factors in Finland. *European Journal of Public Health*, **25**(3), 539–546.

Botstein, D. and Risch, N. (2003). Discovering genotypes underlying human phenotypes: past successes for mendelian disease, future approaches for complex disease. *Nature Genetics*, **33**(3s), 228–237.

Botstein, D., White, R. L., Skolnick, M., and Davis, R. W. (1980). Construction of a genetic linkage map in man using restriction fragment length polymorphisms. *American journal of human genetics*, **32**(3), 314–331.

Browning, B. L. and Browning, S. R. (2011). A fast, powerful method for detecting identity by descent. *American journal of human genetics*, **88**(2), 173–182.

Browning, B. L. and Browning, S. R. (2013). Improving the accuracy and efficiency of identity-by-descent detection in population data. *Genetics*, **194**(2), 459–471.

Browning, B. L. and Browning, S. R. (2016). Genotype Imputation with Millions of Reference Samples. *American journal of human genetics*, **98**(1), 116–126.

Browning, S. R. (2008). Estimation of pairwise identity by descent from dense genetic marker data in a population sample of haplotypes. *Genetics*, **178**(4), 2123–2132.

Browning, S. R. and Browning, B. L. (2010). High-Resolution Detection of Identity by Descent in Unrelated Individuals. *The American Journal of Human Genetics*, **86**(4), 526–539.

Browning, S. R. and Browning, B. L. (2012). Identity by Descent Between Distant Relatives: Detection and Applications. *Annual Review of Genetics*, **46**(1), 617–633.

Buetow, K. H. (1991). Influence of aberrant observations on high-resolution linkage analysis outcomes. *The American Journal of Human Genetics*, **49**(5), 985–994.

Burdett, T., Hall, P., Hasting, E., Hindorff, L., Junkins, H., Klemm, A., MacArthur, J., Manolio, T., Morales, J., Parkinson, H., *et al.* (2016). The nhgri-ebi catalog of published genome-wide association studies. *Available at: www.ebi.ac.uk/gwas. Accessed 2017-01-20, version 1.0.*

Bustamante, C. D., Burchard, E. G., and De La Vega, F. M. (2011). Genomics for the world. *Nature*, **475**(7355), 163–165.

Cai, L., Fisher, A. L., Huang, H., and Xie, Z. (2016). CRISPR-mediated genome editing and human diseases. *Genes & Diseases*, **3**(4), 244–251.

Chakravarti, A. (1999). Population genetics - making sense out of sequence. *Nature Genetics*, **21**, 56–60.

Chen, J., Zhang, J.-G., Li, J., Pei, Y.-F., and Deng, H.-W. (2013). On Combining Reference Data to Improve Imputation Accuracy. *PloS one*, **8**(1).

Choi, Y., Wijsman, E. M., and Weir, B. S. (2009). Case-control association testing in the presence of unknown relationships. *Genetic Epidemiology*, **33**(8), 668–678.

Cirulli, E. T. and Goldstein, D. B. (2010). Uncovering the roles of rare variants in common disease through whole-genome sequencing. *Nature Publishing Group*, **11**(6), 415–425.

Colombo, R. (2007). Dating mutations. *eLS*.

Correns, K. F. J. (1899). Untersuchungen über die Xenien bei *Zea mays*. *Berichte der Deutschen Botanischen Gesellschaft*, **17**, 410–418.

Cotterman, C. W. (1940). *A calculus for statistico-genetics*. Ph.D. thesis, The Ohio State University.

Coventry, A., Bull-Otterson, L. M., Liu, X., Clark, A. G., Maxwell, T. J., Crosby, J., Hixson, J. E., Rea, T. J., Muzny, D. M., Lewis, L. R., Wheeler, D. A., Sabo, A., Lusk, C., Weiss, K. G., Akbar, H., Cree, A., Hawes, A. C., Newsham, I., Varghese, R. T., Villasana, D., Gross, S., Joshi, V., Santibanez, J., Morgan, M., Chang, K., Hale IV, W., Templeton, A. R., Boerwinkle, E., Gibbs, R., and Sing, C. F. (2010). Deep resequencing reveals excess rare recent variants consistent with explosive population growth. *Nature communications*, **1**(8), 131–6.

Cox, D. G. and Kraft, P. (2006). Quantification of the Power of Hardy-Weinberg Equilibrium Testing to Detect Genotyping Error. *Human heredity*, **61**(1), 10–14.

Crow, J. F. (1954). Breeding structure of populations. ii. effective population number. *Statistics and mathematics in biology*, **543**, 556.

Crow, J. F. and Kimura, M. (1970). An introduction to population genetics theory. *An introduction to population genetics theory.*

Daly, M. J., Rioux, J. D., Schaffner, S. F., Hudson, T. J., and Lander, E. S. (2001). High-resolution haplotype structure in the human genome. *Nature Genetics*, **29**(2), 229–232.

de Bakker, P. I. W., Yelensky, R., Pe'er, I., Gabriel, S. B., Daly, M. J., and Altshuler, D. (2005). Efficiency and power in genetic association studies. *Nature Genetics*, **37**(11), 1217–1223.

De Vries, H. M. (1900). Sur la loi de disjonction des hybrides. *Comptes rendus de l'Académie des Sciences*, **130**, 845–847.

Deelen, P., Kanterakis, A., van Dijk, F., Medina-Gomez, C., Kreiner-Møller, E., Rivadeneira, F., Gutierrez-Achury, J., van Enckevort, D., Dijkstra, M., Byelas, H., Genome of Netherlands Consortium, de Bakker, P. I. W., and Swertz, M. A. (2014). Improved imputation quality of low-frequency and rare variants in European samples using the 'Genome of The Netherlands'. *European Journal of Human Genetics*, **22**(11), 1321–1326.

Delaneau, O., Coulonges, C., and Zagury, J.-F. (2008). Shape-IT: new rapid and accurate algorithm for haplotype inference. **9**(1), 540.

Delaneau, O., Marchini, J., and Zagury, J.-F. (2011). A linear complexity phasing method for thousands of genomes. *Nature methods*, **9**(2), 179–181.

Delaneau, O., Zagury, J.-F., and Marchini, J. (2013). Improved whole-chromosome phasing for disease and population genetic studies. *Nature methods*, **10**(1), 5–6.

Devlin, B., Roeder, K., and Wasserman, L. (2001). Genomic control, a new approach to genetic-based association studies. *Theoretical population biology*, **60**(3), 155–166.

Donnelly, K. P. (1983). The probability that related individuals share some section of genome identical by descent. *Theoretical population biology*, **23**(1), 34–63.

Douglas, J. A., Boehnke, M., and Lange, K. (2000). A Multipoint Method for Detecting Genotyping Errors and Mutations in Sibling-Pair Linkage Data. *The American Journal of Human Genetics*, **66**(4), 1287–1297.

Douglas, J. A., Skol, A. D., and Boehnke, M. (2002). Probability of Detection of Genotyping Errors and Mutations as Inheritance Inconsistencies in Nuclear-Family Data. *The American Journal of Human Genetics*, **70**(2), 487–495.

Eberle, M. A., Fritzilas, E., Krusche, P., Kallberg, M., Moore, B. L., Bekritsky, M. A., Iqbal, Z., Chuang, H.-Y., Humphray, S. J., Halpern, A. L., Kruglyak, S., Margulies, E. H., McVean, G., and Bentley, D. R. (2016). A reference data set of 5.4 million phased human variants validated by genetic inheritance from sequencing a three-generation 17-member pedigree. *Genome Research*, **27**(1), 1–9.

Ewens, W. J. (2012a). *Mathematical Population Genetics 1: Theoretical Introduction*, volume 27. Springer Science & Business Media.

Ewens, W. J. (2012b). *Mathematical population genetics 1: theoretical introduction*, volume 27. Springer Science & Business Media.

Fisher, R. (1930a). The genetical theory of natural selection.

Fisher, R. A. (1930b). *The genetical theory of natural selection*. Oxford University Press, Oxford.

Fisher, R. A. (1949). The theory of inbreeding. *The theory of inbreeding*.

Fisher, R. A. (1954). A fuller theory of "junctions" in inbreeding. *Heredity*, **8**(2), 187–197.

Forney, G. D. (1973). The Viterbi Algorithm. In *Proceedings of the IEEE*, pages 268–278.

Frazer, K. A., Murray, S. S., Schork, N. J., and Topol, E. J. (2009). Human genetic variation and its contribution to complex traits. *Nature Reviews Genetics*, **10**(4), 241–251.

Freedman, M. L., Reich, D., Penney, K. L., McDonald, G. J., Mignault, A. A., Patterson, N., Gabriel, S. B., Topol, E. J., Smoller, J. W., Pato, C. N., Pato, M. T., Petryshen, T. L., Kolonel, L. N., Lander, E. S., Sklar, P., Henderson, B., Hirschhorn, J. N., and Altshuler, D. (2004). Assessing the impact of population stratification on genetic association studies. *Nature Genetics*, **36**(4), 388–393.

Fu, W., O'Connor, T. D., Jun, G., Kang, H. M., Abecasis, G., Leal, S. M., Gabriel, S., Altshuler, D., Shendure, J., Nickerson, D. A., Bamshad, M. J., Project, N. E. S., and Akey, J. M. (2012). Analysis of 6,515 exomes reveals the recent origin of most human protein-coding variants. *Nature*, **493**(7431), 216–220.

Fu, Y. X. (1995). Statistical Properties of Segregating Sites. *Theoretical population biology*, **48**(2), 172–197.

Fu, Y.-X. and Li, W.-H. (1999). Coalescing into the 21st Century: An Overview and Prospects of Coalescent Theory. *Theoretical population biology*, **56**(1), 1–10.

Fuchsberger, C., Flannick, J., Teslovich, T. M., Mahajan, A., Agarwala, V., Gaulton, K. J., Ma, C., Fontanillas, P., Moutsianas, L., McCarthy, D. J., Rivas, M. A., Perry, J. R. B., Sim, X., Blackwell, T. W., Robertson, N. R., Rayner, N. W., Cingolani, P., Locke, A. E., Tajes, J. F., Highland, H. M., Dupuis, J., Chines, P. S., Lindgren, C. M., Hartl, C., Jackson, A. U., Chen, H., Huyghe, J. R., van de Bunt, M., Pearson, R. D., Kumar, A., Müller-Nurasyid, M., Grarup, N., Stringham, H. M., Gamazon, E. R., Lee, J., Chen, Y., Scott, R. A., Below, J. E., Chen, P., Huang, J., Go, M. J., Stitzel, M. L., Pasko, D., Parker, S. C. J., Varga, T. V., Green, T., Beer, N. L., Day-Williams, A. G., Ferreira, T., Fingerlin, T., Horikoshi, M., Hu, C., Huh, I., Ikram, M. K., Kim, B.-J., Kim, Y., Kim, Y. J., Kwon, M.-S., Lee, J., Lee, S., Lin, K.-H., Maxwell, T. J., Nagai, Y., Wang, X., Welch, R. P., Yoon, J., Zhang, W., Barzilai, N., Voight, B. F., Han, B.-G., Jenkinson, C. P., Kuulasmaa, T., Kuusisto, J., Manning, A., Ng, M. C. Y., Palmer, N. D., Balkau, B., áková, A. S., Abboud, H. E., Boeing, H., Giedraitis, V., Prabhakaran, D., Gottesman, O., Scott, J., Carey, J., Kwan, P., Grant, G., Smith, J. D., Neale, B. M., Purcell, S., Butterworth, A. S., Howson, J. M. M., Lee, H. M., Lu, Y., Kwak, S.-H., Zhao, W., Danesh, J., Lam, V. K. L., Park, K. S., Saleheen, D., So, W. Y., Tam, C. H. T., Afzal, U., Aguilar, D., Arya, R., Aung, T., Chan, E., Navarro, C., Cheng, C.-Y., Palli, D., Correa, A., Curran, J. E., Rybin, D., Farook, V. S., Fowler, S. P., Freedman, B. I., Griswold, M., Hale, D. E., Hicks, P. J., Khor, C.-C., Kumar, S., Lehne, B., Thuillier, D., Lim, W. Y., Liu, J., van der Schouw, Y. T., Loh, M., Musani, S. K., Puppala, S., Scott, W. R., Yengo, L., Tan, S.-T., Taylor, H. A., Thameem, F., Wilson, G., Wong, T. Y., Njølstad, P. R., Levy, J. C., Mangino, M., Bonnycastle, L. L., Schwarzmayr, T., Fadista, J., Surdulescu, G. L., Herder, C., Groves, C. J., Wieland, T., Bork-Jensen, J., Brandslund, I., Christensen, C., Koistinen, H. A., Doney, A. S. F., Kinnunen, L., Esko, T., Farmer, A. J., Hakaste, L., Hodgkiss, D., Kravic, J., Lyssenko, V., Hollensted, M., Jørgensen, M. E., Jørgensen, T., Ladenvall, C., Justesen, J. M., Käräjämäki, A., Kriebel, J., Rathmann, W., Lannfelt, L., Lauritzen, T., Narisu, N., Linneberg, A., Melander, O., Milani, L., Neville, M., Orho-Melander, M., Qi, L., Qi, Q., Roden, M., Rolandsson, O., Swift, A., Rosengren, A. H., Stirrups, K., Wood, A. R., Mihailov, E., Blancher, C., Carneiro, M. O., Maguire, J., Poplin, R., Shakir, K., Fennell, T., DePristo, M., de Angelis, M. H., Deloukas, P., Gjesing, A. P., Jun, G., Nilsson, P., Murphy, J., Onofrio, R., Thorand, B., Hansen, T., Meisinger, C., Hu, F. B., Isomaa, B., Karpe, F., Liang, L., Peters, A., Huth, C., O'Rahilly, S. P., Palmer, C. N. A., Pedersen, O., Rauramaa, R., Tuomilehto, J., Salomaa, V., Watanabe, R. M., Syvänen, A.-C., Bergman, R. N., Bharadwaj, D., Bottinger, E. P., Cho, Y. S., Chandak, G. R., Chan, J. C. N., Chia, K. S., Daly, M. J., Ebrahim, S. B., Langenberg, C., Elliott, P., Jablonski, K. A., Lehman, D. M., Jia, W., and Ma, R. (2016). The genetic architecture of type 2 diabetes. *Nature*, **536**(7614), 41–47.

Genome of the Netherlands Consortium (2014). Whole-genome sequence variation, population structure and demographic history of the Dutch population. *Nature Genetics*, **46**(8), 818–825.

Gibson, G. (2012). Rare and common variants: twenty arguments. *Nature Reviews Genetics*, **13**(2), 135–145.

Gordon, D., Heath, S. C., Liu, X., and Ott, J. (2001). A Transmission/Disequilibrium Test That Allows for Genotyping Errors in the Analysis of Single-Nucleotide Polymorphism Data. *The American Journal of Human Genetics*, **69**(2), 371–380.

Gordon, D., Finch, S. J., Nothnagel, M., and Ott, J. u. r. (2002). Power and Sample Size Calculations for Case-Control Genetic Association Tests when Errors Are Present: Application to Single Nucleotide Polymorphisms. *Human heredity*, **54**(1), 22–33.

Gore, A., Li, Z., Fung, H.-L., Young, J. E., Agarwal, S., Antosiewicz-Bourget, J., Canto, I., Giorgetti, A., Israel, M. A., Kiskinis, E., Lee, J.-H., Loh, Y.-H., Manos, P. D., Montserrat, N., Panopoulos, A. D., Ruiz, S., Wilbert, M. L., Yu, J., Kirkness, E. F., Izpisua Belmonte, J. C., Rossi, D. J., Thomson, J. A., Eggan, K., Daley, G. Q., Goldstein, L. S. B., and Zhang, K. (2011). Somatic coding mutations in human induced pluripotent stem cells. *Nature*, **471**(7336), 63–67.

Griffiths, R. C. (1991). The Two-Locus Ancestral Graph. In *Selected Proceedings of the Sheffield Symposium on Applied Probability*, pages 100–117. Institute of Mathematical Statistics, Hayward, CA.

Griffiths, R. C. and Marjoram, P. (1996). Ancestral inference from samples of DNA sequences with recombination. *Journal of Computational Biology*, **3**(4), 479–502.

Griffiths, R. C. and Marjoram, P. (1997a). An ancestral recombination graph. *Institute for Mathematics and its Applications*, **87**, 257.

Griffiths, R. C. and Marjoram, P. (1997b). Progress in population genetics and human evolution.

Griffiths, R. C. and Tavaré, S. (1998). The age of a mutation in a general coalescent tree. *Communications in Statistics. Stochastic Models*, **14**(1-2), 273–295.

Gusev, A., Lowe, J. K., Stoffel, M., Daly, M. J., Altshuler, D., Breslow, J. L., Friedman, J. M., and Pe'er, I. (2009). Whole population, genome-wide mapping of hidden relatedness. *Genome Research*, **19**(2), 318–326.

Gutenkunst, R. N., Hernandez, R. D., Williamson, S. H., and Bustamante, C. D. (2009). Inferring the Joint Demographic History of Multiple Populations from Multidimensional SNP Frequency Data. *PLoS Genetics*, **5**(10), e1000695–11.

Haldane, J. (1919). The combination of linkage values and the calculation of distances between the loci of linked factors. *J Genet*, **8**(29), 299–309.

Hardy, G. H. (1908). Mendelian Proportions in a Mixed Population. *Science*, **28**(706), 49–50.

Harris, K. and Nielsen, R. (2013). Inferring Demographic History from a Spectrum of Shared Haplotype Lengths. *PLoS Genetics*, **9**(6).

Hayes, B. J., Visscher, P. M., McPartlan, H. C., and Goddard, M. E. (2003). Novel multilocus measure of linkage disequilibrium to estimate past effective population size. *Genome Research*, **13**(4), 635–643.

Hein, J., Schierup, M., and Wiuf, C. (2004). *Gene genealogies, variation and evolution: a primer in coalescent theory*. Oxford University Press, Oxford.

Henn, B. M., Gutenkunst, R. N., Indap, A. R., Marth, G. T., Clark, A. G., Yu, F., Gibbs, R. A., 1000 Genomes Project, Durbin, R. M., Flicek, P., Gabriel, S. B., Lander, E. S., Wheeler, D., Cibulskis, K., Fennell, T. J., Jaffe, D. B., Shefler, E., Egholm, M., Fulton, R., Bainbridge, M., Challis, D., Sabo, A., Wang, J., Lee, C., Korn, J. M., Sudbrak, R., Auton, A., Iqbal, Z., Desany, B., Dooling, D., Hurles, M. E., MacArthur, D. G., Abyzov, A., Zhang, Z., Garrison, E. P., Banks, E., Handsaker, R. E., Hartl, C., De La Vega, F. M., Alkan, C., Snyder, M., Muzny, D., Reid, J., Quinlan, A. R., Stewart, C., Wu, J., Gravel, S., Sherry, S. T., McVean, G. A., Abecasis, G. R., Koboldt, D. C., Palotie, A., Bustamante, C. D., Schafer, A. J., and Brooks, L. D. (2011). Demographic history and rare allele sharing among human populations. *Proceedings of the National Academy of Sciences*, **108**(29), 11983–11988.

Howie, B., Marchini, J., and Stephens, M. (2011a). Genotype imputation with thousands of genomes. *G3 (Bethesda, Md.)*, **1**(6), 457–470.

Howie, B., Marchini, J., and Stephens, M. (2011b). Genotype Imputation with Thousands of Genomes. *G3 (Bethesda, Md.)*, **1**(6), 457–470.

Howie, B. N., Donnelly, P., and Marchini, J. (2009). A Flexible and Accurate Genotype Imputation Method for the Next Generation of Genome-Wide Association Studies. *PLoS Genetics*, **5**(6), e1000529.

Hudson, R. (1990). Gene genealogies and the coalescent process. *Oxford surveys in evolutionary biology*, **7**(1), 44.

Hudson, R. and Kaplan, N. L. (1985). Statistical Properties of the Number of Recombination Events in the History of a Sample of Dna-Sequences. *Genetics*, **111**(1), 147–164.

Hudson, R. R. (1983). Properties of a neutral allele model with intragenic recombination. *Theoretical population biology*, **23**(2), 183–201.

Hudson, R. R. (2001). Two-locus sampling distributions and their application. *Genetics*, **159**(4), 1805–1817.

Hudson, R. R. (2002). Generating samples under a Wright-Fisher neutral model of genetic variation. *Bioinformatics*, **18**(2), 337–338.

International HapMap 3 Consortium, Schaffner, S. F., Peltonen, L., Dermitzakis, E., Bonnen, P. E., Altshuler, D. M., de Bakker, P. I. W., Deloukas, P., Gabriel, S. B., Gwilliam, R., Hunt, S., Inouye, M., Jia, X., Palotie, A., Parkin, M., Whittaker, P., Yu, F., Chang, K., Hawes, A., Lewis, L. R., Ren, Y., Wheeler, D., Gibbs, R. A., Muzny, D. M., Barnes, C., Darvishi, K., Hurles, M., Korn, J. M., Kristiansson, K., Lee, C., McCarrol, S. A., Nemesh, J., Keinan, A., Montgomery, S. B., Pollack, S., Soranzo, N., Gonzaga-Jauregui, C., Anttila, V., Brodeur, W., Daly, M. J., Leslie, S., McVean, G., Moutsianas, L., Nguyen, H., Zhang, Q., Ghori, M. J. R., McGinnis, R., McLaren, W., Price, A. L., Takeuchi, F., Grossman, S. R., Shlyakhter, I., Hostetter, E. B., Sabeti, P. C., Adebamowo, C. A., Foster, M. W., Gordon, D. R., Licinio, J., Manca, M. C., Marshall, P. A., Matsuda, I., Ngare, D., Wang, V. O., Reddy, D., Rotimi, C. N., Royal, C. D., Sharp, R. R., Zeng, C., Brooks, L. D., and McEwen, J. E. (2010). Integrating common and rare genetic variation in diverse human populations. *Nature*, **467**(7311), 52–58.

International HapMap Consortium (2003). The International HapMap Project. *Nature*, **426**(6968), 789–796.

International HapMap Consortium, Frazer, K. A., Ballinger, D. G., Cox, D. R., Hinds, D. A., Stuve, L. L., Gibbs, R. A., Belmont, J. W., Boudreau, A., Hardenbol, P., Leal, S. M., Pasternak, S., Wheeler, D. A., Willis, T. D., Yu, F., Yang, H., Zeng, C., Gao, Y., Hu, H., Hu, W., Li, C., Lin, W., Liu, S., Pan, H., Tang, X., Wang, J., Wang, W., Yu, J., Zhang, B., Zhang, Q., Zhao, H., Zhao, H., Zhou, J., Gabriel, S. B., Barry, R., Blumenstiel, B., Camargo, A., Defelice, M., Faggart, M., Goyette, M., Gupta, S., Moore, J., Nguyen, H., Parkin, M., Roy, J., Stahl, E., Winchester, E., Ziaugra, L., Shen, Y., Yao, Z., Huang, W., Chu, X., He, Y., Jin, L., Liu, Y., Shen, Y., Sun, W., Wang, H., Wang, Y., Wang, Y., Xiong, X., Xu, L., Waye, M. M. Y., Tsui, S. K. W., Xue, H., Wong, J. T.-F., Galver, L. M., Fan, J.-B., Gunderson, K., Murray, S. S., Oliphant, A. R., Chee, M. S., Montpetit, A., Chagnon, F., Ferretti, V., Leboeuf, M., Olivier, J.-F., Phillips, M. S., Roumy, S., Sallée, C., Verner, A., Hudson, T. J., Kwok, P.-Y., Cai, D., Koboldt, D. C., Miller, R. D., Pawlikowska, L., Taillon-Miller, P., Xiao, M., Tsui, L.-C., Mak, W., Song, Y. Q., Tam, P. K. H., Nakamura, Y., Kawaguchi, T., Kitamoto, T., Morizono, T., Nagashima, A., Ohnishi, Y., Sekine, A., Tanaka, T., Tsunoda, T., Deloukas, P., Bird, C. P., Delgado, M., Dermitzakis, E. T., Gwilliam, R., Hunt, S., Morrison, J., Powell, D., Stranger, B. E., Whittaker, P., Bentley, D. R., de Bakker, P. I. W., Barrett, J., Chretien, Y. R., Maller, J., McCarroll, S., Patterson, N., Pe'er, I., Price, A., Purcell, S., Sabeti, P., Saxena, R., Schaffner, S. F., Sham, P. C., Varilly, P., Altshuler, D., Stein, L. D., Krishnan, L., Smith, A. V., Tello-Ruiz, M. K., Thorisson, G. A., Chakravarti, A., Chen, P. E., Cutler, D. J., Kashuk, C. S., Lin, S., Abecasis, G. R., Guan, W., Li, Y., Munro, H. M., Qin, Z. S., Thomas, D. J., McVean, G., Auton, A., Bottolo, L., Cardin, N., Eyheramendy, S., Freeman, C., Marchini, J., Myers, S., Spencer, C., Stephens, M., Donnelly, P., Cardon, L. R., Clarke, G., Evans, D. M., Morris, A. P., Weir, B. S., Mullikin, J. C., Sherry, S. T., Feolo, M., Skol, A., Zhang, H., Matsuda, I., Fukushima, Y., Macer, D. R., Suda, E., Rotimi, C. N., Adebamowo, C. A., Ajayi, I., Aniagwu, T., Marshall, P. A., Nkwodimmah, C., Royal, C. D. M., Leppert, M. F., Dixon, M., Peiffer, A., Qiu, R., Kent, A., Kato, K., Niikawa, N., Adewole, I. F., Knoppers, B. M., Foster, M. W., Clayton, E. W., Watkin, J., Muzny, D., Nazareth, L., Sodergren, E., Weinstock, G. M., Yakub, I., Onofrio, R. C., Richter, D. J., Birren, B. W., Daly, M. J., Wilson, R. K., Fulton, L. L., Rogers, J., Burton, J., Carter, N. P., Clee, C. M., Griffiths, M., Jones, M. C., McLay, K., Plumb, R. W., Ross, M. T., Sims, S. K., Willey, D. L., Chen, Z., Han, H., Kang, L., Godbout, M., Wallenburg, J. C., L'Archevêque, P., Bellemare, G., Saeki, K., Wang, H., An, D., Fu, H., Li, Q., Wang, Z., Wang, R., Holden, A. L., Brooks, L. D., McEwen, J. E., Guyer, M. S., Wang, V. O., Peterson, J. L., Shi, M., Spiegel, J., Sung, L. M., Zacharia, L. F., Collins, F. S., Kennedy, K., Jamieson, R., and Stewart, J. (2007). A second generation human haplotype map of over 3.1 million SNPs. *Nature*, **449**(7164), 851–861.

International Human Genome Sequencing Consortium (2001). Initial sequencing and analysis of the human genome. *Nature*, **409**(6822), 860–921.

International Human Genome Sequencing Consortium (2004). Finishing the euchromatic sequence of the human genome. *Nature*, **431**(7011), 931–945.

Kaiser, J. (2008). A plan to capture human diversity in 1000 genomes (Science (395)). *Science*, **319**(5868), 1336.

Kang, S. J., Gordon, D., and Finch, S. J. (2004). What SNP genotyping errors are most costly for genetic association studies? *Genetic Epidemiology*, **26**(2), 132–141.

Keinan, A. and Clark, A. G. (2012). Recent explosive human population growth has resulted in an excess of rare genetic variants. *Science*, **336**(6082), 740–743.

Kelleher, J., Etheridge, A. M., and McVean, G. (2016). Efficient Coalescent Simulation and Genealogical Analysis for Large Sample Sizes. *PLoS computational biology*, **12**(5), e1004842–22.

Kimura, M. (1969). The number of heterozygous nucleotide sites maintained in a finite population due to steady flux of mutations. *Genetics*, **61**(4), 893–903.

Kimura, M. and Ota, T. (1973). The age of a neutral mutant persisting in a finite population. *Genetics*, **75**(1), 199–212.

Kingman, J. F. C. (1982a). Exchangeability and the evolution of large populations. *Exchangeability in Probability and Statistics*, pages 97—-112.

Kingman, J. F. C. (1982b). On the genealogy of large populations. *Journal of Applied Probability*, **19**(A), 27–43.

Kingman, J. F. C. (1982c). The coalescent. *Stochastic processes and their applications*, **13**(3), 235–248.

Klein, R. J., Zeiss, C., Chew, E. Y., Tsai, J.-Y., Sackler, R. S., Haynes, C., Henning, A. K., SanGiovanni, J. P., Mane, S. M., Mayne, S. T., Bracken, M. B., Ferris, F. L., Ott, J., Barnstable, C., and Hoh, J. (2005). Complement Factor H Polymorphism in Age-Related Macular Degeneration. *Science*, **308**(5720), 385–389.

Kong, A., Masson, G., Frigge, M. L., Gylfason, A., Zusmanovich, P., Thorleifsson, G., Olason, P. I., Ingason, A., Steinberg, S., Rafnar, T., Sulem, P., Mouy, M., Jonsson, F., Thorsteinsdottir, U., Gudbjartsson, D. F., Stefansson, H., and Stefansson, K. (2008). Detection of sharing by descent, long-range phasing and haplotype imputation. *Nature Genetics*, **40**(9), 1068–1075.

Kruglyak, L. (1999). Prospects for whole-genome linkage disequilibrium mapping of common disease genes. *Nature Genetics*, **22**(2), 139–144.

Kryukov, G. V., Pennacchio, L. A., and Sunyaev, S. R. (2007). Most rare missense alleles are deleterious in humans: implications for complex disease and association studies. *The American Journal of Human Genetics*, **80**(4), 727–739.

Labuda, M., Labuda, D., Korab-Laskowska, M., Cole, D. E., Zietkiewicz, E., Weissenbach, J., Popowska, E., Pronicka, E., Root, A. W., and Glorieux, F. H. (1996). Linkage disequilibrium analysis in young populations: pseudo-vitamin d-deficiency rickets and the founder effect in french canadians. *American journal of human genetics*, **59**(3), 633.

Lander, E. S. (1996). The new genomics: Global views of biology. *Science*, **274**(5287), 536–539.

Lawson, D. J., Hellenthal, G., Myers, S., and Falush, D. (2012). Inference of population structure using dense haplotype data. *PLoS Genetics*, **8**(1), e1002453.

Leutenegger, A.-L., Prum, B., Génin, E., Verny, C., Lemainque, A., Clerget-Darpoux, F., and Thompson, E. A. (2003). Estimation of the Inbreeding Coefficient through Use of Genomic Data. *American journal of human genetics*, **73**(3), 516–523.

Li, N. and Stephens, M. (2003). Modeling linkage disequilibrium and identifying recombination hotspots using single-nucleotide polymorphism data. *Genetics*, **165**(4), 2213–2233.

Li, W. H. (1975). The first arrival time and mean age of a deleterious mutant gene in a finite population. *The American Journal of Human Genetics*, **27**(3), 274–286.

Li, Y., Willer, C., Sanna, S., and Abecasis, G. (2009). Genotype imputation. *Annual review of genomics and human genetics*, **10**, 387–406.

Li, Y., Willer, C. J., Ding, J., Scheet, P., and Abecasis, G. R. (2010). MaCH: using sequence and genotype data to estimate haplotypes and unobserved genotypes. *Genetic Epidemiology*, **34**(8), 816–834.

Lim, E. T., Würtz, P., Havulinna, A. S., Palta, P., Tukiainen, T., Rehnström, K., Esko, T., Mägi, R., Inouye, M., Lappalainen, T., Chan, Y., Salem, R. M., Lek, M., Flannick, J., Sim, X., Manning, A., Ladenvall, C., Bumpstead, S., Hämäläinen, E., Aalto, K., Maksimow, M., Salmi, M., Blankenberg, S., Ardissino, D., Shah, S., Horne, B., McPherson, R., Hovingh, G. K., Reilly, M. P., Watkins, H., Goel, A., Farrall, M., Girelli, D., Reiner, A. P., Stitziel, N. O., Kathiresan, S., Gabriel, S., Barrett, J. C., Lehtimäki, T., Laakso, M., Groop, L., Kaprio, J., Perola, M., McCarthy, M. I., Boehnke, M., Altshuler, D. M., Lindgren, C. M., Hirschhorn, J. N., Metspalu, A., Freimer, N. B., Zeller, T., Jalkanen, S., Koskinen, S., Raitakari, O., Durbin, R., MacArthur, D. G., Salomaa, V., Ripatti, S., Daly, M. J., Palotie, A., and for the Sequencing Initiative Suomi (SISu) Project (2014). Distribution and Medical Impact of Loss-of-Function Variants in the Finnish Founder Population. *PLoS Genetics*, **10**(7), e1004494–12.

Liu, L., Li, Y., Li, S., Hu, N., He, Y., Pong, R., Lin, D., Lu, L., and Law, M. (2012). Comparison of Next-Generation Sequencing Systems. *Journal of biomedicine & biotechnology*, **2012**(7), 1–11.

Loh, P.-R., Palamara, P. F., and Price, A. L. (2016a). Fast and accurate long-range phasing in a uk biobank cohort. *Nature genetics*.

Loh, P.-R., Danecek, P., Palamara, P. F., Fuchsberger, C., Reshef, Y. A., Finucane, H. K., Schoenherr, S., Forer, L., McCarthy, S., Abecasis, G. R., Durbin, R., and Price, A. L. (2016b). Reference-based phasing using the Haplotype Reference Consortium panel. Technical report.

Malécot, G. (1948). Mathematics of heredity. *Les mathematiques de l'heredite.*

Manolio, T. A., Collins, F. S., Cox, N. J., Goldstein, D. B., Hindorff, L. A., Hunter, D. J., McCarthy, M. I., Ramos, E. M., Cardon, L. R., Chakravarti, A., Cho, J. H., Guttmacher, A. E., Kong, A., Kruglyak, L., Mardis, E., Rotimi, C. N., Slatkin, M., Valle, D., Whittemore, A. S., Boehnke, M., Clark, A. G., Eichler, E. E., Gibson, G., Haines, J. L., Mackay, T. F. C., McCarroll, S. A., and Visscher, P. M. (2009). Finding the missing heritability of complex diseases. *Nature*, **461**(7265), 747–753.

Marchini, J. and Howie, B. (2010). Genotype imputation for genome-wide association studies. **11**(7), 499–511.

Marchini, J., Howie, B., Myers, S., McVean, G., and Donnelly, P. (2007). A new multipoint method for genome-wide association studies by imputation of genotypes. *Nature Genetics*, **39**(7), 906–913.

Mardis, E. R. (2006). Anticipating the 1,000 dollar genome. *Genome biology*, **7**(7), 112.

Mardis, E. R. (2017). DNA sequencing technologies: 2006–2016. *Nature Protocols*, **12**(2), 213–218.

Marth, G. T., Yu, F., Indap, A. R., Garimella, K., Gravel, S., Leong, W. F., Tyler-Smith, C., Bainbridge, M., Blackwell, T., Zheng-Bradley, X., Chen, Y., Challis, D., Clarke, L., Ball, E. V., Cibulskis, K., Cooper, D. N., Fulton, B., Hartl, C., Koboldt, D., Muzny, D., Smith, R., Sougnez, C., Stewart, C., Ward, A., Yu, J., Xue, Y., Altshuler, D., Bustamante, C. D., Clark, A. G., Daly, M., DePristo, M., Flicek, P., Gabriel, S., Mardis, E., Palotie, A., Gibbs, R., and 1000 Genomes Project (2011). The functional spectrum of low-frequency coding variation. *Genome biology*, **12**(9), R84.

Maruyama, T. (1974). The age of an allele in a finite population. *Genetical research*, **23**(2), 137–143.

Mathieson, I. and McVean, G. (2012). Differential confounding of rare and common variants in spatially structured populations. *Nature Genetics*, **44**(3), 243–U29.

Mathieson, I. and McVean, G. (2014). Demography and the Age of Rare Variants. *PLoS Genetics*, **10**(8), e1004528.

Maynard Smith, J. (1989). *Evolutionary genetics.* Oxford University Press.

McCarroll, S. A., Kuruvilla, F. G., Korn, J. M., Cawley, S., Nemesh, J., Wysoker, A., Shapero, M. H., de Bakker, P. I. W., Maller, J. B., Kirby, A., Elliott, A. L., Parkin, M., Hubbell, E., Webster, T., Mei, R., Veitch, J., Collins, P. J., Handsaker, R., Lincoln, S., Nizzari, M., Blume, J., Jones, K. W., Rava, R., Daly, M. J., Gabriel, S. B., and Altshuler, D. (2008). Integrated detection and population-genetic analysis of SNPs and copy number variation. *Nature Genetics*, **40**(10), 1166–1174.

McCarthy, M. I., Abecasis, G. R., Cardon, L. R., Goldstein, D. B., Little, J., Ioannidis, J. P. A., and Hirschhorn, J. N. (2008). Genome-wide association studies for complex traits: consensus, uncertainty and challenges. *Nature Publishing Group*, **9**(5), 356–369.

McCarthy, S., Das, S., Kretzschmar, W., Delaneau, O., Wood, A. R., Teumer, A., Kang, H. M., Fuchsberger, C., Danecek, P., Sharp, K., Luo, Y., Sidore, C., Kwong, A., Timpson, N., Koskinen, S., Vrieze, S., Scott, L. J., Zhang, H., Mahajan, A., Veldink, J., Peters, U., Pato, C., van Duijn, C. M., Gillies, C. E., Gandin, I., Mezzavilla, M., Gilly, A., Cocca, M., Traglia, M., Angius, A., Barrett, J. C., Boomsma, D., Branham, K., Breen, G., Brummett, C. M., Busonero, F., Campbell, H., Chan, A., Chen, S., Chew, E., Collins, F. S., Corbin, L. J., Smith, G. D., Dedoussis, G., Dorr, M., Farmaki, A.-E., Ferrucci, L., Forer, L., Fraser, R. M., Gabriel, S., Levy, S., Groop, L., Harrison, T., Hattersley, A., Holmen, O. L., Hveem, K., Kretzler, M., Lee, J. C., McGue, M., Meitinger, T., Melzer, D., Min, J. L., Mohlke, K. L., Vincent, J. B., Nauck, M., Nickerson, D., Palotie, A., Pato, M., Pirastu, N., McInnis, M., Richards, J. B., Sala, C., Salomaa, V., Schlessinger, D., Schoenherr, S., Slagboom, P. E., Small, K., Spector, T., Stambolian, D., Tuke, M., Tuomilehto, J., Van den Berg, L. H., Van Rheenen, W., Volker, U., Wijmenga, C., Toniolo, D., Zeggini, E., Gasparini, P., Sampson, M. G., Wilson, J. F., Frayling, T., de Bakker, P. I. W., Swertz, M. A., McCarroll, S., Kooperberg, C., Dekker, A., Altshuler, D., Willer, C., Iacono, W., Ripatti, S., Soranzo, N., Walter, K., Swaroop, A., Cucca, F., Anderson, C. A., Myers, R. M., Boehnke, M., McCarthy, M. I., Durbin, R., Abecasis, G., and Marchini, J. (2016). A reference panel of 64,976 haplotypes for genotype imputation. *Nature Genetics*, **48**(10), 1279–1283.

McClellan, J. and King, M.-C. (2010). Genetic Heterogeneity in Human Disease. *Cell*, **141**(2), 210–217.

McLaren, W., Gil, L., Hunt, S. E., Riat, H. S., Ritchie, G. R. S., Thormann, A., Flicek, P., and Cunningham, F. (2016). The Ensembl Variant Effect Predictor. *Genome biology*, pages 1–14.

McQuillan, R., Leutenegger, A.-L., Abdel-Rahman, R., Franklin, C. S., Pericic, M., Barac-Lauc, L., Smolej-Narancic, N., Janicijevic, B., Polasek, O., Tenesa, A., MacLeod, A. K., Farrington, S. M., Rudan, P., Hayward, C., Vitart, V., Rudan, I., Wild, S. H., Dunlop, M. G., Wright, A. F., Campbell, H., and Wilson, J. F. (2008). Runs of Homozygosity in European Populations. *The American Journal of Human Genetics*, **83**(3), 359–372.

McVean, G., Awadalla, P., and Fearnhead, P. (2002). A coalescent-based method for detecting and estimating recombination from gene sequences. *Genetics*.

McVean, G. A. T., Myers, S. R., Hunt, S., Deloukas, P., Bentley, D. R., and Donnelly, P. (2004). The fine-scale structure of recombination rate variation in the human genome. *Science*, **304**(5670), 581–584.

Mendel, G. (1866). Versuche über Pflanzenhybriden. *Verhandlungen des naturforschenden Vereines in Brünn*, **4**, 3–47.

Metzker, M. L. (2009). Sequencing technologies — the next generation. *Nature Publishing Group*, **11**(1), 31–46.

Milligan, B. G. (2003). Maximum-Likelihood Estimation of Relatedness. *Genetics*, **163**(3), 1153–1167.

Moore, G. E. (1965). Cramming more components onto integrated circuits. *Electronics*, **38**(8).

Morgan, T. H. (1911). Random segregation versus coupling in Mendelian inheritance. *Science*, **34**(873), 384–384.

Morral, N., Bertranpetit, J., Estivill, X., and Nunes, V. (1994). The origin of the major cystic fibrosis mutation (DF508) in European populations. *Nature*.

Morris, A. and Cardon, L. (2007). Whole genome association. *Handbook of Statistical Genetics, Third Edition*, pages 1238–1263.

Moskvina, V. and Schmidt, K. M. (2006). Susceptibility of Biallelic Haplotype and Genotype Frequencies to Genotyping Error. *Biometrics*, **62**(4), 1116–1123.

Moskvina, V., Craddock, N., Holmans, P., Owen, M., and O'Donovan, M. (2005). Minor genotyping error can result in substantial elevation in type i error rate in haplotype based case control analysis. In *American Journal of Medical Genetics Part B-Neuropsychiatric Genetics*, volume 138, pages 19–19.

Moutsianas, L., Agarwala, V., Fuchsberger, C., Flannick, J., Rivas, M. A., Gaulton, K. J., Albers, P. K., GoT2D Consortium, McVean, G., Boehnke, M., Altshuler, D., and McCarthy, M. I. (2015). The Power of Gene-Based Rare Variant Methods to Detect Disease-Associated Variation and Test Hypotheses About Complex Disease. *PLoS Genetics*, **11**(4), e1005165–24.

Myers, S., Bottolo, L., Freeman, C., McVean, G., and Donnelly, P. (2005). A fine-scale map of recombination rates and hotspots across the human genome. *Science*.

Naidoo, N., Pawitan, Y., Soong, R., Cooper, D. N., and Ku, C.-S. (2011). Human genetics and genomics a decade after the release of the draft sequence of the human genome. *Human Genomics*, **5**(6), 577–622.

Neuhauser, C. (2001). Mathematical models in population genetics. *Handbook of statistical genetics*.

Nordborg, M. (2001). Coalescent theory. *Handbook of statistical genetics*.

O'Connell, J., Gurdasani, D., Delaneau, O., Pirastu, N., Ulivi, S., Cocca, M., Traglia, M., Huang, J., Huffman, J. E., Rudan, I., McQuillan, R., Fraser, R. M., Campbell, H., Polasek, O., Asiki, G., Ekoru, K., Hayward, C., Wright, A. F., Vitart, V., Navarro, P., Zagury, J.-F., Wilson, J. F., Toniolo, D., Gasparini, P., Soranzo, N., Sandhu, M. S., and Marchini, J. (2014). A General Approach for Haplotype Phasing across the Full Spectrum of Relatedness. *PLoS Genetics*, **10**(4), e1004234–21.

Ott, J. (1999). *Analysis of human genetic linkage*. JHU Press.

Pajunen, P., Rissanen, H., Härkänen, T., Jula, A., Reunanen, A., and Salomaa, V. (2010). The metabolic syndrome as a predictor of incident diabetes and cardiovascular events in the Health 2000 Study. *Diabetes and Metabolism*, **36**(5), 395–401.

Palamara, P. F. and Pe'er, I. (2013). Inference of historical migration rates via haplotype sharing. *Bioinformatics*, **29**(13), i180–i188.

Palamara, P. F., Lencz, T., Darvasi, A., and Pe'er, I. (2012). Length Distributions of Identity by Descent Reveal Fine-Scale Demographic History. *The American Journal of Human Genetics*, **91**(5), 809–822.

Palin, K., Campbell, H., Wright, A. F., Wilson, J. F., and Durbin, R. (2011). Identity-by-descent-based phasing and imputation in founder populations using graphical models. *Genetic Epidemiology*, **35**(8), 853–860.

Pasaniuc, B., Zaitlen, N., Shi, H., Bhatia, G., Gusev, A., Pickrell, J., Hirschhorn, J., Strachan, D. P., Patterson, N., and Price, A. L. (2014). Fast and accurate imputation of summary statistics enhances evidence of functional enrichment. *Bioinformatics (Oxford, England)*, **30**(20), 2906–2914.

Pe'er, I., de Bakker, P. I. W., Maller, J., Yelensky, R., Altshuler, D., and Daly, M. J. (2006). Evaluating and improving power in whole-genome association studies using fixed marker sets. *Nature Genetics*, **38**(6), 663–667.

Pennisi, E. (2007). Human Genetic Variation. *Science*, **318**(5858), 1842–1843.

Powell, J. E., Visscher, P. M., and Goddard, M. E. (2010). Reconciling the analysis of IBD and IBS in complex trait studies. *Nature Publishing Group*, **11**(11), 800–805.

Price, A. L., Patterson, N. J., Plenge, R. M., Weinblatt, M. E., Shadick, N. A., and Reich, D. (2006). Principal components analysis corrects for stratification in genome-wide association studies. *Nature Genetics*, **38**(8), 904–909.

Pritchard, J. K. (2001). Are rare variants responsible for susceptibility to complex diseases? *The American Journal of Human Genetics*, **69**(1), 124–137.

Purcell, S., Neale, B., Todd-Brown, K., Thomas, L., Ferreira, M. A. R., Bender, D., Maller, J., Sklar, P., de Bakker, P. I. W., Daly, M. J., and Sham, P. C. (2007). PLINK: a tool set for whole-genome association and population-based linkage analyses. *The American Journal of Human Genetics*, **81**(3), 559–575.

Rabiner, L. R. (1989). A tutorial on hidden Markov models and selected applications in speech recognition. In *Proceedings of the IEEE*, pages 257–286. Alcatel-Lucent Bell Labs, Murray, United States.

Rasmussen, M. D., Hubisz, M. J., Gronau, I., and Siepel, A. (2014). Genome-Wide Inference of Ancestral Recombination Graphs. *PLoS Genetics*, **10**(5), e1004342–27.

Reich, D. E., Cargill, M., Bolk, S., Ireland, J., Sabeti, P. C., Richter, D. J., Lavery, T., Kouyoumjian, R., Farhadian, S. F., Ward, R., and Lander, E. S. (2001). Linkage disequilibrium in the human genome. *Nature*, **411**(6834), 199–204.

Risch, N. and Merikangas, K. (1996). The future of genetic studies of complex human diseases. *Science*, **273**(5281), 1516–1517.

Risch, N., de Leon, D., Ozelius, L., Kramer, P., Almasy, L., Singer, B., Fahn, S., Breakefield, X., and Bressman, S. (1995). Genetic analysis of idiopathic torsion dystonia in Ashkenazi Jews and their recent descent from a small founder population. *Nature Genetics*, **9**(2), 152–159.

Risch, N. J. (2000). Searching for genetic determinants in the new millennium. *Nature*, **405**(6788), 847–856.

Roach, J. C., Glusman, G., Smit, A. F. A., Huff, C. D., Hubley, R., Shannon, P. T., Rowen, L., Pant, K. P., Goodman, N., Bamshad, M., Shendure, J., Drmanac, R., Jorde, L. B., Hood, L., and Galas, D. J. (2010). Analysis of Genetic Inheritance in a Family Quartet by Whole-Genome Sequencing. *Science*, **328**(5978), 636–639.

Roshyara, N. R. and Scholz, M. (2015). Impact of genetic similarity on imputation accuracy. *BMC Genetics*, **16**(1), 1–16.

Rousset, F. (2002). Inbreeding and relatedness coefficients: What do they measure? *Heredity*, **88**(5), 371–380.

Sanger, F. and Coulson, A. R. (1975). A rapid method for determining sequences in DNA by primed synthesis with DNA polymerase. *Journal of molecular biology*, **94**(3), 441–448.

Sanger, F., Nicklen, S., and Coulson, A. R. (1977). DNA sequencing with chain-terminating inhibitors. *Proceedings of the National Academy of Sciences of the United States of America*, **74**(12), 5463–5467.

Scally, A. and Durbin, R. (2012). Revising the human mutation rate: implications for understanding human evolution. *Nature Reviews Genetics*, **13**(10), 745–753.

Schork, N. J., Murray, S. S., Frazer, K. A., and Topol, E. J. (2009). Common vs. rare allele hypotheses for complex diseases. *Current opinion in genetics & development*, **19**(3), 212–219.

Schroff, M. H. (2016). *Genealogical properties of rare variation and their implications for demographic inference*. Ph.D. thesis, University of Oxford.

Serre, J. L., Simon-Bouy, B., Mornet, E., Jaume-Roig, B., Balassopoulou, A., Schwartz, M., Taillandier, A., Boue, J., and Boue, A. (1990). Studies of RFLP closely linked to the cystic fibrosis locus throughout Europe lead to new considerations in populations genetics. *Human genetics*, **84**(5), 449–454.

Shields, D. C., Collins, A., Buetow, K. H., and Morton, N. E. (1991). Error filtration, interference, and the human linkage map. *Proceedings of the National Academy of Sciences of the United States of America*, **88**(15), 6501–6505.

Simons, Y. B., Turchin, M. C., Pritchard, J. K., and Sella, G. (2014). The deleterious mutation load is insensitive to recent population history. *Nature Publishing Group*, **46**(3), 220–224.

Slack, J. (2014). *Genes: A Very Short Introduction*. Oxford University Press, Oxford.

Slatkin, M. (2000). Allele age and a test for selection on rare alleles. *Philosophical Transactions of the Royal Society B: Biological Sciences*, **355**(1403), 1663–1668.

Slatkin, M. (2008a). Inbreeding coefficients and coalescence times. *doi.org*, pages 1–9.

Slatkin, M. (2008b). Linkage disequilibrium – understanding the evolutionary past and mapping the medical future. *Nature Reviews Genetics*, **9**(6), 477–485.

Slatkin, M. and Bertorelle, G. (2001). The use of intraallelic variability for testing neutrality and estimating population growth rate. *Genetics*, **158**(2), 865–874.

Slatkin, M. and Rannala, B. (2000). Estimating allele age. *Annual review of genomics and human genetics*, **1**(1), 225–249.

Sobel, E., Papp, J. C., and Lange, K. (2002). Detection and integration of genotyping errors in statistical genetics. *The American Journal of Human Genetics*, **70**(2), 496–508.

Stam, P. (1980). The distribution of the fraction of the genome identical by descent in finite random mating populations. *Genetical research*, **35**(02), 131.

Stone, M. (1961). The Opinion Pool. *The Annals of Mathematical Statistics*, **32**(4), 1339–1342.

Sturtevant, A. H. (1913). The linear arrangement of six sex-linked factors in drosophila, as shown by their mode of association. *Journal of Experimental Zoology Part A: Ecological Genetics and Physiology*, **14**(1), 43–59.

Su, Z., Marchini, J., and Donnelly, P. (2011). HAPGEN2: simulation of multiple disease SNPs. *Bioinformatics*, **27**(16), 2304–2305.

Tajima, F. (1983). Evolutionary relationship of DNA sequences in finite populations. *Genetics*, **105**(2), 437–460.

Tajima, F. (1993). Measurement of dna polymorphism. *Mechanisms of molecular evolution*, pages 37–59.

Takahata, N. (1993). Allelic genealogy and human evolution. *Molecular Biology and Evolution*, **10**(1), 2–22.

Tavaré, S. (2004). Part I: Ancestral inference in population genetics. In *Lectures on probability theory and statistics*, pages 1–188. Springer.

Tavaré, S., Balding, D. J., Griffiths, R. C., and Donnelly, P. (1997). Inferring coalescence times from DNA sequence data. *Genetics*, **145**(2), 505–518.

Tennessen, J. A., Bigham, A. W., O'Connor, T. D., Fu, W., Kenny, E. E., Gravel, S., McGee, S., Do, R., Liu, X., Jun, G., Kang, H. M., Jordan, D., Leal, S. M., Gabriel, S., Rieder, M. J., Abecasis, G., Altshuler, D., Nickerson, D. A., Boerwinkle, E., Sunyaev, S., Bustamante, C. D., Bamshad, M. J., Akey, J. M., GO, B., GO, S., and Project, N. E. S. (2012). Evolution and Functional Impact of Rare Coding Variation from Deep Sequencing of Human Exomes. *Science*, **337**(6090), 64–69.

Thompson, E. A. (1974). Gene Identities and Multiple Relationships. *Biometrics*, **30**(4), 667.

Thompson, E. A. (1975). The estimation of pairwise relationships. *Annals of human genetics*, **39**(2), 173–188.

Thompson, E. A. (1976). Estimation of age and rate of increase of rare variants. *The American Journal of Human Genetics*, **28**(5), 442–452.

Thompson, E. A. (2008). The IBD process along four chromosomes. *Theoretical population biology*, **73**(3), 369–373.

Thompson, E. A. (2013). Identity by descent: variation in meiosis, across genomes, and in populations. *Genetics*, **194**(2), 301–326.

Tschermak, E. (1900). Über künstliche Kreuzung bei *Pisum sativum*. *Berichte der Deutschen Botanischen Gesellschaft*, **18**, 232–239.

UK10K Consortium, Walter, K., Crooks, L., Memari, Y., Perry, J. R. B., Xu, C., Futema, M., Lawson, D., Iotchkova, V., Schiffels, S., Hendricks, A. E., Li, R., Floyd, J., Wain, L. V., Humphries, S. E., Barrett, J. C., Plagnol, V., Richards, J. B., Greenwood, C. M. T., Timpson, N. J., Soranzo, N., Danecek, P., Barroso, I., McCarthy, S., Tachmazidou, I., Durbin, R., Hurles, M. E., Kennedy, K., Palotie, A., Zeggini, E., Cocca, M., Huang, J., and Min, J. L. (2015). The UK10K project identifies rare variants in health and disease. *Nature*, **526**(7571), 82–90.

Vartiainen, E., Laatikainen, T., Peltonen, M., Juolevi, A., Mannisto, S., Sundvall, J., Jousilahti, P., Salomaa, V., Valsta, L., and Puska, P. (2010). Thirty-five-year trends in cardiovascular risk factors in Finland. *International Journal of Epidemiology*, **39**(2), 504–518.

Venter, J. C., Adams, M. D., Myers, E. W., Li, P. W., Mural, R. J., Sutton, G. G., Smith, H. O., Yandell, M., Evans, C. A., Holt, R. A., Gocayne, J. D., Amanatides, P., Ballew, R. M., Huson, D. H., Wortman, J. R., Zhang, Q., Kodira, C. D., Zheng, X. H., Chen, L., Skupski, M., Subramanian, G., Thomas, P. D., Zhang, J., Miklos, G. L. G., Nelson, C., Broder, S., Clark, A. G., Nadeau, J., McKusick, V. A., Zinder, N., Levine, A. J., Roberts, R. J., Simon, M., Slayman, C., Hunkapiller, M., Bolanos, R., Delcher, A., Dew, I., Fasulo, D., Flanigan, M., Florea, L., Halpern, A., Hannenhalli, S., Kravitz, S., Levy, S., Mobarry, C., Reinert, K., Remington, K., Abu-Threideh, J., Beasley, E., Biddick, K., Bonazzi, V., Brandon, R., Cargill, M., Chandramouliswaran, I., Charlab, R., Chaturvedi, K., Deng, Z., Di Francesco, V., Dunn, P., Eilbeck, K., Evangelista, C., Gabrielian, A. E., Gan, W., Ge, W., Gong, F., Gu, Z., Guan, P., Heiman, T. J., Higgins, M. E., Ji, R.-R., Ke, Z., Ketchum, K. A., Lai, Z., Lei, Y., Li, Z., Li, J., Liang, Y., Lin, X., Lu, F., Merkulov, G. V., Milshina, N., Moore, H. M., Naik, A. K., Narayan, V. A., Neelam, B., Nusskern, D., Rusch, D. B., Salzberg, S., Shao, W., Shue, B., Sun, J., Wang,

Z. Y., Wang, A., Wang, X., Wang, J., Wei, M.-H., Wides, R., Xiao, C., Yan, C., Yao, A., Ye, J., Zhan, M., Zhang, W., Zhang, H., Zhao, Q., Zheng, L., Zhong, F., Zhong, W., Zhu, S. C., Zhao, S., Gilbert, D., Baumhueter, S., Spier, G., Carter, C., Cravchik, A., Woodage, T., Ali, F., An, H., Awe, A., Baldwin, D., Baden, H., Barnstead, M., Barrow, I., Beeson, K., Busam, D., Carver, A., Angela Center, Cheng, M. L., Curry, L., Danaher, S., Davenport, L., Desilets, R., Dietz, S., Dodson, K., Doup, L., Ferriera, S., Garg, N., Gluecksmann, A., Hart, B., Haynes, J., Haynes, C., Heiner, C., Hladun, S., Hostin, D., Houck, J., Howland, T., Ibegwam, C., Johnson, J., Kalush, F., Kline, L., Koduru, S., Love, A., Mann, F., May, D., McCawley, S., McIntosh, T., McMullen, I., Moy, M., Moy, L., Murphy, B., Nelson, K., Pfannkoch, C., Pratts, E., Puri, V., Qureshi, H., Reardon, M., Rodriguez, R., Rogers, Y.-H., Romblad, D., Ruhfel, B., Scott, R., Sitter, C., Smallwood, M., Stewart, E., Strong, R., Suh, E., Thomas, R., Tint, N. N., Tse, S., Vech, C., Wang, G., Wetter, J., Williams, S., Williams, M., Windsor, S., Winn-Deen, E., Wolfe, K., Zaveri, J., Zaveri, K., Abril, J. F., Guigo, R., Campbell, M. J., Sjolander, K. V., Karlak, B., Kejariwal, A., Mi, H., Lazareva, B., Hatton, T., Narechania, A., Diemer, K., Muruganujan, A., Guo, N., Sato, S., Bafna, V., Istrail, S., Lippert, R., Schwartz, R., Walenz, B., Yooseph, S., Allen, D., Basu, A., Baxendale, J., Blick, L., Caminha, M., Carnes-Stine, J., Caulk, P., Chiang, Y.-H., Coyne, M., Dahlke, C., Mays, A. D., Dombroski, M., Donnelly, M., Ely, D., Esparham, S., Fosler, C., Gire, H., Glanowski, S., Glasser, K., Glodek, A., Gorokhov, M., Graham, K., Gropman, B., Harris, M., Heil, J., Henderson, S., Hoover, J., Jennings, D., Jordan, C., Jordan, J., Kasha, J., Kagan, L., Kraft, C., Levitsky, A., Lewis, M., Liu, X., Lopez, J., Ma, D., and Majoros... (2001). The Sequence of the Human Genome. *Science*, **291**(5507), 1304–1351.

Viterbi, A. J. (1967). Error Bounds for Convolutional Codes and an Asymptotically Optimum Decoding Algorithm. *IEEE Transactions on Information Theory*, **13**(2), 260–269.

Voight, B. F. and Pritchard, J. K. (2005). Confounding from Cryptic Relatedness in Case-Control Association Studies. *PLoS Genetics*, **1**(3), e32–10.

Wakeley, J. (2008). *Coalescent Theory: An Introduction*. W. H. Freeman.

Wakeley, J. and Wilton, P. (2016). Coalescent and models of identity by descent. In R. M. Kliman, editor, *Encyclopedia of Evolutionary Biology*, pages 287 – 292. Academic Press, Oxford.

Wang, J. (2005). Estimation of effective population sizes from data on genetic markers. *Philosophical Transactions of the Royal Society B: Biological Sciences*, **360**(1459), 1395–1409.

Watson, J. D. and Crick, F. H. (1953). Molecular structure of nucleic acids; a structure for deoxyribose nucleic acid. *Nature*, **171**(4356), 737–738.

Watterson, G. (1996). Motoo Kimura's Use of Diffusion Theory in Population Genetics. *Theoretical population biology*, **49**(2), 154–188.

Watterson, G. A. (1975). On the number of segregating sites in genetical models without recombination. *Theoretical population biology*, **7**(2), 256–276.

Watterson, G. A. (1976). Reversibility and the age of an allele. I. Moran's infinitely many neutral alleles model. *Theoretical Population Biology*, **10**(3), 239–253.

Weinberg, W. (1908). Über den Nachweis der Vererbung beim Menschen. *Jahreshefte des Vereins für vaterländische Naturkunde in Württemberg.*, **64**, 368–382.

Weissenbach, J. (1993). A second generation linkage map of the human genome based on highly informative microsatellite loci. *Gene*, **135**(1-2), 275–278.

Wheeler, D. A., Srinivasan, M., Egholm, M., Shen, Y., Chen, L., McGuire, A., He, W., Chen, Y.-J., Makhijani, V., Roth, G. T., Gomes, X., Tartaro, K., Niazi, F., Turcotte, C. L., Irzyk, G. P., Lupski, J. R., Chinault, C., Song, X.-z., Liu, Y., Yuan, Y., Nazareth, L., Qin, X., Muzny, D. M., Margulies, M., Weinstock, G. M., Gibbs, R. A., and Rothberg, J. M. (2008). The complete genome of an individual by massively parallel DNA sequencing. *Nature*, **452**(7189), 872–876.

Winkler, H. (1920). *Verbreitung und Ursache der Parthenogenesis im Pflanzen- und Tierreich*. Verlag G. Fischer, Jena.

Wiuf, C. and Hein, J. (1997). On the number of ancestors to a DNA sequence. *Genetics*, **147**(3), 1459–1468.

Wright, S. (1921). Systems of Mating. I. the Biometric Relations between Parent and Offspring. *Genetics*, **6**(2), 111–123.

Wright, S. (1922). Coefficients of Inbreeding and Relationship. *The American Naturalist*, **56**(645), 330–338.

Wright, S. (1931a). Evolution in Mendelian Populations. *Genetics*, **16**(2), 97–159.

Wright, S. (1931b). Evolution in Mendelian Populations. *Genetics*, **16**(2), 97–159.

Yu, N., Zhao, Z., Fu, Y. X., Sambuughin, N., Ramsay, M., Jenkins, T., Leskinen, E., Patthy, L., Jorde, L. B., Kuromori, T., and Li, W. H. (2001). Global patterns of human DNA sequence variation in a 10-kb region on chromosome 1. *Molecular Biology and Evolution*, **18**(2), 214–222.

Zuk, O., Schaffner, S. F., Samocha, K., Do, R., Hechter, E., Kathiresan, S., Daly, M. J., Neale, B. M., Sunyaev, S. R., and Lander, E. S. (2014). Searching for missing heritability: designing rare variant association studies. *Proceedings of the National Academy of Sciences*, **111**(4), E455–64.

1. *I have told you more than I know* [...].
2. *What I have told you is subject to change without notice.*
3. *I hope I raised more questions than I have given answers.*
4. *In any case, as usual, a lot more work is necessary.*

– Fuller Albright